AN ABSTRACT OF THE DISSERTATION OF

Joshua K. Cuzzone for the degree of Doctor of Philosophy in Ocean, Earth, and Atmospheric Science presented on October 1, 2014.

Title: An Interdisciplinary approach towards understanding Late Pleistocene Ice Sheet change.

Abstract approved: _____

Peter U. Clark

The results presented in this dissertation address a number of questions regarding late Pleistocene and Holocene ice-sheet and climate interactions, spanning disciplines involving paleoclimatology and atmospheric science. These studies use various techniques in geochemistry, climate modeling, and ice-sheet modeling to address ice-sheet response to climate and the attendant interactions between the atmosphere and ice-sheets.

An important question in paleoclimatology involves the response of past ice sheets to a warming climate, with the end goal of providing context for understanding the response of future ice sheets to anthropogenic warming. A longstanding question regards the timing and rate of retreat for the Scandinavian Ice Sheet (SIS) during the Holocene. Much work has been done to constrain the retreat of the SIS from the last glacial maximum to the well-defined Younger Dryas moraines, however, little is known regarding the SIS Holocene retreat. Presented is a compilation of 87 ^{10}Be surface exposure ages from Sweden and Norway. These ages provide a high-resolution reconstruction of the SIS deglaciation during the Holocene, and allow for close comparison with proxies of temperature and insolation. The results suggest an

asymmetric deglaciation of the SIS, with retreat forced by both a warming climate and and ice-sheet dynamics depending on time and location. The record also provides a means for evaluating the SIS contribution to Holocene sea-level rise. Combining this with estimates from the Laurentide Ice Sheet and the Greenland Ice Sheet, our results suggest that ~23 m of residual sea-level rise exists at the start of the Holocene. We suggest an Antarctic source, which has implications for understanding the sensitivity of the Antarctic Ice Sheet to Holocene climate change.

Ice-sheets exert a large presence on the overlying atmosphere, with these interactions influencing the general circulation and ultimately the surface mass balance of the ice sheet. Prior work has indicated striking differences in the atmospheric circulation between the LGM and present day. Using a fully coupled climate simulation of the last deglaciation, the atmospheric circulation is studied, with respect to the stationary waves and storm tracks. For this study, we focus on the LIS. Our results show an enhanced stationary wave, forced mechanically by the topography of the LIS along western North America, which provides moisture, driven by enhanced ridging. This mechanism provides a positive feedback, whereby a larger ice sheet drives a more positive wintertime mass balance. Eventually, as the ice sheet melts, this stationary wave weakens, and the moisture flux decreases. Over the eastern LIS, coupled atmosphere and ice-sheet dynamics conspire to weaken the storm track at the LGM. As the ice melts, however, the storm track becomes broader and strengthens. The storm track becomes an efficient means for moisture delivery to the eastern LIS, with this relationship strengthening through the deglaciation. We suggest that enhanced wintertime accumulation from the strengthening storm track may have played a strong role in

offsetting summertime ablation along the eastern LIS, and thus may be a reason why the LIS terminated over eastern North America.

Another longstanding question in paleoclimatology involves the role of CO_2 and insolation on driving the deglaciation of the great Northern hemisphere ice sheets. To investigate this question we one way coupled the 3-dimensional thermomechanical ice-sheet model, Glimmer to climate simulations of the last deglaciation using GENMOM. We first built up a realistic LIS, constrained by the best available reconstructions of the area and volume, by perturbing parameters to obtain the best fit. Once a suitable spun-up LGM LIS was created, we forced the deglaciation of the LIS using climate simulations of the last deglaciation using either varying insolation only, and varying CO_2 only. Our results show similar trends in the deglaciation of the LIS relative to simulations of the deglaciation forced with all forcings (CO_2 and insolation). Upon further inspection, our results prove that the one way coupling scheme is unable to capture the influence of the separate forcings. Instead, the topography boundary condition used to drive the climate simulations dictates the distribution of heat and moisture, and thus the deglaciation. Our results show that in order to properly simulate the response of the LIS to CO_2 and insolation only forcings, an asynchronous coupling scheme or coupled climate-ice-sheet models should be used.

An Interdisciplinary approach towards understanding Late Pleistocene Ice Sheet Change

by

Joshua K. Cuzzone

A DISSERTATION

Submitted to

Oregon State University

in partial fulfillment of

the requirements for the

degree of

Doctor of Philosophy

Presented October 1, 2014

Commencement June 2015

Doctor of Philosophy dissertation of Joshua K. Cuzzone presented October 1, 2014.

APPROVED:

_____

Major Professor, representing Ocean, Earth, and Atmospheric Sciences

_____

Dean of the College of Earth, Ocean, and Atmospheric Science

_____

Dean of the Graduate School

I understand that my dissertation will become part of the permanent collection of Oregon State University libraries. My signature below authorizes release of my dissertation to any reader upon request.

_____

Joshua K. Cuzzone, Author

ACKNOWLEDGMENTS

The body of work presented in this dissertation is a culmination of efforts by many, who have helped me achieve my scientific goals as a graduate student. Peter Clark, my advisor has guided me through the rigorous steps in becoming a PhD, and has pushed me to become a better scientist along the way. Thank you Peter for taking me on as a student, and allowing me to explore my own scientific ideas along my journey in graduate school. You have been an exceptional mentor, who has always expected the best from his students. Thank you for pushing me to always improve. The opportunities given to me during my time at OSU will serve me well in my academic future, and I cannot begin to express my gratitude for all of your help.

A few years ago, as a master student at the University of Wisconsin-Madison, I made the great journey across the road from the Atmospheric Science building to the Geology building. I took glacial geology, taught by Anders Carlson, and thus began my curiosity of paleoclimatology. I really thank you Anders, for opening my eyes to the field of glacial geology and paleoclimatology. I owe much of my success to your efforts and of course, to connecting me with Peter. I thank you for always being available to answer any questions I had along the way, and supportive of my academic goals.

To Steve Hostetler, thank you for always being available to listen my ideas, particularly regarding my storm track research. I can recall some early meeting my first year, where I was not prepared well express my ideas on the subject. You have always been supportive and encouraging, and I cannot thank you enough for your help.

To Justin Wettstein, thank you so much for making the leap to be a member on my committee as well as a co-author on one of my papers. I came to you during a very busy transition for you as a new professor. Your interest in my research has been exceptional, and has helped foster my intellectual growth regarding atmospheric dynamics. I feel as if I have gained a good friend, and I appreciate all of your efforts and help along this journey.

To my committee members, thank you again. I cannot express my thanks in such few words. Also, thank you to my graduate representative, Andrew Valls for agreeing to serve on my committee, particularly at short notice.

To my teachers along the way, thank you for all of your help and efforts. In particular, I thank you Alan Mix. Alan was a large motivation behind one of my thesis chapters, after taking his paleoceanography class. Alan, you have been a great mentor and teacher. I have learned a great deal about paleoclimatology and statistics from you and thank you very much for all of your help. Edward Brook was instrumental in my academic growth as well. Thank you Ed for your valuable insight into cosmogenic surface exposure techniques. To Jay Alder, thank you for putting up with my pestering regarding modeling. You have been patient with me and an excellent mentor over the years. Thank you for all of your help.

My academic growth would not be possible without the help and mentorship of Shaun Marcott. Shaun, I cannot express my thanks for your patience in teaching me everything related to cosmogenic surface exposure dating. I know it was a tough task to show an atmospheric scientist around the lab, but I am incredibly grateful for your help. Also, thank you for your wise words regarding “getting through” graduate school. I feel I

have gained a good friend and colleague, and I look forward to possible collaboration in the future.

Graduate school would not be possible without the love and support of my friends. To my 5040 family, Lalo, Amoreen, Iria, Alberto, Guinness, and Molly, I cannot express how much you all mean to me. Your support over the years has been instrumental to my success. And to Iria, Amoreena, and Alberto, thank you for keeping me well fed over the years! To Lalo, my partner in crime on the trail. Riding bikes means so much to us, and I am glad we were able to foster an incredibly strong friendship on and off the bike. I will miss riding together on a daily basis, but look forward to a future full of fun times on the bike.

To my officemates, Cody Beedlow, Aaron Barth, Nilo Bill, Andrea Balbas, and Jeremy Hoffman. You have all been instrumental in my growth and have offered so much in terms of friendship. I know I have made friends for life and I cannot wait to see what the future holds for us all.

Lastly, my family has been incredibly supportive over the years. Your love and support has kept me going over the years, and I cannot begin to express my thanks. Thank you mom for instilling a scientific curiosity in me that has endured well into my academic career. I remember turning over rocks at the beach with you, in search of sea critters, while other kids were off playing in the pool. To my father, thank you for always teaching me that my best effort is what counts, and not the outcome. I cannot begin to express my thanks for your hard work and sacrifice to allow me to pursue my goals and aspirations. To my parents, you have been instrumental in my success and I cannot express how fortunate I am. To my older brother Daniel, my role model and best friend.

Thank you for always being there for me, pushing me when I was down, and letting me know that things will be ok. You are the hardest working person I know, and I have learned so much from you. Thank you for all of your support over the years.

CONTRIBUTIONS OF AUTHORS

Chapter 2 - P.U. Clark co-wrote the manuscript and conceived the project with A. Carlson. F. He performed the transient climate simulation. B. Wholfarth and J.P. Lunkka helped with field sampling and interpretation. S. Marcott assisted with lab procedures. D. Ullman assisted with data analysis and interpretation. M. Caffee assisted with ^{10}Be analysis.

Chapter 3 – J. Wettstein co-wrote the manuscript. J. Alder carried out the climate simulation. S. Hostetler and P.U. Clark helped with interpretation.

Chapter 4 – J. Alder carried out the climate simulations and helped setup the ice-sheet model. P.U. Clark and S. Hostetler helped with interpretation and analysis.

TABLE OF CONTENTS

TABLE OF CONTENTS (Continued) Page

TABLE OF CONTENTS (Continued) Page

LIST OF FIGURES

LIST OF FIGURES (Continued)

Figure Page

LIST OF TABLES

An Interdisciplinary approach towards understanding Late Pleistocene Ice Sheet Change

Chapter 1

Introduction

1.1 Foreword

Presently, climatologists are faced with a daunting task in understanding how our earth will respond to anthropogenic climate change. Many steps have been taken over the past decades to improve observation networks and complex climate models used to predict future changes. These steps, however, are limited temporally as predictions can only be verified against present data, with the future remaining unknown. Often, the paleoclimate record has served as a strong metric to evaluate past changes to our climate in response to certain forcings, thus offering a glimpse of where we may be heading in the future.

The study of paleoclimatology provides a context for future climate change, and allows scientists to evaluate the role of natural forces in shaping our climate. This metric has allowed climatologists to conclude that present and future changes to our climate are being forced primarily by human activities (IPCC, 2013). Much work is needed, however, to understand the sensitivity of our climate to these anthropogenic forcings, the role they play in altering the cryosphere, and how changes will conspire to affect sea level. Since the study of paleoclimatology spans many aspects of earth science, it is a useful tool for addressing these questions. In this dissertation, issues related to paleoclimatology are addressed with respect to past ice sheet sensitivity and sea-level

rise, past ice-sheet-atmosphere interactions, and the sensitivity of the ice sheets to changes in insolation and CO_2.

The main objective of this body of work is to evaluate past ice-sheet response to climate change over the last deglaciation and early Holocene. Because the cryosphere is intimately coupled with the climate system, attempting to answer these questions involves insight and analysis from a broad spectrum of disciplines. The motivation for this work surrounds the response of present day ice sheets, namely the Greenland Ice Sheet and the West Antarctic Ice Sheet, to anthropogenic climate change. These questions are focused, but not limited to, the response and rate of ice sheet melt to a warming climate and their respective contribution to future sea-level rise. The response of these ice sheets to future changes involves a complex set of parameters including influence from the atmosphere and ocean, as well as ice dynamics. The work presented here does not attempt to strictly answer these questions nor evaluate the future response of ice sheets to a warming climate. Rather, the aim of this research is to gain insight into how large ice sheets have responded to past climate change, how the atmosphere and ice-sheets have interacted in the past, and how greenhouse gases may have influenced the trajectory of past ice sheets using an ice-sheet model. The role of paleoclimatology in answering critical questions regarding the future state of our climate first lies in understanding the influence of past climate changes on our earth system.

1.2 Project Objectives

In chapter 2, the deglaciation of the Scandinavian Ice Sheet (SIS) is reconstructed using cosmogenic surface exposure dating using ^{10}Be. Much work has been done to understand the deglaciation of the SIS during the last deglaciation (Lundqvist and

Wohlfarth, 2001; Lunkka et. al., 2004; Rinterknecht et. al., 2006), yet the timing and rate of its retreat during the Holocene remains unknown. Using surface exposure dating, we constrain the final termination of the SIS, providing a context of its sensitivity to a changing climate. Accordingly, we constrain the SIS contribution to Holocene sea-level rise and estimate remaining sources to determine the sensitivity of other ice sheets.

In chapter 3 we use a state of the art climate simulation of the last deglaciation to evaluate the role of the changing atmospheric circulation on the surface mass balance of the Laurentide Ice Sheet (LIS). Many studies have indicated differences in the present day and last glacial maximum atmospheric circulation regime (Manabe and Broccoli, 1985; Roe and Lindzen (2001); Li and Battisti, 2008). Superimposed on changes do to a warming climate through the last deglaciation, changes in the atmospheric circulation would certainly have altered the mass balance of the Laurentide ice sheet through changes in temperature and moisture advection. Here we evaluate changes in storm tracks and the stationary wave pattern over the last deglaciation. We employ statistical tests to estimate the role each of these changes played in the surface mass balance of the LIS, with implications for its final termination.

Understanding the sensitivity of the great Northern Hemisphere ice sheets to changes in CO2 and insolation during the last deglaciation has been an important question in paleoclimatology. In chapter 4, a simulation of the LIS deglaciation from the last glacial maximum (LGM) is undertaken by one way coupling the ice-sheet model Glimmer (Rutt et. al., 2009) to climate output from GENMOM (Alder et. al., 2011). Parameter space is evaluated to allow for the closest simulated ice volume and area compared to the best

available reconstructions. Using the simulated LGM LIS, sensitivity tests are performed to evaluate the role of CO_2 and insolation on the deglaciation.

1.3 References

Alder, J.R., and S.W. Hostetler. (2014). Global climate simulations at 3000 year intervals for the last 21,000 years with the GENMOM coupled atmosphere-ocean model. C*limates of the past discussion,* **10**(4), 2925-2978.

IPCC, 2013: Summary for Policymakers. In: Climate Change 2013: The Physical Science Basis. Contribution of Working Group I to the Fifth Assessment Report of the Intergovernmental Panel on Climate Change [Stocker, T.F., D. Qin, G.-K. Plattner, M. Tignor, S.K. Allen, J. Boschung, A. Nauels, Y. Xia, V. Bex and P.M. Midgley (eds.)]. Cambridge University Press, Cambridge, United Kingdom and New York, NY, USA

Li, C., and D. S. Battisti (2008), Reduced Atlantic Storminess during Last Glacial Maximum: Evidence from a Coupled Climate Model, *J. Climate*, ***21***(14), 3561–3579, doi:10.1175/2007JCLI2166.1.

Lundqvist, Jan, 1986a, Late Weichselian glaciation and deglaciation in Scandinavia. in V. Sibrava, D. Q. Bowen, and G. M. Richmond, ed., pp. 269-292, Quaternary Glaciations in the Northern Hemisphere. Pergammon Press, New York. 514 pp.

Lunkka, J. P., Johansson, P., Saarnisto, M. And Sallasmaa, O. 2004. Glaciation of Finland. In Ehlers, J., Gibbard, P. (Eds), Extent and Chronology of Glaciations. INQUA Commission on Glaciation. Elsevier, p. 93 – 100.

Manabe, S., and A. J. Broccoli (1985), The influence of continental ice sheets on the climate of an ice age, *J. Geophys. Res.*, 90, 2167-2190, doi:10.1029/JD090iD01p02167.
Marshall, S.J., and G.K.C. Clarke (1999), Modeling North American freshwater runoff through the last glacial cycle, *Quaternary Research,* **52**, 300–315.

Rinterknecht, V., Clark, P. U., Raisbeck, G. M., Yiou, F., Bitinas, A., Brook, E. J., Marks, L., Zelcs, V., Lunkka, J. P., Pavlovskaya, I. E., Piotrowski, J. A., Raukas, A. 2006. The Last Deglaciation of the Southeastern Sector of the Scandinavian Ice Sheet. Science. **311**, 5766, p. 1449-1452.

Roe, G.H. and R.S. Lindzen. 2001a. The mutual interaction between continental-scale ice sheets and atmospheric stationary waves. *J. Climate*, **14**(7), 1450–1465.

Rutt, I. C., Hagdorn, M., Hulton, N. R. J., and Payne, A. J. 2009. The glimmer community ice sheet model. Journal of Geophysical Research, 114(F2).

Chapter 2

A high-resolution ^{10}Be chronology for the final deglaciation of the Scandinavian Ice Sheet and implications for Holocene sea-level rise

Josh Cuzzone[1], Peter U. Clark[1], Anders E. Carlson[1], David Ullman[1], Feng He[2], Vincent R. Rinterknecht[3], Juha Pekka Lunkka[4], Barbara Wohlfarth[5], Shaun A. Marcott[6], Marc Caffee[7]

[1] College of Earth, Ocean, and Atmospheric Science, Oregon State University, Corvallis, OR 97331, USA

[2] Center for Climatic Research and Department of Atmospheric and Oceanic Sciences, University of Wisconsin, Madison, WI 53706, USA

[3] School of Geography and Geosciences, University of Saint Andrews, St. Andrews, United Kingdom

[4] Department of Geosciences, University of Oulu, Oulu, Finland

[5] Department of Geologic Sciences, University of Stockholm, Stockholm, Sweden

[6] Department of Geosciences, University of Wisconsin, Madison, WI 53706, USA

[7] Department of Physics and Astronomy, Purdue University, West Lafayette, IN 47907

Submitted to the Science

2.1 Absract

The last deglaciation of the Scandinavian Ice Sheet (SIS) from ~21,000 to 13,000 years ago is well dated by several hundred ^{10}Be and ^{14}C ages (Rinterknecht et al., 2006, Heine et. al., 2009, Johnsen et. al., 2009, Larsen et. al., 2012, Anjar et. al., 2014), constraining the response of the SIS to climate change and its contribution to global sea-level rise. The subsequent retreat history after ~13,000 years ago is established primarily from Baltic-Sea varve records, but there are large uncertainties in this chronology due to missing varves (Wohlfarth et al., 1995), and the varve record only extends to ~62.5 °N in the Baltic Sea, leaving a substantial fraction of final SIS retreat history largely unconstrained. Here we develop a high-resolution chronology for the final deglaciation of the SIS based on 87 ^{10}Be cosmogenic exposure dates sampled along three transects spanning southern to northern Sweden and Finland. Combining this new chronology with 221 existing ^{10}Be ages on deglaciation since the Last Glacial Maximum shows most rapid rates of ice-margin retreat around the times of the onset of the Bølling-Allerød warm period and of the Holocene, identifying a strong response of SIS mass balance to variations in the Atlantic meridional overturning circulation and associated climate change. Ice-volume estimates constrained by our new chronology suggest that the SIS contributed ~9 m sea-level equivalent to global sea-level rise between 14.5 ka and final deglaciation 10 ka, with highest rates of rise occurring during the Bølling-Allerød and a threefold decrease during the Younger Dryas. When combined with the estimated contribution from the Laurentide and Greenland ice sheets, our results suggest that the Antarctic Ice Sheet contributed ~20 m of global sea-level rise between 13 ka and 3 ka, when present sea level was reached.

2.2 Methods

We sampled glacial erratics for ^{10}Be dating at 16 sites along three transects across Sweden and Finland, with each transect beginning near the inferred Younger Dryas ice margin and converging to where flow lines indicate final deglaciation of the Scandinavian Ice Sheet (SIS) in northwestern Sweden (Boulton et. al., 2001) (Figure 1). We only sampled boulders above the highest shoreline of the Baltic Ice Lake, which inundated large areas surrounding the present Gulf of Bothnia during ice retreat. Individual surface exposure ages were calculated using the western Norway production rate (Goehring et. al., 2012). We corrected ages for the effect of glacio-isostatic uplift on production rate through time. Chauvenet's criterion was used to remove outliers, with the final ages reported for each site representing either the arithmetic mean or error-weighted mean of the sample population, and corresponding uncertainties are reported as the standard error or error-weighted uncertainty, respectively (see Appendix A for description of choice).

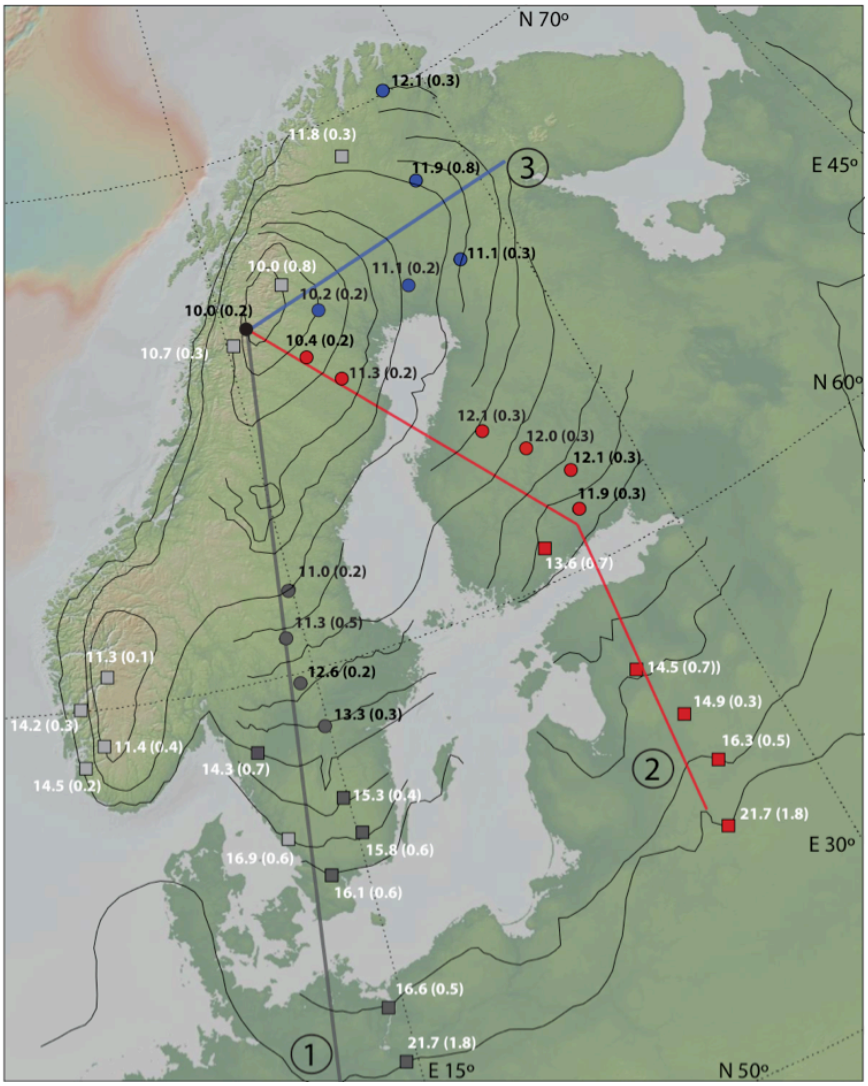

Figure 2.1. Retreat history for the Scandinavian Ice Sheet beginning at the LGM. Contours indicate mapped ice retreat lines (Lundqvist et. al., 2004; Lunkka et al., 2004). Ages are expressed either as the straight mean and standard error, or the error weighted mean age and error weighted external uncertainty (see Appendix A for explanation of choice). Colored lines indicate transects drawn for use in the time-distance transect diagram, with the colored circles and squares indicating the ages used for each transect (1: Sweden – Dark Grey, 2: Finland - Red, 3: Northern Finland - Blue (see figure 2). Circles indicate ages derived from the current study, and squares indicate prior chronology (Tschudi et. al., 2000; Rinterknecht et. al. 2004; Rinterknecht et. al., 2005; Rinterknecht et. al., 2006; Rinterknecht et. al., 2007; Linge et. al., 2007; Rinterknecht et. al., 2008; Heine et. al., 2009; Johnsen et. al., 2009; Stroeven et. al., 2011; Larsen et. al., 2012Mangerud et. al., 2013; Briner et al., 2014; Anjar et. al., 2014). Light grey squares indicate ages not used in the time-distance

Our three transects are perpendicular to inferred isochrones of ice retreat established from regional ice-flow indicators or moraines (Lundqvist, 1986, Boulton et al., 2001, Lunkka et. al., 2004), with an approximate spacing of 100 km between each sampled site. For transects 1 and 2, we include 190 previously published ^{10}Be ages that extend coverage along each transect to the southern SIS position at the LGM (Figure 1) (Table S3). All of these ages were recalculated using the western Norway production rate (Goehring et. al., 2012), thus producing a standardized data set encompassing the entire deglaciation of the SIS from its southern LGM limit to its final site of deglaciation in northwestern Sweden. We use the isochrones to extrapolate the age of those sites that are not directly on the transect to the transect, and then use all of the ages to establish average retreat rates of the SIS margin along each transect.

2.3 Results

Recalculated ages suggest that retreat from the southern SIS LGM margin began 21.7 ± 2 ka. Our new ages indicate that final deglaciation of the SIS occurred in northwestern Sweden at 10 ± 0.2 ka, which is in good agreement with ^{10}Be ages from the same isochrone 100 km to the northeast (10.0 ± 0.8 (Linge et. Al., 2006) (Figure 1). Throughout this deglacial period, variations in ice-margin retreat rates along each transect are similar, indicating coherent ice-sheet-wide responses to climate forcing. Figure 2 compares this retreat history to 65ºN summer insolation and a reconstruction of 30-90°N temperature (Shakun et. al., 2012, Marcott et. al., 2013) in order to evaluate the relation between ice-margin retreat and deglacial climate change (Figure 2).

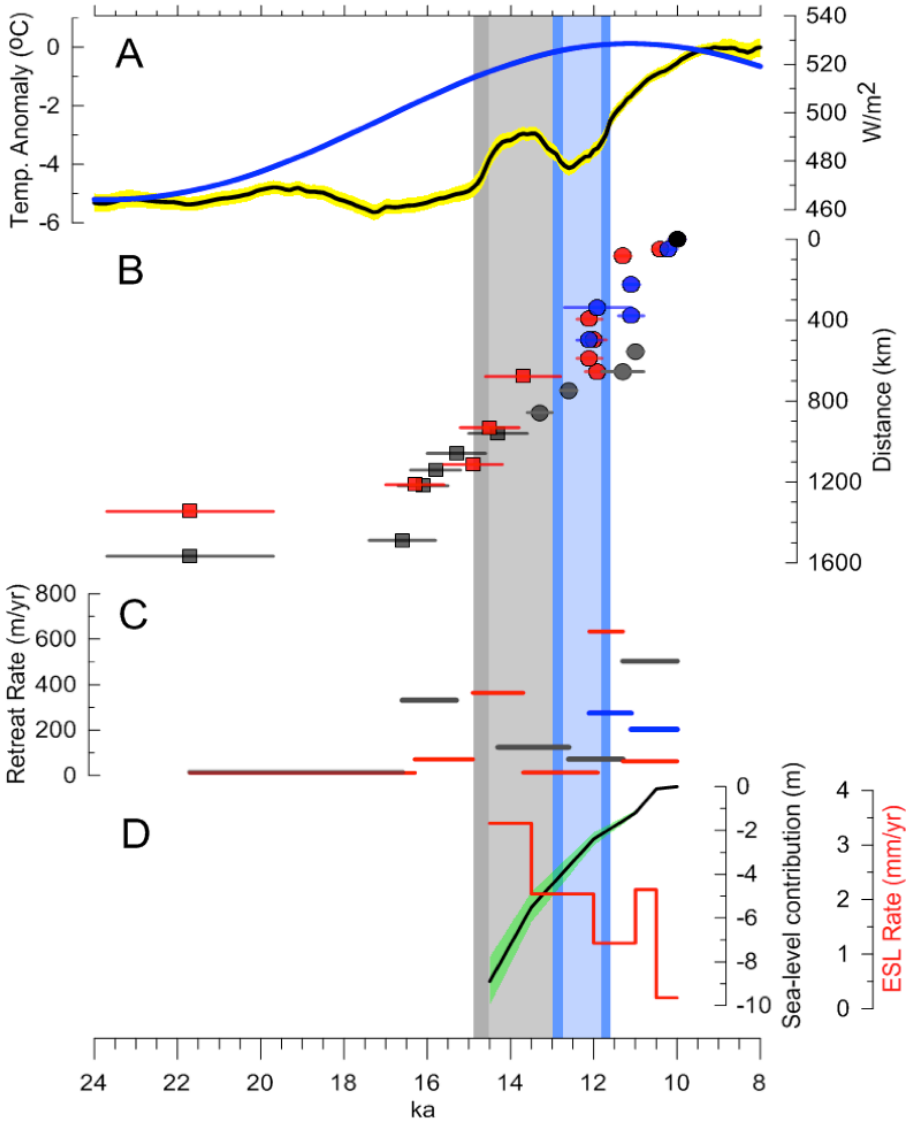

Figure 2.2. Time-Distance diagram showing retreat along transects (see Figure 1), decreasing towards the termination point in Northwest Sweden are shown in panel B. Ages are shown as the straight mean and standard error, or the error-weighted mean age and error-weighted external uncertainty (see Supporting Online Material for explanation of choice). Temperature anomaly and 1-sigma uncertainty is shown for 90 - 30°N (Shakun et. al., 2012; Marcott et. al., 2013) in panel A. Retreat rates along the transects are shown in Panel C. The sea level contribution from the SIS (see Supporting Online Material for calculation), and the corresponding rate of sea-level contribution is shown in Panel D. The grey rectangle corresponds to the Bølling-Allerød warm interval, with the dark grey rectangle indicating the 2-sigma uncertainty of onset. The blue rectangle corresponds to the Younger Dryas cold interval, with the dark blue rectangles indicating the 2-sigman uncertainty for onset and termination (Rasmussen et. al., 2006).

Based on the chronology derived from the recalculated ^{10}Be ages, the southern SIS margin retreated slowly from its LGM position (~21 ka) to the first major recessional moraine across the Baltic plain (Pomeranian moraine) (~16.5 ka). Insofar as there was little change in regional temperature during this period, this retreat was likely in response to the corresponding increase in high-latitude summer insolation and associated feedbacks (Carlson and Winsor, 2012; He et al., Nature, 2013) (Figure 2). A significant increase in retreat rates along transect 1 then occurred between 16.6 ± 0.8 ka and 16.1 ± 0.6 ka, ~2,000 yr before the onset of the Bølling-Allerød warm period, which has been attributed to a dynamical control on this sector of the SIS associated with drawdown by the Norwegian Channel ice stream (Larsen et. al., 2012). In contrast, retreat rates along transect 2 do not increase significantly until the abrupt warming at the onset of the Bølling-Allerød period (Figure 2), indicating that retreat of this sector of the SIS was largely influenced by a temperature control on the surface mass balance. Retreat rates along both transects then remain relatively high during the Bølling-Allerød.

Our new chronology for sites along transect 1 extends the SIS retreat history from southern Sweden to the site of final deglaciation in the northwestern Swedish highlands (Figure 1). Deglaciation from our first sampled site (Swe-1) occurred at 13.3 ± 0.3 ka, which agrees with radiocarbon ages suggesting deposition of the nearby Levene moraine >13.2 cal ka BP (Lundqvist et. al., 2001). This and the age from the next site along this transect suggest continued high rates of ice-margin retreat during the Bølling-Allerød, whereas the age from Swe-3 suggests a reduced rate during the Younger Dryas (Figure 2). Our remaining ages on this transect suggest that ice-margin retreat then accelerated

during the early Holocene. We note that the Swe-5 age (11.3 ± 0.2 ka) on transect 2 occurs on a well-defined isochrone (Lundqvist et. al., 1986, Boulton et. al., 2001) that intersects transect 1 to the southwest (Figure 1). Inclusion of this age on transect 1 suggests an even greater acceleration after the start of the Holocene, with near-instantaneous retreat over ~500 km at ~11.3 ka, followed by slow retreat associated with the final phase of SIS deglaciation over the Swedish highlands. This response to the abrupt onset of Holocene warming likely reflects a rapid rise of the equilibrium line altitude (ELA), with an initial episode of rapid ice loss through high ablation rates below the ELA followed by diminishing rates of loss as the ice-margin retreated to higher elevations, decreasing the ablation area.

On transect 2, the recalculated age of the Salpausselkä I moraine (SSI) in southeastern Finland (13.6 ± 0.7 ka) and our new age from the Salpausselkä II moraine (SSII) (11.9 ± 0.1 ka), less than 50 km up ice from the SSI moraine, suggest a reduced retreat rate during the Younger Dryas (Figure 2). Retreat from the SSII moraine coincides with the drainage of the Baltic Ice Lake, which is dated to 11.6 ± 0.1 cal ka (Saarnisto et. al., 2001) and thus in good agreement with our new age. This age, combined with the next three ages on this transect, are all within uncertainty of each other, indicating a rapid, near-instantaneous retreat of the southeastern Finnish sector of the SIS, similar to the episode of rapid retreat of the southwestern Swedish sector documented by our ages along transect 1. Within uncertainties, however, this episode of rapid retreat across southern Finland corresponds to the abrupt warming that marks the start of the Holocene whereas the retreat across southern Sweden occurred a few hundred years later (Figure 2). Insofar as both retreat episodes are likely in response to the abrupt warming, the

earlier retreat of the Finnish margin may reflect an additional dynamical contribution of mass loss from calving in the proglacial lake that was in contact with much of this margin during retreat (Andrén et. al., 2011). The remaining ages on transect 2 then suggest that retreat from the Swedish coast (11.3 ± 0.3 ka) proceeded at a relatively slow rate until final deglaciation 10 ± 0.2 ka, consistent with our chronology for transect 1.

Transect 3 begins at a site within a moraine complex inferred to be Younger Dryas in age (Sollid et. al., 1973, Lunkka et. al., 2004), which is confirmed by our age from this site (12.1 ± 0.4 ka). Our age from site Fin-6 (11.9 ± 0.8 ka) is in good agreement with a ^{10}Be age of 11.8 ± 0.3 ka (Stroeven et al., 20011) that occurs near the same isochrone (Figure 1). The remaining ages along this transect then suggest a similar retreat history as for transect 2, with higher rates at the end of the Younger Dryas and lower rates during the earliest Holocene (Figure 2).

We assess the contribution of the SIS to global mean sea-level rise for six times between 14.5 ka and final deglaciation ~10 ka when there are sufficient constraints on isochrones ages to establish ice-sheet areas (Boulton et al., 2001). We convert ice area to ice volume using a well-established relationship for an ice sheet on a hard bed, thus providing a maximum estimate (see Supplementary Information). We estimate that between 14.5 ka and 10.0 ka, the SIS contributed 8.9±1.1 m to global mean sea level, which is 1-3 m more than estimated in the ICE-5G model (Peltier, 2004) (Fig. S4). Highest rates of associated sea-level rise occurred during the Bølling-Allerød and lowest rates during the Younger Dryas (Figure 2D), consistent with our retreat history.

Figure 3 combines the SIS sea-level contribution for the last 13 kyr with the contribution from the Laurentide Ice Sheet (LIS) (Carlson and Clark, 2012), which is

derived in the same way and thus also represents a maximum amount, and from the Greenland Ice Sheet (Lecavalier et al., 2014). We subtract this combined Northern Hemisphere ice-sheet contribution from global mean sea level (Lambeck et. al., In Press) (see Supplement) to derive a residual sea-level contribution of 19.5 m from the Antarctic Ice Sheet (AIS), which is the only other possible source at this time. Our results are similar to the estimate of 17.3 m in the ICE-5G model (Peltier, 2004), although the greatest rates of rise in our reconstruction occur earlier (11.5 ka to 7.5 ka versus 9 ka to 6 ka). A large AIS contribution to Holocene sea-level rise is consistent with evidence of episodic mass loss suggested from iceberg-rafted debris, particularly during the mid-early Holocene (Weber et. al., 2014), and from ^{10}Be ages from West and East Antarctica that suggest widespread ice-sheet surface lowering of at least 100-400 m (Figure 3).

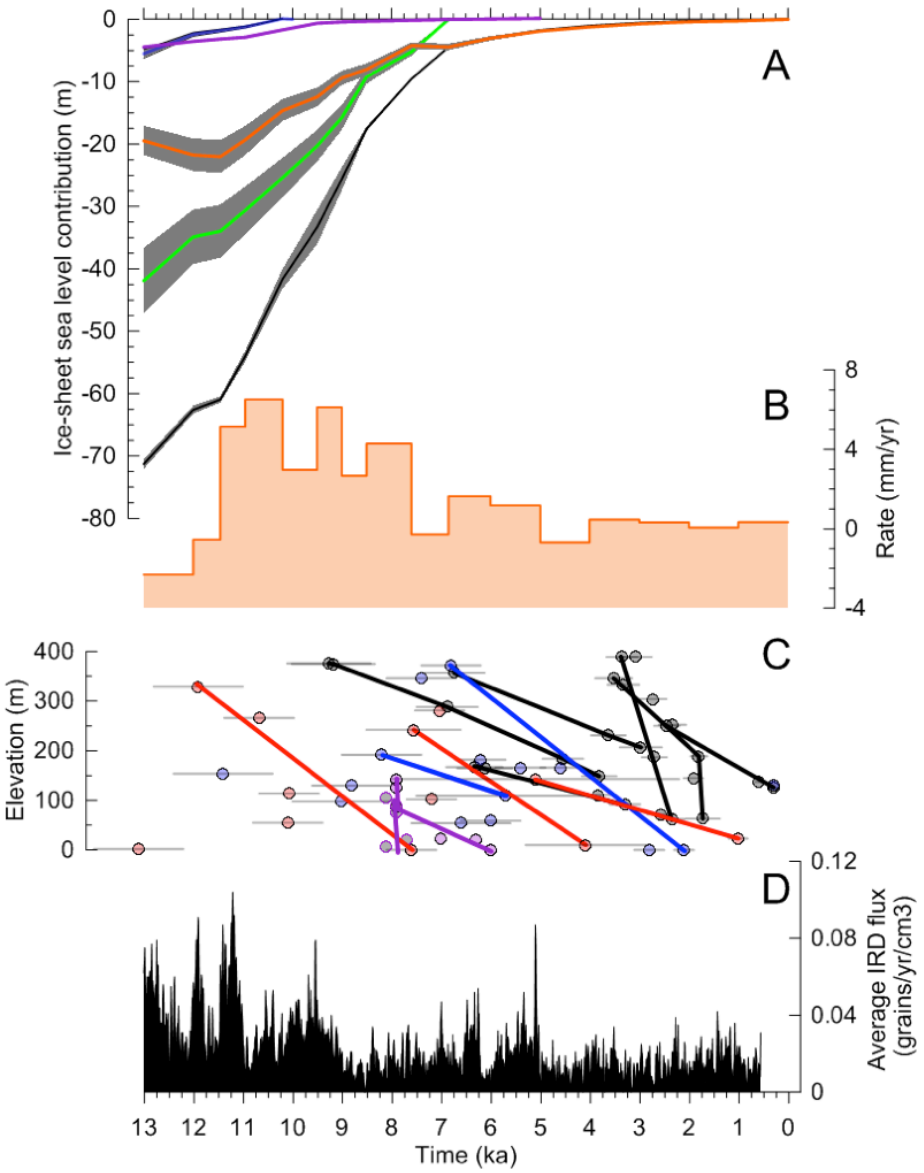

Figure 2.3. Calculated sea-level contribution from the SIS (Blue) (current study), LIS (Green) (Carslon et al., 2008; Ullman et. al., In Prep), and Greenland (Magenta) (Lecavalier et. al., 2014) is shown in panel A. The residual is calculated as the difference between the LIS+SIS from the modeled eustatic sea level component (Black) (Lambeck et. al., In Press). Show in Panel B is the ESL rate in mm/yr for the residual from Panel A. In Panel C are cosmogenic surface exposure ages using ^{10}Be as a function of elevation in Antarctica (Stone et. al., 2003 (Black circles); Mackintosh et. al., 2007 (Red circles); Bentley et al., 2010 (Blue circles), Johnson et. al., 2014 (Magenta circles). Error shown is the 1-sigma uncertainty. Lines show the corresponding trend for sample populations, and indicate thinning of Antarctica through the late Pleistocene and early Holocene. Panel D represents the Antarctic IRD flux from Weber et. al., 2014.

2.4 Conclusions

Estimates of the amount of excess ice in the AIS during the last glaciation differ by >15 m global mean sea-level equivalent (Lambeck et. al., In Press), with implications for understanding the role of the AIS in deglacial climate change (Weaver et al., 2003, Liu et al., 2009) as well as for constraining its present-day mass loss from the Gravity Recovery and Climate Experiment (GRACE) satellite by accounting for ongoing glacio-isostatic adjustment. Our results support those reconstructions (Peltier, 2004; Lambeck et. al., In Press) that indicate that significantly greater excess ice was present than has been used in models to correct GRACE measurements (Whitehouse et al., 2012), suggesting that corresponding estimates of present-day mass loss (Shepherd et al., 2012) should be revised downwards.

2.6 References

Andrén, T., Björck, S., Andrén, E., Conley, D., Lambeck, K., Zillén, L., Anjar, J., 2011. The development of the Baltic Sea basin during the last 130 ka. In: Harff, J.,Björck, S., Hoth, P. (Eds.), The Baltic Sea Basin as a Natural Laboratory. Springer-Verlag, Berlin, Heidelberg, pp. 75-97

Anjar, J., Laresen, N. K., Hakansson, L., Moller, P., Linge, H., Fabel, D., Xu, S. 2014. A 10 Be-based reconstruction of the last deglaciation in southern Sweden. *Boreas*. **43,** 132–148.

Bard, E., Hameline, B., Arnold, M., Montaggiono, L., Cabioch, G., Faure, G., Rougerie, F. 1996. Deglacial sea-level record from Tahiti corals and the timining of global meltwater discharge. Nature. **382**, 241-244.

Bentley, M.J., Fogwill, J., Le Brocq, A.M., Hubbard, A.L., Sugden, D.E., Dunai, T.J., Freeman, S.P.H.T. 2010. Deglacial history of the West Antarctic Ice Sheet in the Weddell Sea embayment: Constraints on past ice volume change. *Geology*. **38**, pp 411-414. Doi:10.1130/G30754.1

Boulton, G.S., Dongelmans, P., Punkari, M., Broadgate, M., 2001.

Paleoglaciology of an ice sheet through a glacial cycle: the European ice sheet through the Weichselian. Quaternary Science Reviews **20**, 591–625.

Briner, J.P., Svendsen, J.I., Mangerud, J., Lohne, Ø.S., Young, N.E. (2014). A ^{10}Be chronology of the southwestern Scandinavian Ice Sheet history during the Late Glacial period. Journal of Quaternary Science, v. **29,** p. 370-380.

Bromley, G.R.M., Putnam, A.E., Rademaker, K.M., Lowell, T.V., Schaefer, J.M., Hall, B., Winckler, G., Birkel, S.D., Borns, H.W. 2014. Younger Dryas deglaciation of Scotland driven by warming summers. *PNAS*. **117**(11):6215-9 DOI: 10.1073/pnas.1321122111.

Carlson, A., Legrande, A. N., Oppo, D., Came, R.E., Schmidt, G. A., Anslow, F.S., Licciardi, J.M., Obbink, E.A. 2008. Rapid early Holocene deglaciation of the Laurentide ice sheet. Nature Geoscience. **1**, 620-624.

Carlson, A.E., and Clark, P.U. 2012, Ice-sheet sources of sea-level rise and freshwater discharge during the last deglaciation: Reviews of Geophysics, v. **50**, doi: 10.1029/ 2011RG000371.

Cato, I. 1987: On the definitive connection of the Swedish Time Scale with the present. Sverige Geologiska Undersokning Ca. **68**, 1-55.

Clark, P.U., Mix, A.C. 2002. Ice sheets and sea level of the Last Glacial Maximum. Quaternary Science Reviews. **21**, 1-7.

Donner, J. 1995. The Qauternary History of Finland. (World and regional Geology 7). Cambridge, Cambridge University Press, 200pp.

Dyke, A.S., 2004. An outline of North American Deglaciation with emphasis on central and northern Canada. In: Ehlers, J., Gibbard, P.L. (Eds.), Quaternary Glaciations: Extent and Chronology. Elsevier, Amsterdam, pp. 373–424.

Fairbanks, R. 1989. A 17,000-year glacio-eustatic sea level record: influence of glacial melting rates on the Younger Dryas event and deep-ocean circulation. Nature. **342**, 637-642.

Goehring, B., Strand, O.L., Mangerud, J., Inge Svendsen, J, Gyllencreutz, R., Schaefer, J., Finkel, R. 2012. Late Glacial and Holocene Be-10 production rates for western Norway. Journal of Quaternary Science, v. **27**, pp. 89-96.

Gyllencreutz, R., Mangerud, J., Svendsen, JI., Lohne, O. 2007. DATED-A GIS based reconstruction and dating database of the Eurasian deglaciation. Geologic Survey of Finland, Special Paper **46**, 113-120.

He, F., J. D. Shakun, P. U. Clark, A. E. Carlson, Z. Liu, B. L. Otto-Bliesner, and J. E.

Kutzbach (2013), Northern Hemisphere forcing of Southern Hemisphere climate during the last deglaciation, Nature, **494**(7435), 81-85.

Heine, K., Reuther, A. U., Thieke, H. U., Schulz, R., Schlaak, N. & Kubik, P. W. 2009: Timing of Weichselian ice marginal positions in Brandenburg (northeastern Germany) using cosmogenic in situ 10Be. Zeitschrift für Geomorphologie **53**, 433–454.

Johansson, P. 1995. The deglaciation in the eastern part of the Weichselian ice divide in Finnish Lapland. Geological Survey of Finland Bulletin, **383**, 72pp.

Johnsen, T.F., Alexanderson, H., Fabel, D. and Freeman, S.P.H.T. 2009.
New 10Be cosmogenic ages from the Vimmerby moraine confirm the timing of Scandinavian Ice Sheet deglacia- tion in southern Sweden. Geogr. Ann. **91** A (2): 113-120.

Johnson, J.S., Bentley, M.J., Smith, J.A., Finkel, R.C., Rood, D.H., Gohl, K., Balco, G., Larter, R.D., Schaefer, J.M. 2014. Rapid thinning of Pine Island Glacier in the Early Holocene. *Science*. **343**, 999. Doi:10.1126/science/1247385.

Lambeck, K., Rouby, H., Purcell, A., Sun, Y., Sambridge, M. In press. Sea Level and Global Ice Volumes From the Last Glaicial Maximum to the Holocene. *PNAS*.

Lecavalier, B.S., Milne, G.A., Simpson, M. J.R., Wake, L., Huybrechts, P., Tarasov, L., Kjeldsen, K. K., Funder, S., Long, A. J., Woodroffe, S., Dyke, A.S., Larsen, N. K. 2014. A model of Greenland ice sheet deglaciation constrained by observations of relative sea level and ice extent. *Quaternary Science Reviews,* **102**, 54-84
doi: 10.1016/j.quascirev.2014.07.018

Larsen, N. K., Linge, H., Håkansson, L. & Fabel, D. 2012: Investigating the last deglaciation of the Scandinavian Ice Sheet in south- west Sweden with 10Be exposure dating. Journal of Quaternary Science **27**, 211–220.

Licciardi, J.M., Clark, P.U., Jenson, J.W., and MacAyeal, D.R., 1998,
Deglaciation of a soft-bedded Laurentide Ice Sheet: Quaternary Science Reviews, v. **17**, p. 427-448.

Linge, H., Olsen, L., Brook, E.J., Darter, J.R., Mickelson, D.M., Raisbeck,
G.M. & Yiou, F. 2007. Cosmogenic nuclide surface exposure ages from Nordland, northern Norway: implications for deglaciation in a coast to inland transect. Norwegian Journal of Geology, vol. **87**, pp. 269-280. ISSN 029-196X.

Liu, Z., B. L. Otto-Bliesner, F. He, E. C. Brady, R. Tomas, P. U. Clark, A. E. Carlson, J. Lynch-Stieglitz, W. Curry, E. Brook, D. Erickson, R. Jacob, J. Kutzbach, and J. Cheng (2009): Transient Simulation of Last Deglaciation with a New Mechanism for Bølling-Allerød Warming. Science, **325**, 310-314, doi:10.1126/science.1171041.

Lundqvist, Jan, 1986a, Late Weichselian glaciation and deglaciation in Scandinavia. in V. Sibrava, D. Q. Bowen, and G. M. Richmond, ed., pp. 269-292, Quaternary Glaciations in the Northern Hemisphere. Pergammon Press, New York. 514 pp.

Lundqvist, J. & Wohlfarth, B. A. 2001. Timing and east-west correlation of South Swedish ice marginal lines during the late Weichselian. Quaternary Science Reviews **20** (10), 1127–1148.

Lundqvist, J. 2004. Glacial history of Sweden. In: Ehlers, J., Gibbard, P.I. (eds), Quaternary glaciations: extent and chronology, Part 1: Europe. Developments in Quaternary Science 2. Amsterdam: Elsevier, 271–294.

Lunkka, J. P., Johansson, P., Saarnisto, M. And Sallasmaa, O. 2004. Glaciation of Finland. In Ehlers, J., Gibbard, P. (Eds), Extent and Chronology of Glaciations. INQUA Commission on Glaciation. Elsevier, p. 93 – 100.

Mackintosh, A., White, D., Fink, D., Gore, D.B., Pickard, J., Fanning, P.C. 2007. Exposure ages from mountain dipsticks in Mac. Robertson Land, East Antarctica, indicate little change in ice-sheet thickness since the Last Glacial Maximum. *Geology*. **35**, pp. 551-554. Doi:10.1130/G23503A.1

Mangerud J, Goehring BM, Lohne ØS, et al. 2013. Collapse of marine-based outlet glaciers from the Scandinavian Ice Sheet. Quaternary Science Reviews **67**: 8–16.

Marcott, S.A., Shakun, J.D., Clark, P.U., Mix, A.C. 2013. A Reconstruction of Regional and Global Temperature for the Past 11,300 Years. **339** (6124), 1198-1201. DOI:10.1126/science.1228026.

Peltier, W.R., 2004. Global Glacial Isostasy and the Surface of the Ice-Age Earth: The ICE-5G (VM2) Model and GRACE, Ann. Rev. Earth and Planet. Sci., **32**, 111-149.

Rasmussen, S.O., Andersen, K.K., Svenson, A.M., Steffensen, J.P., Vinther, B.M., Clausen, H.B., Siggard-Andersen, M.L., Johnsen, S.J., Larsen, L.B., Dahl-Jensen, D., Bigler, M., Rothlisberger, R., Fischer, H., Goto-Azuma, K., Hansson, M.E., Ruth, U. 2006. A new Greenland ice core chronology for the last glacial termination. *J. Geophys. Res.*, **111**, D06102, doi:10.1029/2005JD006079.

Rinterknecht, V. R., Bitinas, A., Clark, P. U., Raisbeck, G. M., Yiou, F.,Brook, E. J. 2008. Timing of the last deglaciation in Lithuania. BOREAS. **37**, 3, p. 426-433.

Rinterknecht, V., Pavlovskaya, I. E., Clark, P. U., Raisbeck, G. M., Yiou, F., Brook, E. J. 2007. Timing of the last deglaciation in Belarus. Boreas. **36**, 3, p. 307-313.

Rinterknecht, V., Clark, P. U., Raisbeck, G. M., Yiou, F., Brook, E. J., Tschudi, S., Lunkka, J. P. 2004. Cosmogenic ^{10}Be dating of the Salpausselkä I Moraine in southwestern Finland. Quaternary Science Reviews. **23**, 23-24, p. 2283-2289.

Rinterknecht, V., Marks, L., Piotrowski, J. A., Raisbeck, G. M., Yiou, F., Brook, E. J. & Clark, P. U. 2005. Cosmogenic 10Be ages on the Pomeranian Moraine, Poland. Boreas. **34**, 2, p. 186-191.

Rinterknecht, V., Clark, P. U., Raisbeck, G. M., Yiou, F., Bitinas, A., Brook, E. J., Marks, L., Zelcs, V., Lunkka, J. P., Pavlovskaya, I. E., Piotrowski, J. A., Raukas, A. 2006. The Last Deglaciation of the Southeastern Sector of the Scandinavian Ice Sheet. Science. **311**, 5766, p. 1449-1452.

Saarnisto, J., and T. Saarinen. 2001. Deglaciation chronology of the Scandanavian Ice Sheet from the Lake Onega Basin to the Salpausselka End Moraines. Global and Planetary Change. **31**: 387-405.

Shakun, J. D., Clark, P. U., He, F., Marcott, S. A., Mix, A. C., Liu, Z., Otto-Bliesner, B. L, Schmittner, A., and Bard, E. 2012. Global warming preceded by increasing carbon dioxide concentrations during the last deglaciation. Nature,**484**, 49-54.

Shepherd, A., Irvins, E.R., Geruo, A., Barletta, V.R., Bentley, M.J., Bettadpur, S., Briggs, K.H., Bromwich, D.H., Forsberg, R., Galin, N., Horwath, M., Jacobs, S., Joughin, I., King, M.A., Lenaerts, J.T.M., Li, J., Lightenberg, S.R.M., Luckman, A., Luthcke, S.B., McMillan, M., Meister, R., Milne, G., Mouginot, J., Muir, A., Nicolas, J.P., Paden, J., Payne, A.J., Pritchard, H., Rignot, E., Rott, H., Sorensen, L.S., Scambos, T.A., Scheuchl, B., O. Schrama, E.J., Smith, B., Sundal, A.V., van Angelen, J.H., van de Berg, W.J., van den Broeke, M.R., Vaughan, D.G., Velicogna, I., Wahr, J., Whitehouse, P., Wingham, D.J., Yi, D., Young, D., Zwally, H.J. 2012. A Reconciled Estimate of Ice-Sheet Mass Balance. *Science*. **338**, pp. 1183-1189. DOI: *10.1126/science.1228102*

Sollid, J.L., Andersen, S., Hamre, M., Kjeldsen, O., Salvigsen, O., Sturos, S., Tveita, T., Wilhelmsen, A. 1973. Deglaciation of Finmark, North Norway. Norsk Geografisk Tidskrift, **27**, 233-325.

Stone, J.O., Balco, G.A., Sugden, D.E., Caffee, M.W., Sass,L.C., Cowdery, S.G., Siddoway, C. 2003. Holocene deglaciation of Marie Byrd Land, West Antarctica. Science.**299**, 99-102.

Stroeven, A.P., Fabel, D., Harbor, J.M., Fink, D., Caffee, M.W., Dahlgren, T., 2011. Importance of sampling across an assemblage of glacial landforms for interpreting

cosmogenic ages of deglaciation. Quaternary Research **76**, 148-156.

Stromberg, B. 1989: Late Weichselian deglaciation and clay varve chronologyin east central Sweden. Sverige Geologiska Undersokning Ca **73**, 1-70.

Tarasov, L., and Peltier, W. R. 2004. A geophysically constrained large ensemble analysis of the deglacial history of the North American ice sheet complex, Quat. Sci. Rev. vol **23**, 359-388.

Tschudi, S., Ivy-Ochs, S., Schlu ¨ chter, C., Kubik, P.W., Rainio, H. 2000.^{10}Be dating of Younger Dryas Salpausselka ¨I formation in Finland. Boreas **29**, 287–293.

Ullman, D.J., Carlson, A.E., Clark, P.U., Cuzzone, J., Winsor, K., Caffee, M. In Prep. Abrupt collapse of the Labrador Dome of the Laurentide Ice Sheet linked to 8.2 ka event.

Weaver, A.J., Saenko, O.A., Clark, P.U., Mitrovica, J.X. 2003. Meltwater Pulse 1A from Antarctica as a Trigger of the Bølling-Allerød Warm Interval. *Science*. **299**, pp. 1709-1713.

Weber, M.E., Clark, P.U., Kuhn, G., Timmerman, A., Sprenk, D., Gladstone, R., Zhang, X., Lohman, G., Menviel, L., Chikamoto, M.O., Friedrich, T., Ohlwein, C. 2014. Millennial-scale variability in Antarctic ice-sheet discharge during the last deglaciation. Nature. **510**, 134-138. Doi:10.1038/nature13397

Whitehouse, P. L., Bentley, M.J., Milne, G., King, M.A., Thomas, I.D. 2012. A new glacial isostatic adjustment model for Antarctica: calibrated and tested using observations of relative sea-level change and present-day uplift rates. *Geophysical Journal International*. **190**, pp. 1464-1482. doi: 10.1111/j.1365-246X.2012.05557.x

Wohlfarth, B., Björck, S., Possnert, G. & Brunnberg, L. 1995. A comparison between radiocarbon dated Late Weichselian calendar-year chronologies. *Journal of Coastal Research* Special Issue No. 17: Holocene Cycles: Climate, Sea Levels and Sedimentation, pp. 45–48.

Chapter 3

The relative contributions from storm tracks and stationary waves on the winter surface mass balance of the Laurentide Ice Sheet through the last deglaciation

Joshua Cuzzone[1*], Jay Alder[2], Justin Wettstein[1], Steve Hostetler[2], Peter U. Clark[1]

[1]*College of Earth, Ocean, and Atmospheric Sciences, Oregon State University, Corvallis, OR 97331*

[2]*U.S. Geological Survey, Oregon State University, Corvallis, OR 97331*

Submitted to the Climate Dynamics

3.1 Abstract

Prior research using climate models of varying complexity indicates changes in transient activity (storm tracks) and stationary waves between present day and the Last Glacial Maximum (LGM). These differences likely influenced the surface mass balance of the Northern Hemisphere ice sheets through the last deglaciation (21 – 9 ka). We evaluated the LGM and deglacial changes in the wintertime Northern hemisphere storm track and stationary wave patterns over the Laurentide Ice Sheet (LIS) using a fully coupled AOGCM, GENMOM. Changes in the surface mass balance over the LIS were evaluated with respect to the strength and position of the storm tracks and stationary waves, an essential component to the extratropical hydrologic cycle. Our results indicate varying regional sensitivity of the LIS to atmospheric circulation. In the west, an enhanced stationary wave exerts a large influence on the mass balance of the Cordilleran Ice Sheet through enhanced moisture advection. In contrast, storm tracks play a major role in enhancing accumulation along the southern and eastern margin of the LIS with increasing amplitude as the storm tracks become more vigorous and broad later in the deglaciation as the LIS melted. Increased accumulation from the storm tracks may have partially offset summer melt through the deglaciation, allowing the eastern LIS to persist longer than other areas of the ice sheet.

3.2 Introduction

Throughout the last deglaciation (21-9 ka), global climate evolved in response to increasing CO_2 (*Shakun et. al.*, 2012) and insolation (*Alley et al.,* 2002), which drove the demise of the great northern hemisphere ice sheets. Although these forces played a significant role in increasing ice-sheet ablation, they also worked to alter the background

atmospheric circulation with respect to the heat, momentum, and moisture transport. Because the surface mass balance of ice sheets are closely associated with the climate and atmospheric circulation, these changes would certainly play a critical role in either enhancing or dampening the forced response of increasing CO_2 and insolation. Recently, *Boos* (2012) showed that changes in the hydrologic cycle between the Last Glacial Maximum (LGM, 21,000 yr before present) and present day (PD) were closely associated with changes in large-scale atmospheric circulation with transient eddies providing the majority of poleward moisture transport. Relatedly, *Hofer et al*. (2012) found that up to 60% of the LGM-to-preindustrial (PI) precipitation changes over southwestern Europe could be explained by changes in atmospheric circulation, with the remaining difference attributed to reduced evaporation. Both of these results are consistent with variability in Greenland ice-core accumulation rates during the last deglaciation, which *Kapsner et al*. (1995) interpreted as being associated with changes in storm tracks (i.e. dynamic change in the atmospheric circulation) rather than with thermodynamic changes expected from a warming climate.

Although transient eddies dominate the zonal mean flux of heat and moisture in the Northern Hemisphere, stationary waves drive large regional fluxes, especially during winter. Several studies have concentrated on the role of stationary waves in the growth and maintenance of the Laurentide Ice Sheet (LIS), with a particular focus on the topographic forcing of the atmospheric flow by the ice sheet (*Lindmen and Oerlemans,* 1987*; Cook and Held,* 1988*; Shin and Barron,* 1989*; Roe and Lindzen,* 2001*; Liakka and Nilsson,* 2010; Ullman et. al., 2014). *Roe and Lindzen* (2001) explored feedbacks between ice sheet topography and the prominence of stationary waves by simulating the

growth of a single ice sheet on an idealized continent using a stationary wave model coupled to an ice-sheet model. They concluded that the topography of the ice sheet significantly influences the stationary wave pattern, which acts as a feedback onto the ice-sheet mass balance and configuration by affecting heat and moisture fluxes on time scales equivalent to ice sheet growth and decay.

Stationary waves are dynamically linked to the transient eddies that make up the storm tracks, as evidenced both in reanalyses (*Wettstein and Wallace*, 2010) and in idealized general circulation model experiments (*Kaspi and Schneider*, 2013). Stationary waves modulate local baroclinicity and thus the position and development within the storm tracks (*Kaspi and Schneider*, 2013), whereas the release of latent heat within storm tracks can act to enhance the stationary wave pattern (*Hoskins and Karoly*, 1981). Thus, the extratropical heat, moisture, and momentum budgets are a consequence of both transient and stationary waves as well as the dynamics of their interaction.

Modeling studies that have examined changes in storm tracks in the vicinity of the LGM Northern Hemisphere (NH) ice sheets found a reduction in their intensity and a southeastward displacement over the North Atlantic, relative to their modern configuration (*Li and Battisti*, 2008; *Donahoe and Battisti*, 2009; *Laine et al*., 2009). Such changes would likely have influenced the mass balance of both the Fennoscandian and North American ice sheets, as synoptic-scale variability tends to dominate the wintertime mid-latitude flux of moisture, heat, and momentum over the North Atlantic. Accordingly, some studies have proposed that variability in the storm tracks may have played an important role in the buildup and maintenance of the NH ice sheets during the LGM (*Manabe and Broccoli*, 1985; *Dong and Valdes*, 1998; *Kageyama et al*., 1999).

Because these studies did not evaluate changes through the deglaciation, however, investigating the evolving role of stationary wave and storm track contributions to ice sheet surface mass balance (SMB) could not performed.

Changes in solar radiation and topographic forcing from ice sheets occurred in the transition from the LGM through the last deglaciation, which would necessarily lead to changes in the mean state and variability of the atmospheric general circulation. Here, we investigate the relative contributions of the stationary waves and the transient eddies that make up the storm track on the SMB of the LIS from the LGM to 9 ka using a fully-coupled AOGCM, GENMOM (*Alder et al*. 2011; *Alder and Hostetler*, 2014). By examining changes in the stationary and transient components during the last deglaciation, we assess how each component contributed to the SMB of the LIS.

3.3 Methods

We examine output from GENMOM, which is the GENESIS [Global Environmental and Ecological Simulation of Interactive Systems] version 3 atmospheric GCM (*Thompson and Pollard,* 1997*)* coupled to MOM2 [Modular Ocean Model version 2] (*Pacanowski,* 1996*)*. The coupling between the two models and the present-day simulations are described in more detail in *Alder et al*. (2011). The AGCM has 18 vertical (sigma) levels and a spectral T31 resolution, which translates to a nominally 3.75° horizontal resolution. MOM2 also is run on a T31 horizontal grid, but with 20 vertical levels. We use output for 21 ka (LGM), 15 ka, 12 ka, 9 ka, PI, and PD simulations. Detailed information regarding these deglaciation experiments using GENMOM can be found in *Alder et al*. (2014). The simulations include appropriate boundary conditions for insolation (*Berger*, 1978), surface topography, ocean

bathymetery, ice-sheet height and area, and atmospheric greenhouse gases including CO_2 (*Monnin et al*., 2001), CH_4 (*Brook et al*., 2000), and N_2O (*Sowers et al*., 2003) for each time slice. The NH ice sheets are prescribed based on the ICE-4G reconstructions (*Peltier*, 1994) except for the LIS, where the reconstructions from *Licciardi et al*. (1998) (herein the L98 reconstructions) replace ICE4G. The LIS reconstructions of L98 and ICE-4G are similar in spatial extent, but the L98 reconstruction is generally higher than ICE4G, particularly at 12 ka and 9 ka. For comparison with PD storm tracks, we use the 2.5° resolution, 1990-2010 European Centre for Medium-Range Weather Forecasts (ECMWF) 6 hourly Era-Interim Reanalysis (*Simmons et al*., 2007, with updates).

3.4 Results

3.4.1 Surface mass balance in different seasons

The SMB of an ice sheet is controlled primarily by winter accumulation and summer ablation. In colder (or wetter) climates, winter accumulation can exceed summer ablation, causing ice sheet growth. The deglaciation of the NH ice sheets occurred when summer ablation exceeded winter accumulation largely in response to increasing summer insolation and CO_2 (*Alley et al*., 2002; *Shakun et al*., 2012). The changing influence of transient and stationary waves in the atmospheric circulation could have enhanced or diminished the radiatively forced retreat of the ice sheets by altering winter accumulation.

We compute the SMB as the liquid water equivalent of precipitation minus evaporation and runoff (*P-E-R*) (*Pollard and Thompson*, 1997; *Hostetler et al*., 1999) using daily model output. Runoff is simply partitioned between mass lost from the grid cell (70%) and mass assumed to refreeze (30%), (*Marshall and Clarke*, 1999). Figure 1 shows the SMB for winter (DJF) and summer (JJA) through the deglaciation.

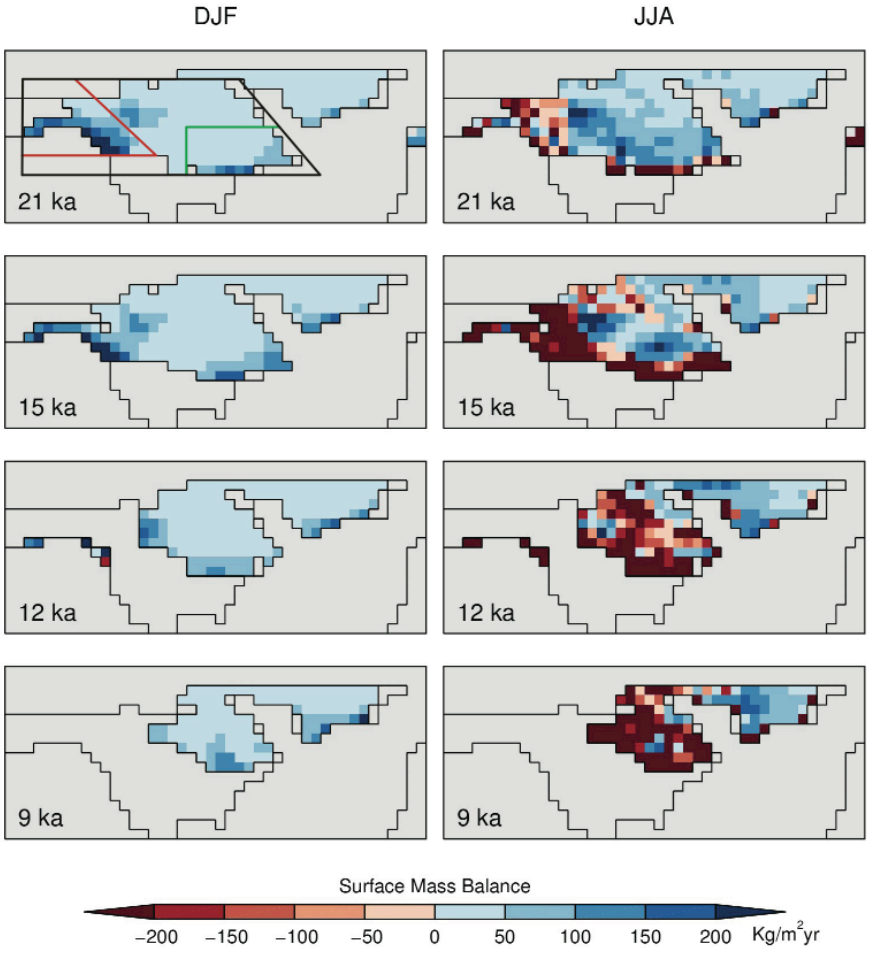

Figure 3.1. DJF and JJA surface mass balance over ice-covered gridcells for GENMOM simulations at 21 ka, 15 ka, 12 ka, and 9 ka. The subdomains of the Cordilleran (red) and southeast Laurentide (green), and Cordilleran + Laurentide (Black) are indicated, and defined in the text

At 21 ka, ablation rates are high during JJA along the southern margin of the LIS and the Cordilleran Ice Sheet (CIS), and this ablation-dominated area expands into the interior of the ice sheet during the deglaciation. On an annual and area-averaged basis, summer ablation dominates the SMB (not shown), which would lead to the loss of the LIS and CIS in a manner generally consistent with the aforementioned ice sheet reconstructions. In contrast, net accumulation occurs over the entire ice sheet in DJF throughout the deglaciation, with the highest accumulation rates over the CIS and the southeastern sector of the LIS. Because these areas exhibit correspondingly high summer ablation, high accumulation rates would have caused less negative net SMB, thus modulating the rate of ice-sheet retreat that would have occurred under less winter accumulation.

We assess the influence of stationary waves and storm tracks on DJF accumulation patterns over the LIS during the last deglaciation. We focus on DJF as winter is the season of peak intensity in stationary waves, transient eddies, and ice sheet accumulation. Winter is also the season with the most pronounced LIS influence on atmospheric circulation. We do not analyze JJA because the storm tracks are weaker and more diffuse in summer due to oceanic and continental heating and associated changes in the temperature structure of the atmosphere. Summertime storms that contributed to accumulation may have occurred along the ice-sheet margin as a result of baroclinic instability associated with mesoscale and convective development (*Bromwich et al.*, 2005) but those contributions were likely small compared with those during winter.

3.4.2 Large-scale circulation

The upper tropospheric (300 hPa) zonal wind and the stationary wave pattern in 500 hPa geopotential height during the LGM and PD are shown in Figure 2 to demonstrate large-scale changes in atmospheric circulation. Like many other LGM simulations [e.g., *Li and Battisti*, 2008; *Laine et al*., 2009; Ullman et. al., 2014], GENMOM simulates a stronger and more zonal jet over the Atlantic as compared with the more southwest-to-northeast oriented PD jet. These changes occur simultaneously with enhanced low-level baroclinicity and reduced transient eddy activity during the LGM (Figure 3), consistent with other climate models and previous studies (*Li and Battisti*, 2008; *Donahoe and Battisti*, 2009). During the LGM, the stationary wave pattern is substantially enhanced relative to the PD, especially over western North America (Figure 2). A stronger stationary wave reflects the topographic forcing of the atmosphere by the CIS and LIS, consistent with *Roe and Lindzen* (2001) and *Liakka and Nilsson* (2010). Lower geopotential heights over northeastern North America and the northern North Atlantic during the LGM, coupled with higher geopotential heights over the southern (subtropical) North Atlantic, are consistent with a strengthened and more zonally-oriented Atlantic jet during the LGM.

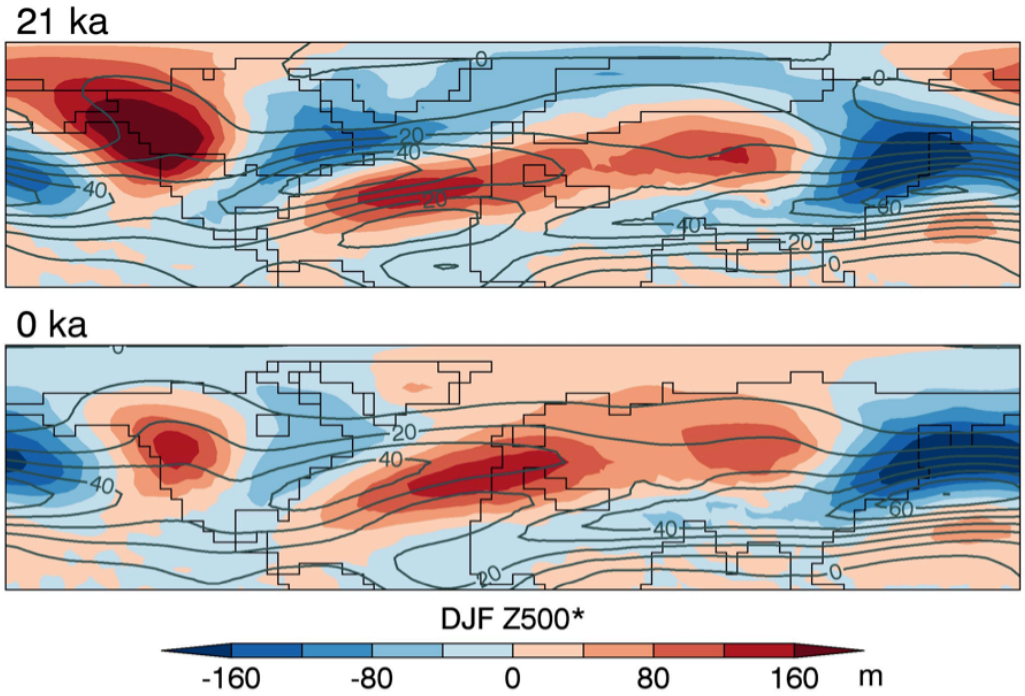

Figure 3.2. A). DJF 300 hPa zonal wind (contours, 10 ms^{-1} interval) for GENMOM LGM (21 ka) and present day (0 ka) simulations. DJF Z_{500}* (color shading, 40 m interval), computed as $Z_{500} - [Z_{500}]$, where [] indicates the zonal mean

3.4.3 Storm tracks

We used the daily fields from GENMOM and Era-Interim to calculate the lower tropospheric eddy heat flux as a proxy for overall storm track activity and as a single storm track indicator with a close link to atmospheric heat and moisture transport. For each time slice, we analyze 50 years of DJF 6-hourly model output. We applied a sixth-order, high-pass Butterworth filter, with a nominal frequency cutoff of 8 days to emphasize synoptic-scale motions. We filter the meridonal wind *(v)* and temperature (*T*) fields separately and then multiply them to derive the 850 hPa eddy heat flux ($v'T'_{850}$,

where primes denote departures from the time mean). The climatological-mean seasonal cycle was removed from the 6-hourly output.

Figure 3 shows the storm tracks for both Era-Interim output and the simulated LGM through PD time slices. The PD GENMOM run displays ~23% weaker transient eddy heat flux than the Era-Interim over the Northern Hemisphere, consistent with other modeling studies (*Kageyama et al*., 1999; *Chang and Guo*, 2012) that found the intensity of the simulated storm track to be proportional to the horizontal resolution of the model and thus attenuated in lower resolution GCMs. Compared to Era-Interim, GENMOM exhibits a somewhat more zonal orientation and the simulated storm track does not extend into the northern North Atlantic. Era-Interim and GENMOM agree well, however, when comparing the overall spatial distribution of storm tracks. A spatial correlation of 0.88 over the North Atlantic basin (20-70°N, 270-360°E) indicates that the overall structure of the storm track is well simulated and this is especially the case in the vicinity of the southeastern LIS.

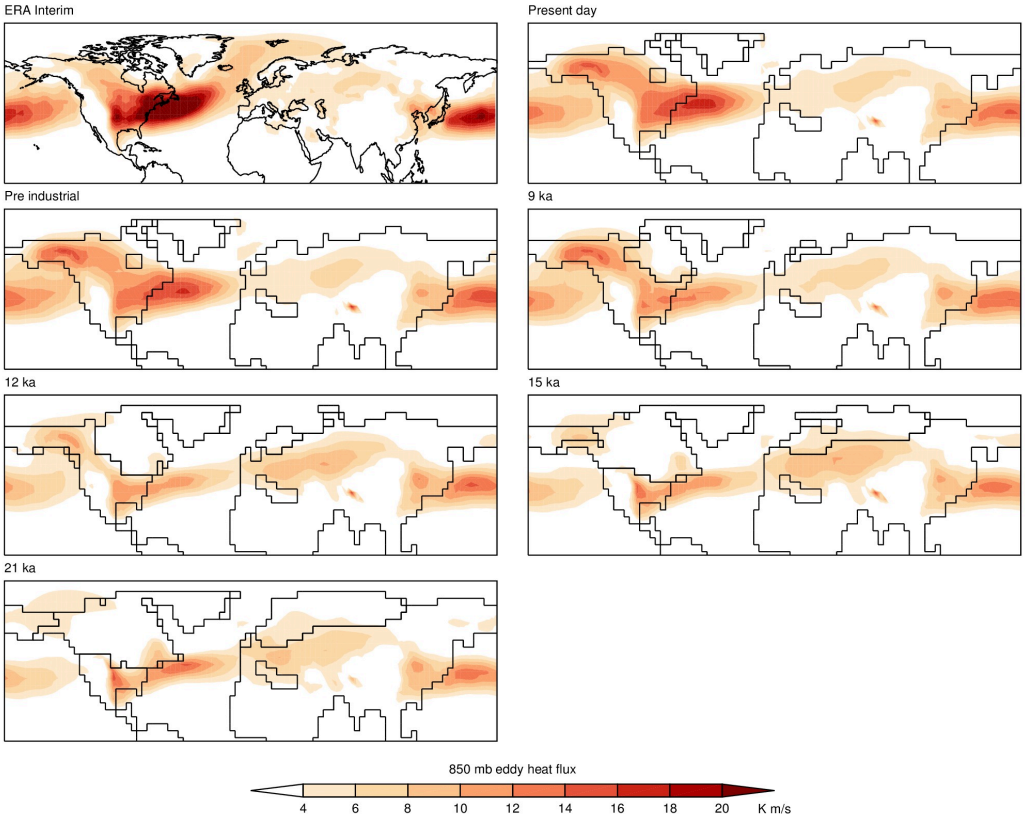

Figure 3.3. DJF eddy heat flux $v'T'$ (Kms^{-1}) at 850 hPa for Era-Interim (1990-2010) and the GENMOM simulations at 21ka, 15ka, 12ka, 9ka, preindustrial, and present day. See text for additional details

Relative to PI, the LGM (21 ka) simulation exhibits a weak storm track that is displaced to the southeast (Figure 3). These changes occur contemporaneously with a stronger, sharper, and more zonally-oriented jet during the LGM (Figure 2). The area-averaged eddy activity during the LGM is weaker than that of the PI by 22% over eastern North America and the North Atlantic (15°-65°N, 90W-0°W), consistent with differences found in a higher resolution version of CCSM3 (*Li and Batisti*, 2008). The topographic forcing of the LIS confines storm activity to the southern LIS margin, resulting in an

eastward extension of the storm track towards the Iberian Peninsula, Mediterranean, and northern Europe (Figure 3).

The overall decrease in LGM storm track activity is somewhat counter-intuitive, considering the LGM was more favorable for baroclinic development in response to a much steeper lower tropospheric temperature gradient from the presence of the ice sheets. The decrease in North Atlantic eddy activity may be related to decreased seeding from the Pacific or increased stability in the upstream jet entrance region (*Donahoe and Battisti*, 2009), the influence of stronger temperature gradients on a more barotropically-driven subtropical jet (*Li and Wettstein*, 2012), or to a combination of these and other factors. Although a number of mechanisms could be explored to explain the reduction in Atlantic storm activity during the LGM, these are beyond the scope of our study. The salient point is that GENMOM exhibits an evolution in the jet, stationary waves, and transient eddy characteristics from the LGM to the modern day that are both broadly consistent with previous results and potentially important for the SMB associated with ice sheet growth and decay.

Compared to the LGM (21 ka), storm activity over the same eastern North America and North Atlantic region (15°-65°N, 90W-0°W) weakens slightly by ~8% at 15 ka (Figure 3). At 12 ka, 9 ka, and PI, storm activity increases progressively as the NH ice sheets recede. In particular, storm activity over the North Atlantic strengthens and shifts upstream toward North America and toward the present-day geographical distribution. The European sector simultaneously experiences a decrease in storm activity over time as the storm track becomes increasingly confined to the upstream North Atlantic (Figure 3).

3.4.4 Composite Analysis

To evaluate relationships between ice sheet SMB and either quasi-stationary waves or the storm tracks, we compute composites according to periods of high and low SMB for either zonal anomalies in the 500-hPa geopotential height (Z_{500}*) or 850-hPa transient eddy heat flux ($v'T'_{850}$), respectively. The climatological-mean seasonal cycle is removed from all of the SMB, transient, and stationary fields. We use a compositing technique as it avoids the assumption of a linear relationship between variables. We confine our analysis to the LIS (42°-80°N, 189°-317°E) and the CIS (46°-72°N, 210°-255°E) (LIS + CIS), the CIS, and the southeastern sector of the LIS (SE LIS) (46°-60°N, 260°-310°E) (See Figure 1 for locations of domains). For the analysis, the Greenland Ice Sheet was masked out. For the CIS, we used the LIS mask from L98 to separate the LIS and CIS along the saddle between the two ice sheets. We define high SMB as those periods when the area-weighted sum of the SMB exceeds the mean plus one-half standard deviation of the SMB over the specified domain. Correspondingly, low SMB is defined as those periods when the SMB falls below the mean minus one-half standard deviation.

We display results as composite differences, which are the difference between the high SMB composites and the low SMB composites. During DJF, between 26-29% of samples satisfy the criteria for both high and low composites, and samples are distributed relatively evenly between the two composites. These numbers are roughly what would be expected based on a normally distributed variable and indicate our composites are not dominated by either the high or low state. Individual high and low states were evaluated for physical consistency with the displayed composite differences.

3.4.5 Relationship between stationary waves, storm tracks, and ice sheet surface mass balance

Stationary waves

LIS + CIS

The left column of Figure 4 shows the corresponding stationary wave pattern given the SMB composite difference. At 21 ka, a quadrapole structure is found over North America, with ridging and higher heights over the CIS and the eastern LIS, and associated troughs over Alaska, the southern Great Plains, and downstream over the Atlantic. This pattern is essentially repeated at 15 ka. At 12 ka, there are only a few grid cells of ice remaining over the CIS and the robustness of this association diminishes. The entire Z_{500}* pattern changes at 9 ka, as geopotential height anomalies shift eastward near the remnant ice over the southeast LIS.

CIS

The association between the stationary waves (middle column, Figure 4) and the CIS SMB is positive, however, obvious association between SMB and ridging is evident over the CIS with lower heights over Alaska. This positive signal is confined to the CIS, indicating the tight coupling between the stationary wave and the surface mass balance in this region. This pattern is repeated at 15 ka and 12 ka, when only a few ice covered grid cells remain in the CIS. Accordingly, the gradient of the *Z_{500}* pattern is closely associated with* the ice-sheet topography, which is strongest at 21 ka and progressively decreases in the 15 ka and 12 ka time slice experiments.

Southeastern LIS (SE LIS)

Higher geopotential heights over Baffin Bay and lower heights over northwestern Canada (i.e. mostly an east-west dipole) are associated with increased SMB over the SE LIS at 21 ka (Figure 4). The east-west dipole relationship intensifies at 15 ka and 12 ka. The overall gradient rotates approximately 30 degrees clockwise between 21 ka and 15 ka and approximately 30 to 45 degrees clockwise between 12 ka and 9 ka. Even though the SMB-Z_{500}* relationship can generally be characterized by this east-west dipole over North America, there are substantial differences in the placement of the highs and lows and the associated pressure gradient in each time slice. The association between SMB over the SE LIS and stationary waves may reflect their role in the SMB of the southeastern sector of the LIS following the retreat and absence of the CIS, or it may simply reflect physically-consistent wave-wave interactions associated with a SMB-storm track relationship over the SE LIS. We will return to an exploration of the prior two topics.

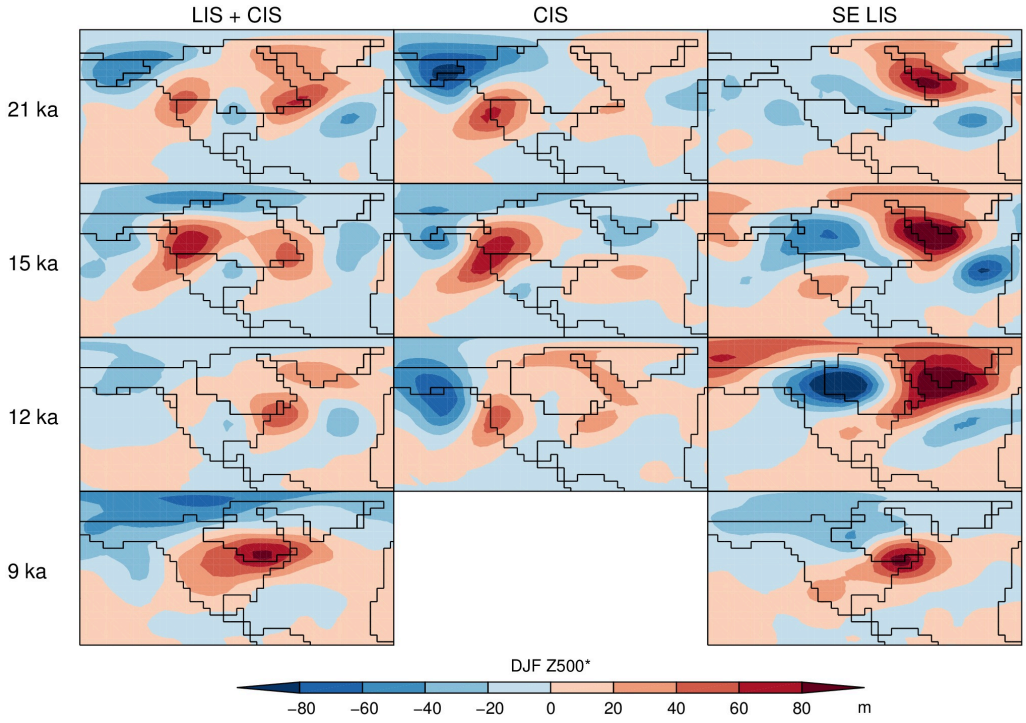

Figure 3.4. Composite differences of DJF Z500* computed as the difference between time samples exhibiting high and low surface mass balance. Each column represents the area over which the composites were computed

Storm tracks

LIS + CIS

When the eddy activity composite differences are conditioned on SMB over the combined LIS and CIS, increased SMB is associated with increased eddy activity at 21 ka especially over eastern North America and particularly over the southeastern sector of the LIS (Figure 5 – top left). The area of high eddy activity remains over the southeastern LIS during 15 ka and 12 ka, becoming broader later in the deglaciation. At 9ka, when the LIS has retreated to the Labrador and Keewatin regions, the SMB-storm track relationship broadens and extends further northward, following an expansion of the storm track during 9 ka (Figure 3). During these intervals, eddy activity weakens over the CIS, indicating limited influence of the storm track on the SMB of the CIS during winter.

CIS

Defining the SMB composites over the CIS yield difference patterns that are both difficult to physically interpret and largely insignificant (Figure 5 – middle column), suggesting that the role of the Pacific storm track was not an important influence on the SMB of the CIS, except perhaps marginally in the 12 ka simulation.

Southeastern LIS

Over the SE LIS, the association between SMB and eddy activity occurs in each of the four time slice experiments, but the association is weakest at 21 ka and strongest at 9 ka (Figure 4 – right column). The association broadens spatially at 12 ka, consistent with a broadening of the storm track later in the deglaciation (Figure 3). At 9ka, the association of SMB with high eddy activity remains focused over the SE LIS, but extends further west into North America and intensifies overall.

These results clearly show the strong influence of the storm track on the SMB of the SE LIS. The spatial correlations of the eddy heat flux index [total eddy heat flux over the southeastern LIS box] and SMB increase from 0.4 at 21 ka to 0.54 at 9 ka, both of which are significant using a student's t-test. The monotonic increase in the correlations

through the time slices indicates the emerging prominence of the storm track in providing enhanced moisture delivery to the SE LIS through the deglaciation.

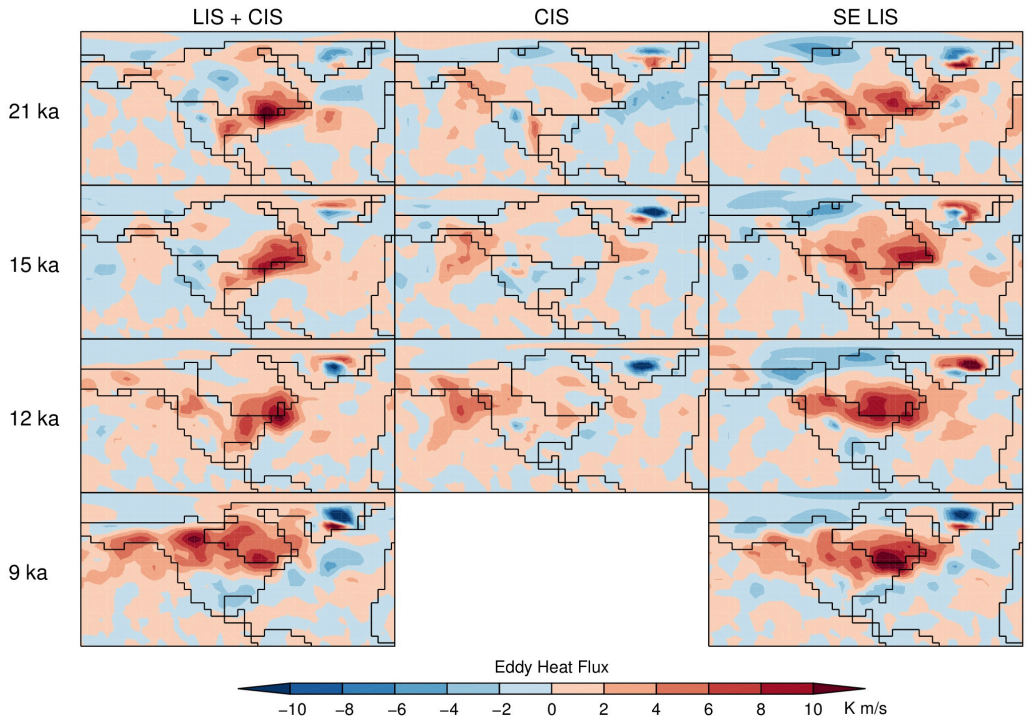

Figure 3.5. Composite differences in DJF 850 hPa eddy heat flux ($v'T'_{850}$) computed as the difference between time samples exhibiting high and low surface mass balance. High and low surface mass balance composites were calculated over the domains indicated for each column

3.4.6 Moisture Flux Convergence

The composites highlight the strong relationship between the storm track and the SMB over the SE LIS. The stationary wave pattern also shares a relationship with the SMB, albeit weaker, over the southeastern LIS. To further examine the influence of each component of the atmospheric flow on the SMB, we evaluate the low-level (850 hPa) moisture flux convergence associated with the time series indices of eddy heat flux ($v'T'_{850}$) and stationary wave (Z_{500}*) strength over the SE LIS (Figures 6 and 7, respectively). We restrict this analysis to the SE LIS where we have shown that the storm track exhibits a strong influence throughout the deglaciation.

In the PD climate, transient eddies are responsible for a majority of the moisture flux in the extratropical hydrologic cycle (*Peixoto and Oort,* 1992). To evaluate deglacial changes in moisture flux, we calculated the 850-hPa horizontal moisture flux convergence (MFC) as:

$$(1) \qquad -\nabla \bullet (qV_h) = -u\frac{\partial q}{\partial x} - v\frac{\partial q}{\partial y} - q\left(\frac{\partial u}{\partial x} + \frac{\partial v}{\partial y}\right)$$

where ∇ is the gradient operator (multiplied by -1 to calculate convergence rather than divergence), V is the horizontal wind vector that can be decomposed into its zonal (u) and meridional (v) components, and q is the specific humidity. This equation describes both the advection of specific humidity by the mean flow and the convergence of specific humidity gradients. For the MFC composites, an index was constructed for each time slice (21 ka, 15 ka, 12 ka, 9 ka) to identify periods when the eddy heat flux over the southeastern LIS (see Figure 1**)** exceeded the mean plus one-half standard deviation (i.e. high storm activity) and when the eddy heat flux fell below the mean minus one-half standard deviation (i.e. low storm activity).

Transient eddy contribution

Composite differences in MFC conditioned on eddy heat flux are shown in Figure 6. A band of convergence near and over the southeastern margin of the LIS is consistently associated with enhanced eddy heat flux during each time slice experiment (Fig. 6). Bands of negative MFC (divergence) equatorward of the SE LIS margin may

indicate moisture source regions. At 9 ka, as the ice sheet retreats to the Labrador and Keewatin regions, MFC dominates over the eastern Labrador sector. The spatial structure of the 850 hPa MFC suggests a consistent anticyclonic flow of the Bermuda High off the east coast of North America associated with the coherence between the eddy heat flux over the SE LIS, the North Atlantic storm track, and larger-scale features of the atmospheric circulation.

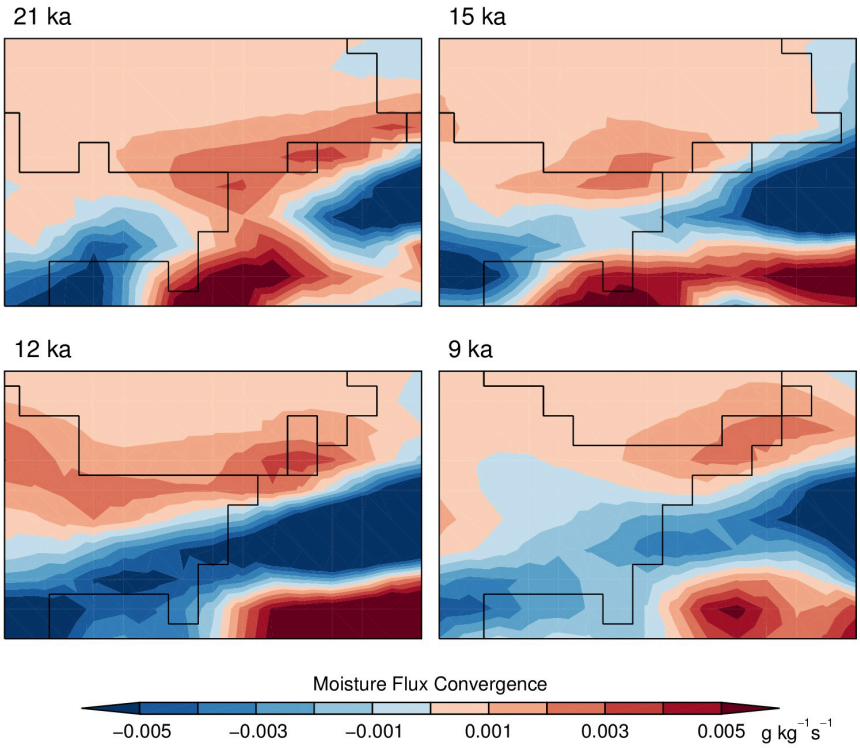

Figure 3.6. Composite differences in DJF moisture flux convergence computed as the difference between samples exhibiting high and low 850 hPa eddy heat flux ($v'T'_{850}$) over the southeastern Laurentide domain (lat-lon ranges if no box designating this in Fig. 1)

Stationary wave contribution

To assess the stationary wave contributions to MFC over the SE LIS, we

constructed composites conditioned on time indices for the Z_{500}* patterns over the SE LIS shown in Fig.7. To create the composites of time samples exhibiting high and low Z_{500}* patterns, we constructed reference maps over the southeastern LIS through the deglaciation for each time slice in Figure 4. For this analysis, we restricted our domain to 140°W to 0°W longitude, and 45°N to 88°N latitude. Results were not qualitatively affected by the domain selection as long as the patterns shown in Figure 5 were captured. The 6-hourly Z_{500}^{*} output was spatially regressed onto the one reference map produced for each time slice experiment. By performing this spatial regression and applying the correct area-weighting for each time slice, a 50-year time series of the Z_{500}* reference pattern was generated for each experiment. High and low MFC composites conditioned on the strength of the Z_{500}* reference pattern were identified similar to the storm activity composite by applying a one-half standard deviation threshold.

Composite differences in MFC conditioned on the Z_{500}* reference map index are shown in Figure 7. The MFC associated with the reference stationary wave patterns exhibits MFC over many of the areas associated with storm activity, but is generally weaker and less confined to regions along the LIS margins (except perhaps at 15 ka). Unlike the MFC composite difference associated with high storm activity, the MFC associated with the reference stationary wave patterns does not exhibit a consistent and coherent structure during the deglaciation, especially near the SE LIS. Perhaps the clearest indication of a varying relationship between stationary waves and MFC is demonstrated in the moisture flux divergence (instead of convergence) over the SE LIS at 9 ka, although closer inspection reveals that the MFC associated with the reference Z_{500}* patterns is rather different in each of the time slice experiments. It is worth noting that the varying MFC (and divergence in the 9 ka experiment) associations with the reference stationary wave patterns occur despite a consistently strong and positive winter SMB over the margin of the SE LIS in each time slice experiment (Fig. 1).

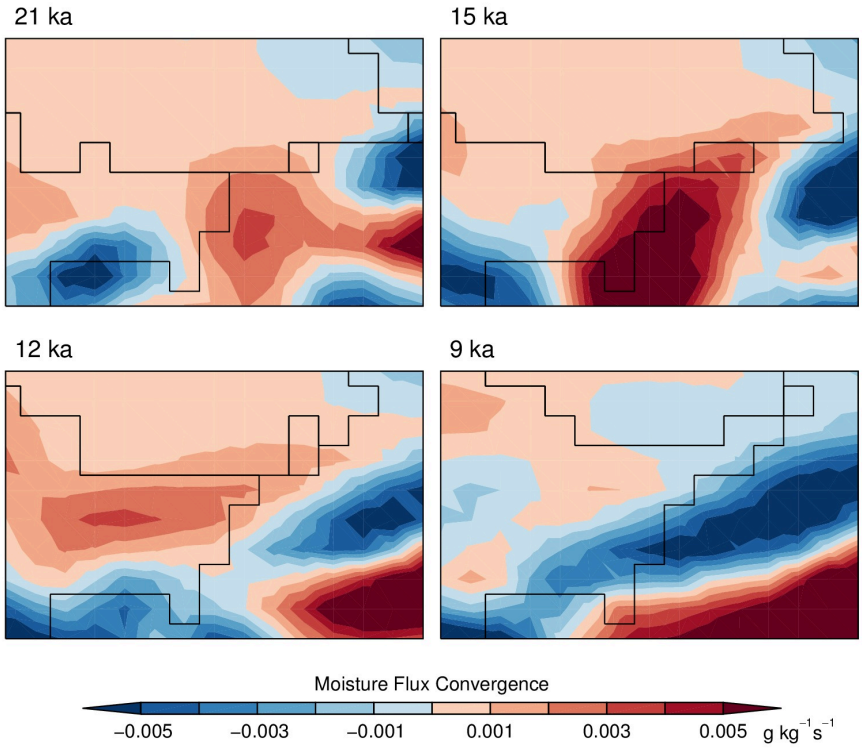

Figure 3.7. DJF moisture flux convergence computed as the difference between samples corresponding to high and low Z_{500}* over 140°W:0°W longitude, and 45°N to 88°N latitude

3.5 Discussion and conclusions

Understanding the influence of the large-scale atmospheric circulation on the SMB of the LIS is important for exploring how feedbacks between the atmosphere and ice sheet may have governed the deglacial evolution of the LIS. We assessed the relative roles of storm tracks and stationary wave patterns on the SMB of the LIS. In particular, we have identified an important storm track contribution to winter accumulation over the SE LIS throughout the deglaciation (until at least 9 ka). This storm track contribution to winter SMB likely modulated the retreat of the ice sheet from this sector during the

deglaciation, consistent with findings from Carlson et al. (2009).

Our analysis reconfirms the strong connection between the stationary wave pattern forced topographically by the CIS and its positive feedback to the SMB over the CIS. Winter accumulation over the CIS is primarily driven by uplift of the southwesterly mean flow forced by increased ridging over western North America, in agreement with *Roe and Lindzen* (2001). The stationary wave is most pronounced at 21 ka when the LIS was at its maximum extent and height. This interaction exemplifies a positive feedback between the topography and the stationary wave pattern, whereby higher topography and ice sheet extent excite a stronger stationary wave and, ultimately, increased SMB. Conversely, as the CIS ablates and loses elevation through the deglaciation in response to increasing insolation and greenhouse gas radiative forcing, the corresponding stationary wave pattern weakens, resulting in decreased moisture advection over the CIS and corresponding reductions in atmospheric SMB contributions, which further contributes to the overall ablation of the CIS.

A general conclusion from our results is that different sectors of the great North American ice sheets were associated with qualitatively different SMB contributions at the LGM and during the subsequent deglaciation. One clear indication of this is the mostly opposite DJF Z_{500}* anomaly pattern associated with the CIS and with the SE LIS composite differences in SMB in the vicinity of the CIS (compare the middle and right columns of Fig. 4). Given the well-understood interaction of topography and the stationary wave over the CIS, the mostly opposite pattern indicates the two regions must experience substantially different interactions with the atmospheric circulation.

Over the SE LIS, the response of the stationary waves and storm tracks is most

likely a result of closely coupled wave-wave interactions (e.g., *Wettstein and Wallace*, 2010; *Kaspi and Schneider*, 2013), which differs from the apparent dominance of the stationary wave contribution over the CIS. Thus, although the stationary waves influence the SMB of the SE LIS through a dynamic coupling with the storm tracks, (see Figure 4, right column), the SMB there is predominately affected by the storm tracks (see Table 1 – positive relationship between surface mass balance and $v'T'_{850}$); although, consistent with other studies (*Li and Battisti*, 2008; *Donahoe and Battisti*, 2009), the storm track at 21 ka is weakened relative to the PD (See Figure 3). As the ice sheet is reduced in height and extent through the deglaciation the storm track broadens, becomes more vigorous, and is presumably more effective at delivering moisture to the SE LIS. Thus, in contrast to the feedbacks governing the stationary wave and topography over the CIS, there is an inverse relationship between the storm track and topography over the SE LIS that constitutes a negative (damping) feedback on ice sheet growth and decay. These results are not only important for understanding the dynamical interactions between ice sheets and the atmosphere, but also emphasize the distinctly different ways the atmosphere can influence the surface mass balance. Accordingly, our results might help to explain the fact that the final termination of the LIS occurred over eastern North America (Dyke, 2004; Carlson et al., 2007; Carlson et al., 2009).

Southeast Sector	$v'T'_{850}$ (k m/s)	Z_{500}* (m)	**SurfaceMass Balance** (kg/m2 yr)
21ka			
μ	2	-350	88
σ^2	28	3422	2100
15ka			
μ	2.6	-340	162
σ^2	37.4	3846	3114
12ka			
μ	3.3	-239	173
σ^2	25.4	4385	2993
9ka			
μ	6.7	-311	198.8
σ^2	53.2	5327	4602

Table 3.1 Mean and variance of $v'T'_{850}$, Z_{500}*, and surface mass balance for the Southeast Sector of the LIS (SE LIS), over all time slices

3.6 Acknowledgements

We thank Dimitry Smirnov, Katie Holman and Aaron Donahoe for their comments regarding the manuscript. We acknowledge support from the U.S. National Science Foundation Sedimentary Geology & Paleobiology Program (grant number EAR-0958417) to PUC.

3.7 References

Alder, J.R., and S.W. Hostetler. (2014). Global climate simulations at 3000 year intervals for the last 21,000 years with the GENMOM coupled atmosphere-ocean model. C*limates of the past discussion,* **10**(4), 2925-2978.

Alder, J. R., S. W. Hostetler, D. Pollard, and A. Schmittner (2011), Evaluation of a present-day climate simulation with a new coupled atmosphere-ocean model GENMOM, *Geosci. Model Dev.*, ***4***(1), 69–83, doi:10.5194/gmd-4-69-2011.
Alley, R. B., Brook, E. J, Anandakrishnan, S. (2002). A northern lead in the orbital band: north-south phasing of Ice-Age events. *Quat. Sci. Rev.* **21**, 431–441.

Berger, A. L. (1978), Long-term variations of daily insolation and Quaternary climatic changes, *Journal of the Atmospheric Sciences*, ***35***(12), 2362–2367.

Boos, W. R. (2012), Thermodynamic Scaling of the Hydrological Cycle of the Last Glacial Maximum, *J. Climate*, ***25***(3), 992–1006, doi:10.1175/JCLI-D-11-00010.1.

Brook, E. J., S. Harder, J. Severinghaus, E.J. Steig, and C.M. Sucher (2000), On the origin and timing of rapid changes in atmospheric methane during the last glacial period, Global Biogeochem. Cycles, **14(**2), 559–572.

Carlson, A.E., Clark, P.U., Raisbeck, G.M., and Brook, E.J. 2007. Rapid Holocene deglaciation of the Labrador Sector of the Laurentide Ice Sheet: Journal of Climate, v. **20**, p. 5126-5133.

Carlson, A.E., Anslow, F.S., Obbink, E.A., LeGrande, A.N., Ullman, D.J., and Licciardi, J.M. 2009. Surface-Melt Driven Laurentide Ice-Sheet Retreat during the Early Holocene: Geophysical Research Letters, v. **36**, doi: 10.1029/2009GL040948.

Chang, E. K. M., Y. Guo, X. Xia, and M. Zheng (2012), Storm Track Activity in IPCC AR4/CMIP3 Model Simulations, *J. Climate*, 120630072710003, doi:10.1175/JCLI-D-11-00707.1.

Cook, K.H. and I.M. Held. 1988. Stationary waves of the ice age climate. J. Climate, **1**(8), 807–819.

Donohoe, A and D.S. Battisti (2009), Causes of reduced Atlantic storm activity in a CAM3 simulation of the last glacial maximum, *Journal of Climate,* **22**, 4793–4808.

Dong, B., and P. J. Valdes (1998), Simulations of the Last Glacial Maximum climates using a general circulation model: prescribed versus computed sea surface temperatures, *Climate Dynamics*, **14**, 571-591.

Dyke, A.S. (2004), An outline of North American deglaciation with emphasis on central and northern Canada. In: Ehlers J., Gibbard P.L. (eds.) Quaternary glaciations-extent and chronology, Part II. 2b, Elsevier, Amsterdam, 373-424.

Fettweis, X., M. Tedesco, M. R. Van de Broeke, and J. Ettema (2011), Melting trends over the Greenland ice sheet 52 (1958–2009) from spaceborne microwave data and regional climate models, *The Cryosphere*, **5**, 359-375.

Hofer, D., C. C. Raible, A. Dehnert, and J. Kuhlemann (2012), The impact of different glacial boundary conditions on atmospheric dynamics and precipitation in the North Atlantic region, *Clim. Past*, ***8***(3), 935–949, doi:10.5194/cp-8-935-2012.

Hoskins, B. J. and D. J. Karoly, 1981: The steady linear response of a spherical atmosphere to thermal and orographic forcing. J. Atmos. Sci., **38**, 1179–1196.

Hostetler, S.W., P.U. Clark, P.J. Bartlein, A.C. Mix, and N.G. Pisias (1999), Atmospheric transmission of North Atlantic Heinrich Events, *J. Geophysical Research,* **104**(D4), 3947-3952.

Kageyama, M., P. Valdes, G. Ramstein, C. Hewitt, and U. Wyputta (1999), Northern Hemisphere storm tracks in present day and Last Glacial Maximum climate simulations: A comparison of European PMIP models, *J. Climate*, **12,** 742.

Kapsner, W. R., R. B. Alley, C. A. Shuman, S. Anandarkrishnan, and P. M. Grootes (1995), Dominant influence of atmospheric circulation on snow accumulation in Greenland over the past 18,000 years, *Nature*, ***373***(6509), 52–54.

Laîné, A., M. Kageyama., D. Salas-Mélia., A. Voldoire., G Riviere., G. Ramstein., S. Planton., S. Tyteca., and J.Y. Peterschmitt (2009), Northern Hemisphere storm tracks during the Last Glacial Maximum in the PMIP2 ocean-atmosphere coupled models: Energetic study, seasonal cycle, precipitation, *Climate Dyn.*, **32,** 593–614.

Liakka, J., Nilsson, J. 2010. The impact of topographically forced stationary waves on local ice-sheet climate. *J. Glaciology.* **56**, 534-544.

Li, C., and D. S. Battisti (2008), Reduced Atlantic Storminess during Last Glacial Maximum: Evidence from a Coupled Climate Model, *J. Climate*, ***21***(14), 3561–3579, doi:10.1175/2007JCLI2166.1.

Li, C. and J.J. Wettstein, 2012: Thermally driven and Eddy-driven Jet Variability in Reanalysis. *J. Climate*, **25**, 1587-1596, doi:10.1175/JCLI-D-11-00145.1.

Licciardi, J., P.U. Clark, J.W. Jenson, and D.R. Macayeal (1998), Deglaciation of a soft-bedded Laurentide ice sheet, *Quaternary Science Reviews,* **17**, 427-448.

Lindeman, M. and J. Oerlemans, 1987. Northern Hemisphere ice sheets and planetary waves: a strong feedback mechanism. *Journal of Climatology*, **7**, 109-117.

Manabe, S., and A. J. Broccoli (1985), The influence of continental ice sheets on the

climate of an ice age, *J. Geophys. Res.*, 90, 2167-2190, doi:10.1029/JD090iD01p02167.
Marshall, S.J., and G.K.C. Clarke (1999), Modeling North American freshwater runoff through the last glacial cycle, *Quaternary Research,* **52**, 300–315.

Monnin, E., A. Indermühle, A. Dallenbach, J. Fluckiger, B. Stauffer, T. F. Stocker, D. Raynaud, and J. M. Barnola (2001), Atmospheric CO2 concentrations over the last glacial termination, *Science*, ***291***(5501), 112–114, doi:10.1126/science.291.5501.112.

Pacanowski, R. C. 1996. MOM 2 Version 2.0 (Beta) Documentation: User's Guide and Reference Manual, NOAA GFDL Ocean Technical Report 3.2, 329 pp.

Peixoto, J. P., and A. H. Oort (1992), Physics of Climate, American Institute of Physics, 520 pp.

Peltier, W. R. (1994), Ice age Paleotopography, *Science*, **265**, 195-201.

Pollard, D., and S. L. Thompson (1997), Climate and ice-sheet mass balance at the last glacial maximum from the GENESIS version 2 global climate model, *Quaternary Science Reviews*, ***16***(8), 841–863.

Roe, G.H. and R.S. Lindzen. 2001a. The mutual interaction between continental-scale ice sheets and atmospheric stationary waves. *J. Climate*, **14**(7), 1450–1465.

Shakun, J.D., Clark, P.U., He, F., Marcott, S. A., Mix, A.C., Liu, Z., Otto-Bliesner, B., Schmittner, A., Bard, E. 2012. Global warming preceded by increasing carbon dioxide concentrations during the last deglaciation. *Nature*. **484**, 49-54. doi:10.1038/nature10915

Shinn, R.A., Barron, E.J. 1989. Climate Sensitivity to Continental Ice Sheet Size and Configuration.*J. Climate*.**2**,1517-1537.

Simmons, A., S. Uppala, D. Dee, and S. Kobayashi (2007), Era-Interim: New ECMWF reanalysis products from 1989 onwards, *ECMWF Newsletter,* **110**, 25-35, ECMWF, Reading, United Kingdom.

Sowers, T., Alley, R.B., and Jubenville, J. (2003), Ice Core Records of Atmospheric N2O Covering the Last 106,000 Years, *Science*, **301**, 945-948.

Thompson, S. L. and Pollard, D. 1997. Greenland and Antarctic mass balances for present and doubled CO2 from the GENESIS version 2 global climate model, J. Climate, **10**, 871–900.

Ullman, D. J., LeGrande, A. N., Carlson, A. E., Anslow, F. S., and Licciardi, J. M.: . 2014. Assessing the impact of Laurentide Ice Sheet topography on glacial climate, Clim. Past, **10**, 487-507, doi:10.5194/cp-10-487-2014.

Wettstein, J.J., and J.M. Wallace, 2010: Observed Patterns of Month-to-Month Storm

Track Variability and Their Relationship to the Background Flow. *J. Atmos. Sci.,* **67**, 1420-1437, doi: 10.1175/2009JAS3194.1.

Yin, J. H. (2005), A consistent poleward shift of the storm tracks in simulations of 21st century climate, *Geophysical Research Letters*, ***32***(18), L18701, doi:10.1029/2005GL023684**.**

Chapter 4

Modeling the Laurentide Ice Sheet through the last deglaciation using the 3-dimensional, thermomechanical ice-sheet model, Glimmer: Sensitivity to model parameters, CO_2, and insolation.

Cuzzone, J.[1], Alder, J.[2], Clark, P.U.[1], Hostetler, S.[2]

[1]College of Earth, Ocean, and Atmospheric Sciences, Corvallis, OR

[2] US Geological Survey, College of Earth, Ocean and Atmospheric Sciences, Oregon State University, Corvallis, Oregon 97331, United States

4.1 Abstract

Feedback mechanisms and sensitivity to external forcings are not fully understood with regards to the deglaciation of the large northern hemispheric ice sheets beginning at the Last Glacial Maximum (LGM). Climate and ice-sheet modeling experiments have played an important role in increasing our knowledge of the forces that influence large ice sheets, with the last deglaciation serving as an important benchmark to help evaluate the role of external forcings and feedbacks that may shape the future trajectory of present day ice sheets. Using climate model output over the last deglaciation to force an ice-sheet model can be a computationally expensive undertaking that first requires extensive testing of model parameter space. Here, a one-way coupling scheme is used to simulate the last deglaciation of the Laurentide Ice Sheet (LIS) by coupling climate model output from GENMOM, to the three-dimensional thermomechanical ice-sheet model, Glimmer. This setup is used as it achieves fast simulation times, allowing parameter space to be explored to optimize the simulation of the LIS. First, a constant LGM climatology is applied to Glimmer for 50,000 years, and the resulting ice thickness and volume are analyzed. These simulations are re-run to optimize the paramter space in Glimmer that results in the best fit of the Laurentide Ice Sheet (LIS) volume and thickness when compared to the best available reconstructions. Simulations are then carried out across the last deglaciation, beginning with the LIS at the LGM. The results verify the use of the Genmom climatology, as it is capable of reproducing the deglaciation of the LIS, when input into Glimmer. We next test the sensitivity of the LIS during the last deglaciation to greenhouse gases (GHG) and insolation. Because of the one-way coupling scheme, our method is unsuccessful in establishing the individual roles of each

forcing on the deglaciation of the LIS. Instead, we find that the topography boundary condition used to simulate the climate in Genmom, overwhelmingly determines the deglactiation of the LIS. To assess the relative roles of CO_2 and insolation, an asynchronous coupling scheme or a fully coupled ice-sheet climate model should be implemented.

4.2 Introduction

To evaluate changes in the behavior and response of ice sheets to a warming climate, we often use the paleoclimate record of past ice sheet changes to evaluate their sensitivity to warming. Using the geologic record as a benchmark for past ice sheet margin migration coupled with estimates of ice sheet volume, ice sheet models have been employed to test the sensitivity of ice sheets over a range of time scales. Many studies focus on the last deglaciation as a means to evaluate ice sheet model skill and the response to various forcings and feedbacks controlling ice sheet changes. Often, intermediate complexity climate models are used to simulate the climate over the last glacial cycle (Bonelli et. al., 2009; Ganopolski et. al., 2010) and force an ice sheet model either offline or interactively with the simulated climate. Because the simulation of the climate is computationally expensive for fully coupled atmosphere and ocean climate models (AOGCMs), these itermediate complexity models are useful. Another method used to simulate ice sheet growth and decay over the last glacial cycle involves constructing a climate index from the Greenland $\delta^{18}O$ ice core record to create temperature and precipitation fields needed to force an ice sheet model, of which have been implemented in a number of studies (Marshall et. al., 2000;2002; Tarasov and

Peltier, 2004; Zweck and Huybrechts, 2005; Charbit et. al., 2007). Temperature and precipitation fields are interpolated from present day reanalysis such as ERA-40 (Uppala et. al., 2005) or NCEP (Kalnay et. al., 1996) reanalysis across the last deglaciation using the isotope record as an index. The interpolated anomaly is added onto these fields to construct a temperature and precipitation forcing used as boundary conditions for the ice sheet model. Since this forcing does not include dynamic changes to the climate that would otherwise be simulated in a fully coupled climate model, corrections such as elevation-drying effects need to be included to simulate realistic ice sheet volumes (Marshall et. al., 2002). Therefore, although the index method provides a means of initial conditions used to simulate ice volume, a climate model that accounts for these dynamics is often a better platform to force an ice-sheet model with.

Aside from the climate forcings, many studies have also indicated a high sensitivity to model and climate boundary conditions on the simulation of the Northern Hemisphere ice sheets (Hebler et. al., 2008; Zweck and Huybrechts, 2005), of which the positive degree day factors and the ice softness parameters (used to determine ice flow) were shown to impact the ice volume the greatest. Basal sliding processes were shown to influence the geometry of the simulated ice sheet the greatest (Marshall et. al., 2002; Tarasov and Peltier, 2004). With respect to climate, Hebler et. al. (2008) and Zweck and Huybrechts (2005) determined that uncertainty in the climate forcing influenced the simulation of the Northern Hemisphere ice sheets greater than those associated with parametric uncertainty. Accordingly, using a suite of climate simulations from different models, Charbit et. al. (2007) found the LGM ice sheets exhibited a high sensitivity to changes in the climate forcing.

Here we employ the use of a fully coupled atmosphere and ocean climate model (GENMOM), that has been used to simulate the climate of the last deglaciation at specific time segments (see Alder et. al., 2014 for full description), to force the 3-dimensional thermo-mechanical ice-sheet model, Glimmer (Rutt et. al., 2009). Simulating the deglaciation of the Laurentide Ice Sheet (LIS) has recently been achieved by Gregoire et. al. (2012), using a more coarse climate model compared to GENMOM. The benefit of a more coarse climate model allowed Gregoire et. al. (2012) to simulate the deglaciation transiently, rather than through time segments which will be described in our methods. Rather than capture the deglaciation of the LIS in a transient state, however, our goal is to capture the sensitivity of the buildup and deglaciation of the LIS to a range of parameters within Glimmer.

4.3 Methods

4.3.1 Ice-Sheet Model

We use the Glimmer 3-dimensional thermo-mechanical ice sheet model for this study. Glimmer has been verified against EIMSINT standards (Rutt et. al., 2009), has been used to simulate the Greenland Ice Sheet during the Pliocene (Lunt et. al., 2008) and the future (Stone et. al., 2010), and has recently been used to simulate the deglaciation of the LIS (LIS) (Gregoire et. al., 2012). The model applies the shallow ice approximation (SIA) to compute ice thickness and temperature on a three dimensional grid. The SIA works well for slow ice flow dominated by vertical shear, but breaks down where fast flow dominates (e.g. ice shelves, ice streams), as longitudinal stresses become important. Thickness changes are computed from the surface mass balance and horizontal ice flux

divergence, and deformation is resolved through the determination of ice temperature in three dimensions. Glimmer also includes a simple isostasy model and can account for varying basal sliding.

4.3.2 Climate Forcing

We force Glimmer with output from GENMOM, which is the GENESIS [Global Environmental and Ecological Simulation of Interactive Systems] version 3 atmospheric GCM (Thompson and Pollard, 1997) coupled to MOM2 [Modular Ocean Model version 2] (Pacanowski, 1996). The AGCM has 18 vertical (sigma) levels and a spectral T31 resolution which translates to a nominally 3.75° horizontal resolution. MOM2 also is run on a T31 horizontal grid, but with 20 vertical levels. The climate simulations were performed at specific time segments throughout the last deglaiation (21ka, 18ka, 15ka, 12ka, 9ka, 6ka, 3ka, PI, and PD). Details regarding the paleoclimate simulations we use to drive Glimmer can be found in Alder et al. (2014). Because these simulations span the entire deglaciation, simulation of the deglaciation of the LIS is possible. The simulations all include appropriate boundary conditions for insolation (Beger, 1978), surface topography, ocean bathhymettry, ice-sheet height and area, and atmospheric greenhouse gases including CO_2 (Monnin et al., 2001), CH_4 (Brook et al., 2000), and N_2O (Sowers et al., 2003) for each time slice. The Northern Hemisphere ice sheets are prescribed based on the ICE-4G reconstructions (Peltier, 1994) except for the LIS, where the reconstructions from Licciardi et al. (1998) replace ICE-4G. The LIS of Licciardi et al. (1998) and ICE-4G are similar in spatial extent but differ in topography, with ICE-4G thickness generally lower at 12ka and 9ka (See Figure 1 for comparison with Ice-5g and

Ice-6G). For the build up phase of the simulations, we drive Glimmer with monthly averaged (300 yr. avg.) precipitation and temperature. For the deglaciation, we also drive glimmer using temperature and precipitation fields from the deglacial snapshots (Figure 2).

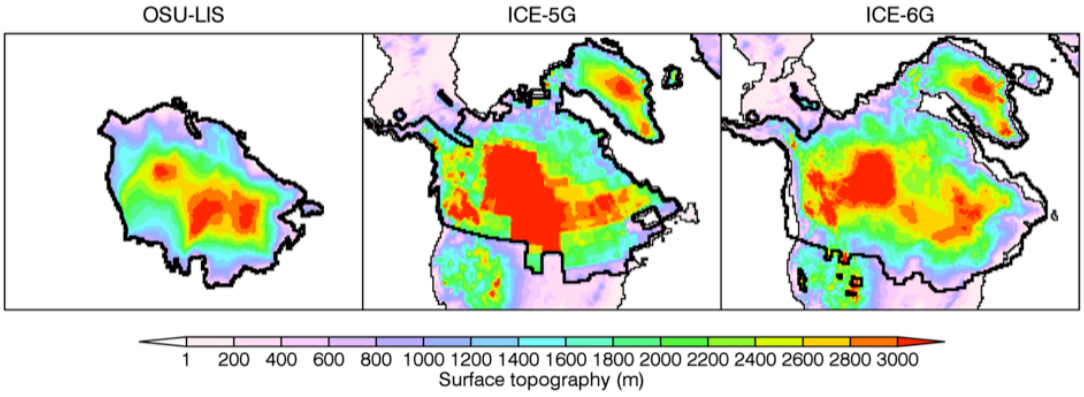

Figure 4.1. Surface elevation maps for the OSU-LIS reconstruction (Licciardi et. al., 1998), Ice-5G (Peltier, 2004), and Ice-6G .

4.3.3 LGM spin-up and sensitivity tests

We begin our glacial simulation using present day topography and ice thickness from the ETOPO1 dataset (Amante and Eakins, 2009). The area over North America was defined to cover the extent of the Laurentide and Cordilleran Ice Sheets. Following Gregoire et al. (2012), ETOPO1 data was projected onto the grid using bilinear interpolation (File provided by Lauren Gregoire). A Lambert Equal Area Azimuthal projection (Snyder, 1987) was chosen for its ease with continent mapping. The domain is shown in Figure 3, with mapping details shown in Table 1. Although this study does not seek to evaluate change over Greenland, we include Greenland Ice Sheet to ease with development of the Inuitian portion of the LIS.

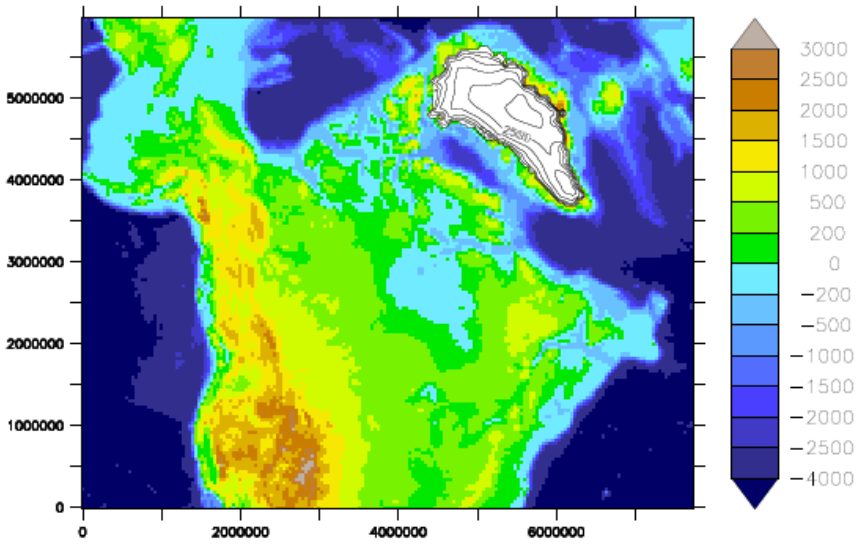

(a) North America

Figure 4.3. Bedrock topography (in m) used as the initial condition for the LIS simulations. Topography and bedrock are taken from ETOPO1 projected onto a Cartesian grid using bilinear interpolation (see Table X for mapping details). Scale is in meters. File and accompanying map was provided for by Lauren Gregoire.

Projection Details	North America
Map Projection	Lambert Equal Area Azimuthal
Resolution	40km
Central Longitude (°)	-95
Central Latitude (°)	45
False easting (m)	3848380
False northing (m)	1082320
Grid Size	194 x 150

Table 4.1. Mapping projection details used for the Glimmer simulations.

4.3.4 Boundary Conditions

In table 2, Glimmer parameters are identified with their corresponding values. These parameters are not well constrained by observations, so often, tuning of these parameters are needed to arrive at a realistic result with respect to simulated ice sheet extent and volume. It should be noted that these parameter values would vary based upon specific geographic locations. These simulations are limited to area-wide parameters, which do not vary spatially. These main parameters are lapse rate, Pdd of snow, Pdd of ice, a flow enhancement factor, mantle relaxation time (relating to isostasy), and the geothermal heat flux. We adjust the laspe rate to 5 K km^{-1}, based upon results from Abe-Ouchi (2007). Before testing the sensitivity of ice-sheet buildup to the parameters, we choose to first simulate the build up of the LIS using the standard Glimmer setup.

Parameters	Value Used	Min	Max	Unit
$PDD_{snow}(\alpha_s)$	3	2	5	mm d^{-1} °C^{-1}
$PDD_{ice}(\alpha_{ice})$	8	7	12	mm d^{-1} °C^{-1}
Flow Factor	3	1	10	none
Mantle Relaxation time	1000	300	9000	years
Geothermal Heat Flux	50	35	65	W m^{-2}
Marine Limit	-200	-100	-500	m

Table 4.2. Parameters used in the ice sheet simulations with the range of values tested, and the values used to create the "Tuned" ice sheet, and deglaciation simulations.

4.3.5 Ice-sheet build-up methodology

Various methods have been used to simulate the build up of ice sheets in models. Beginning at the present day topography, the ice sheet model was forced with a constant LGM climate over 50,000 years, until ice volume and extent reached equilibrium following (Huybrechts and T'siobbel, 1997). Often, equilibrium was reached much earlier in our simulations. Although this method is limited in that it does not begin the simulation of the LIS through a glacial cycle, this method has been shown to more adequately simulate the build up of the LIS in prior work using Glimmer (Gregoire et. al., 2012) rather than using a climate index to simulate the buildup through the last glacial cycle.

4.4 Results – parameter testing

The results from the initial simulation of the LIS indicate that too much ice is present both in extent and volume (Figure 4). To address these issues, we simulated the buildup of the LIS across varied parameter space to tune the model to fit the known limits of the LGM LIS, and estimated volume. For this section, refer to Table 2 for range of parameter values and Figure 5 and 6.

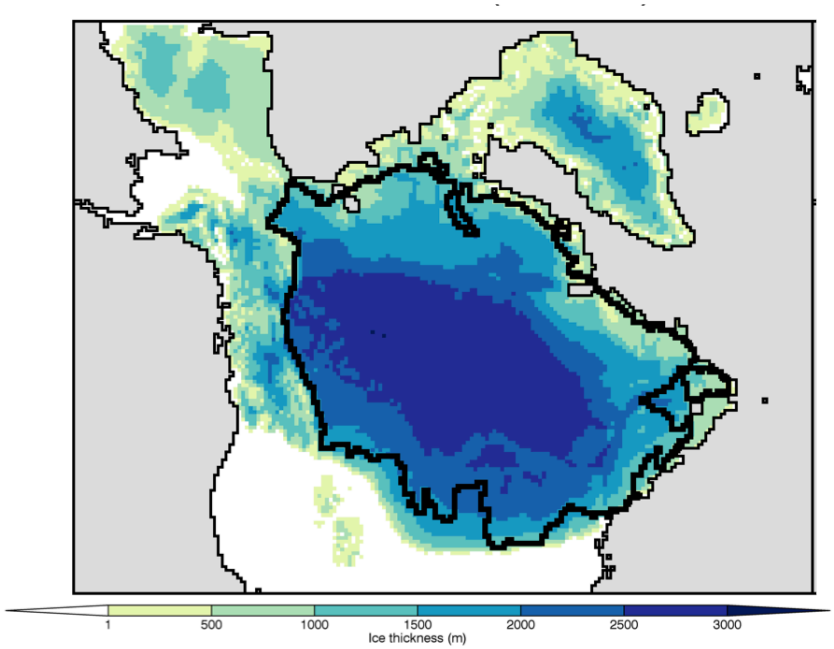

Figure 4.4. Initial LGM simulation for the LIS and Cordilleran Ice Sheet, using default Glimmer input parameters, no isostasy, and no basal sliding. Ice extends too far south of LGM margins, interior thickness is greater than would be expected from reconstructions (Licciardi et. al., 1998; Peltier, 2004). Also, too much ice exists over Beringia.

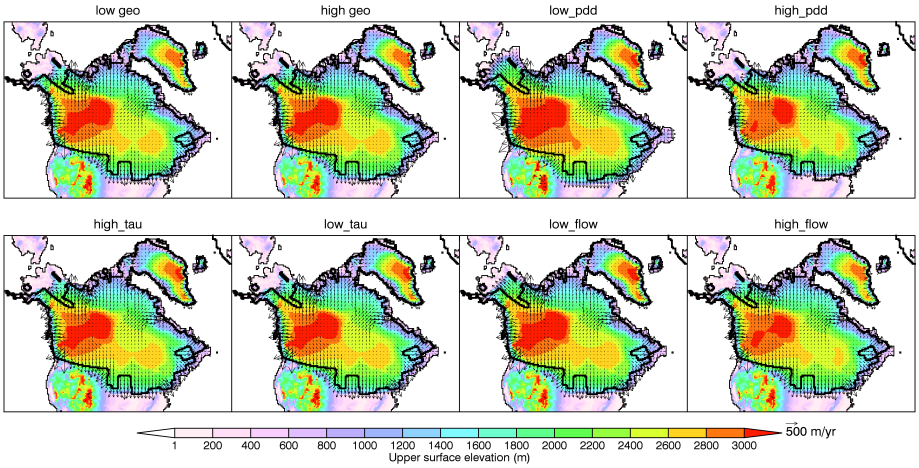

Figure 4.5. Ice surface elevation for the 21ka sensitivity simulations (see Table 1 for values used in each test case). Vectors indicate the magnitude of the U and V ice velocity. The 500 m/yr vector is shown as a reference.

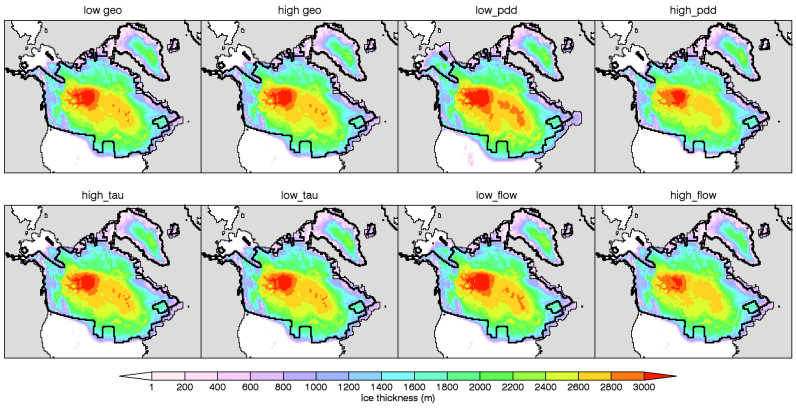

Figure 4.6. Ice sheet thickness for each of the sensitivity runs, defined by the parameters in Table 1.

4.4.1 Basal Sliding

Basal sliding plays an important role in ice-sheet dynamics, where basal temperature dictates melt and thus sliding. It is a key component towards modeling the LIS more accurately, allowing for increases in ice velocity and migration of the ice sheet towards lower elevations.

To test the role of basal sliding, we allowed the ice sheet to respond to a consistent area-wide basal sliding of 0.5 mm yr^{-1} Pa^{-1}. Ice-sheet volume greatly increases by 38% over the LIS, in response to lower basal sliding (Figure 7). The structure of the ice sheet continues to have a single dome, with the ice margin retreated slightly northward compared to the standard run. When the basal sliding is increased to 10 mm yr^{-1} Pa^{-1}, ice sheet volume decreases by 7% from the standard run.

4.4.2 PDD factors

The PDD factors have a large influence on the amount of ice melt that occurs in the ice-sheet model. These factors assume a positive relationship between ablation and temperature and therefore, changes in these variables could have a large effect on the ice sheet extent and volume. To complicate matters, Glimmer cannot input spatially varying PDD factors, which would change given the large geographic extent of the LIS. Large insolation changes, which occurred over the last deglaciation, would also affect the PDD factors, of which cannot be reconciled here.

With these limitations, we test the sensitivity to PDD factors by simulating ice sheet growth with high and low PDD factors. The high simulation has a PDD of snow at 5 mm

d^{-1} $°C^{-1}$ and a PDD of ice at 12 mm d^{-1} $°C^{-1}$. The low simulation uses a PDD of snow at 2 mm d^{-1} $°C^{-1}$ and a PDD of ice at 7 mm d^{-1} $°C^{-1}$.

When compared to the standard PDD run, the high PDD simulation reduces the ice volume by 13% (Figure 7). The southern margin recedes northward, and the development of the Cordilleran ice sheet is limited (Figure 6). The low PDD simulation has its volume increase by 16%, an ice margin, which is too far south, and too much ice over Beringia. Collectively, these changes occur across all of the ice sheet area, but have its largest effects along the southern margin. Finding the right PDD factors for this study was based upon similarity to the reconstructions of ice volumes from ICE-5G (Peltier 2004) and Licciardi et al. (1998), with extent from Dyke (2004).

4.4.3 Geothermal Heat Flux

The geothermal heat flux has important influence on ice-sheet sliding. Increasing the flux to 65 mWm^{-2} allows the LIS to become closer to the melting point, and in many locations, the LIS becomes warm bedded. This leads to basal sliding (condition is met when there is water). Ice sheet volume only decreases marginally by 3%, however, the maximum ice sheet thickness decreases by 9% (Figure 7). This indicates that increased sliding due to a larger geothermal heat flux, allows the ice sheet to become more flat. Lowering the geothermal heat flux, does the opposite, and may strengthen the ice stream development.

4.4.4 Flow Factor

The flow factor is a dimensionless variable used to describe ice softness. In Glimmer, this value is usually set at 3, and applies to all areas of the ice sheet. When the

factor is decreased to 1, ice volume and thickness both increase, by 5% and 9% respectively (Figure 7). Increasing the flow factor to 10 has less of an effect, with ice volume and thickness decreasing due to enhanced flow by 5% and 3%.

4.4.5 Isostasy

To account for isostatic processes, Glimmer can vary the response times of the mantle. Serving as an important constraint on the ice-elevation feedback, we varied this number from 300 to 9000 years. When the mantle is slower to adjust, ice would build up to a higher altitude, and a positive feedback would initiate whereby more mass is located above the equilibrium line. This would ultimately allow more ice to accumulate over time. With a faster responding mantle, ice would load the surface, depress it faster, and thus would remain lower with respect to the equilibrium line. Our results show marginal changes for the slower responding mantle (9000 yrs), with ice volume and thickness increasing by 3 and 2% (Figure 7). Very little change occurs with the faster responding mantle of 300 yrs. Although not investigated here, isostatic processes may play a larger role over a full glacial cycle (Abe-Ouchi, 2013).

4.4.6 Addition of subglacial sediments

Geologic evidence supports the notion that the LIS was not a single domed ice sheet, and instead had three distinct domes (Dyke, 1982). Sediment deformation incorporated into ice sheet models have been shown to influence the character of the LIS dynamics, by enhancing ice streaming (Marshall et al., 2002; Tarasov and Peltier, 2004). These methods have either allowed varying basal sliding based upon

sediment thickness (Marshall et al., 2002) or have resolved till viscosity to account for deformation (Tarasov and Peltier, 2004).

To test the role of subglacial sediments on ice doming over the LIS, we took advantage of Glimmers capability to use sediment masks. We used the sediment mask from Laske and Masters (1997) following methods from Gregoire et. al. (2012) (Figure 8). This mask denotes areas where sediment thickness is below 20m, and thus hard bedded, and areas where sediment thickness is above 20m. The sliding only ensues where there is basal water, however, higher velocities are a result of thicker, more deformable sediment. Values are set at 5 mm yr^{-1} Pa^{-1} where there are sediments greater than 20m in thicknesses and 0.5 mm yr^{-1} Pa^{-1} elsewhere. The effect of varying basal sliding on the ice volume is marginal (< 4%). Ice stream definition is much improved and the single dome structure is not present with the addition of sediments, although the structure does not replicate all of the known domes of the LIS (Figure 9).

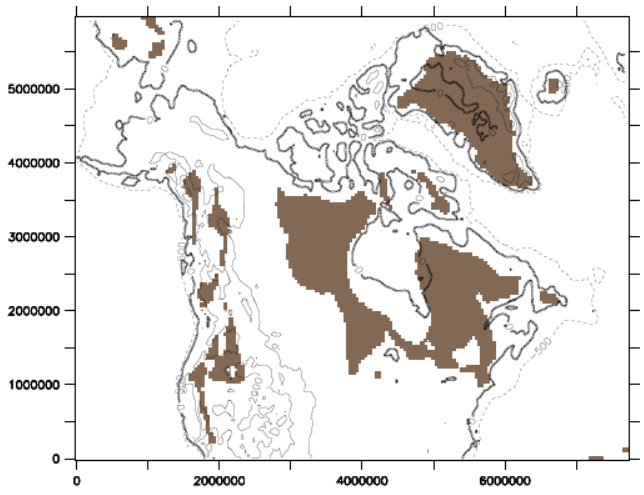

Figure 4.8. Sediment map for North America from Laske and Masters (1997). Brown areas indicate areas of bare rock, where sediment thickness is less than 20m. White areas are where sediment is greater than 20m and considered soft bedded. Masks and figure provided for by Lauren Gregoire.

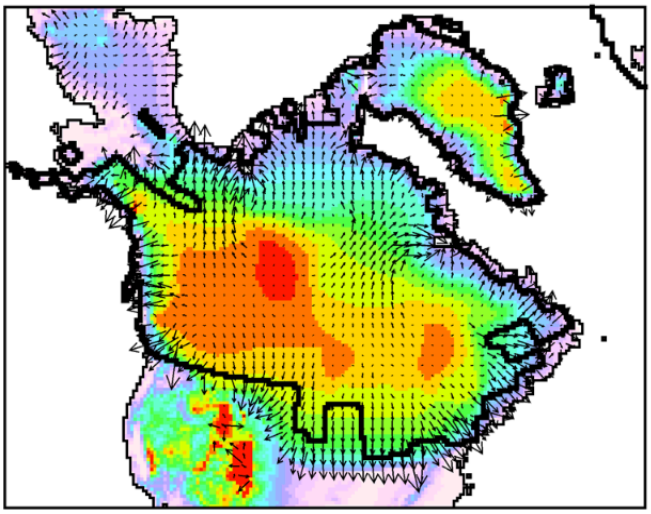

Figure 4.9. Ice surface elevation for the 21ka "Tuned" simulation. Vectors indicate the magnitude of the U and V ice velocity. The 500 m/yr vector is shown as a reference.

4.4.7 Tuned Ice Sheet – Description of ice-sheet buildup

With the sensitivity of input parameters assessed, we run Glimmer using the parameters defined in Table 2. Shown in Figure 10 are the areas of accumulation and ablation during the LGM simulation. Much of the accumulation is confined to western North America, where the Cordilleran ice sheet grows. This signal is forced primarily by the increased ridging of 500mb heights across western North America in the input climatology (see Alder et. al., 2014). Since the climatology for 21ka reflects the boundary condition of Ice-4G and Licciardi et. al. (1998), the buildup of the ice sheet is confined to

where precipitation maximizes as a result of the topography. Accordingly, accumulation is also high across the southeastern margin of the LIS.

Once ice builds up over the Cordilleran mountains and over Quebec initially, these regions grow large enough until both portions merge over central Canada. Over the Cordilleran ice sheet, accumulation rates are high at ~1 m yr^{-1} on the upslope side of the mountains. Over the LIS, accumulation rates are much lower, with the exception of the southeastern LIS. The simulation for the LIS has two defined domes (Figure 9) where the Keewatin and Labrador domes have been defined (Dyke, 2004). Accumulation is higher over the domes (Figure 10), and lower over Hudson Bay where softer sediments allow for faster basal velocity (Figure 10), and thus lower ice sheet thickness. The southern LIS has a much steeper gradient of slope, primarily forced by the high accumulation in this region, whereas the northern LIS is flatter in response to less accumulation but also less ablation. Compared with the paleo ice streams described in Stokes and Tarasov (2010), Glimmer simulates many of the paleo ice streams, which is improved by the varying basal sliding boundary condition. For this simulation, it takes Glimmer ~20,000 model years to reach an equilibrium state, although we run the simulations for 50,000 years. Once the LIS and Cordilleran are defined, the domes begin to become more defined, in part due to varying basal sliding conditions for hard and soft beds.

Our simulation of the build up is not the focus of the study, and should not be considered realistic, although the simulation matches the ice extent of Dyke (2004) well. When the LIS is confined to the boundaries in Ice-5G, Glimmer simulates a volume of $27x10^6$ km^3 compared to $31x10^6 km^3$ for Ice-5G. When confined to the margins of Licciardi et. al.

(1998), Glimmer simulates virtually the same volume. Although the input climatology used the Licciardi et. al. (1998) LIS and a boundary condition for topography, this result gives confidence to the fact that Glimmer can reconstruct a reasonable, and almost identical ice sheet as the initial boundary condition for the climate simulation.

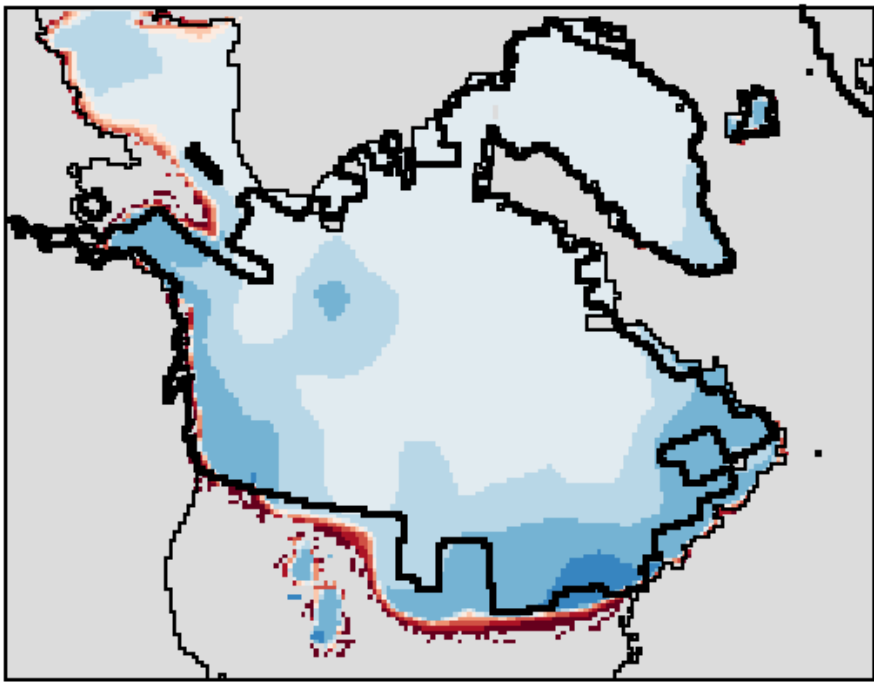

Figure 4.10. Accumulation and ablation for the 21ka "tuned" simulation. Areas in blue denote accumulation, and areas in red denote ablation.

4.5. Modeling the LIS through the last deglaciation

With an LIS that matches the extent (Dyke, 2004) and volume (Licciardi et. al., 1998; Peltier, 2004) well, we use this as our boundary condition to simulate the deglaciation of the LIS. The Genmom temperature and precipitation climatology from 18ka, 15ka, 12ka, 9ka, and 6ka are used to drive Glimmer (Alder et. al., 2014) throughout

the deglaciation. Explained in more detail in Alder et. al. (2014), the Genmom simulations used appropriate boundary conditions for greenhouse gases, insolation, and ice-sheet topography. The temperature and precipitation climatology is shown in Figure 11, and has been tested against existing paleo-climate proxies (Alder et. al., 2014). Gregoire et al. (2012) force Glimmer with transient climate output across the deglaciation in 1000 yr. timesteps. Here we use an absolute forcing at discrete time intervals (18ka, 15ka, 12ka, 9ka, and 6ka). The goal of this work is to validate that the climatology from Genmom produces an LIS resembling reconstructions at these time intervals. Accordingly, the process of the deglaciation should not be considered useful or realistic here. Only the end state of the simulation, after the specific climatology is applied, should be considered.

4.6. Methodology

Monthly mean precipitation and temperature from each time segment from the GENMOM simulations are used to drive the pdd model (Figure 11). Glimmer has the built in capacity to hotstart using a preexisting ice sheet. The deglaciation begins using the spun-up LIS. This includes the ice-sheet thickness and temperature fields, which are used to compute the ice velocities. Lastly, the same input parameters used to create the tuned LGM LIS are kept constant throughout the deglaciation experiment. The climate forcing from the 18ka simulation from GENMOM is forced onto the 21ka LIS. This simulation is run for 50,000 years, although the new ice sheet reaches near equilibrium usually after 25,000 years. This method continues by forcing the new LIS with the next time segments climate fields, with the last climate forcing at 6ka.

4.7. Deglaciation

Beginning at 21ka, the simulated LIS contained 26 million km^3 of ice volume (using the ICE-5g mask). The deglaciation of the LIS is slow when forced with the 18ka climate, with the LIS containing 25 million km^3 of ice volume. Shown in Figure 12, this ice loss mainly occurs along the southern margin, although interior regions gain mass, possibly associated with a thermodynamically driven moister environment as the climate warms out of the LGM. By 15ka, deglaciation continues to be slow, with ice volume for the LIS at 24 million km^3. By this time the Cordilleran has begun to lose mass and the saddle between the Cordilleran and LIS begins to encroach southward. The largest change in the LIS occurs during the 12ka forcing. At this time period, boreal summer insolation peaks, and the LIS loses much of its volume down to 13 million km^3. During this interval the Cordilleran ice sheet melts almost completely, for the exception of ice over higher elevations. The LIS western margin pulls eastward greatly, whereas the southeast margin pulls back slightly in comparison. By 9ka, the Keewatin dome begins to disappear from the simulation, and most of the ice is confined to the Labrador sector over the eastern LIS. Again, the southeast margin pulls northward much slower than the western LIS. At 9ka, the LIS only contains 8 million km^3 of ice volume. By 6ka, the LIS is gone, and the only remnant ice remaining exists over the Northern Cordilleran and over Baffin Island.

Compared to the Ice-5G mask, our simulated ice volume is ~17% less at 21ka and 18ka (Figure 13 – left panel). This number becomes less at 15ka, and at 12ka our simulated ice volume is ~12% greater than Ice-5g. Ice loss in Ice-5g accelerates at a much greater rate than our simulation during the interval between 15ka and 12ka. By

9ka, our simulation agrees with the Ice-5g reconstruction well. When the LIS is masked to the margins used in Licciradi et. al., (1998), the agreement with our simulation is improved (Figure 13 – right panel). This may not be surprising considering the boundary condition for the LIS in GENMOM was the Licciardi et. al., (1998) reconstruction. Therefore, the climate produced in Genmom, is verified by the deglaciation of the LIS, which follows the reconstruction.

Area wise, our simulation agrees well with the Liccardi et al. (1998) reconstruction (Figure 13 – right panel), of which areal limits are derived from Dyke and Prest (1986). Much of the LIS is confined to these limits (see black outline in Figure 10). At 12ka, the western LIS has pulled back away from the mapped limits, but overall agreement with respect to area is good.

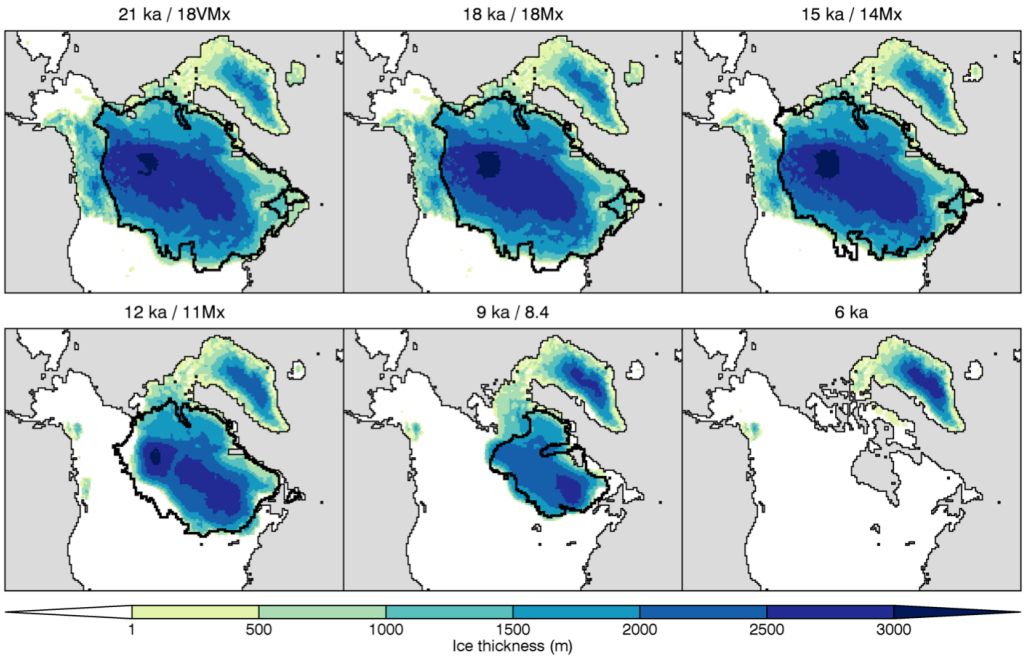

Figure 4.12. Ice sheet thickness for each individual time segment. Ages to the left of the (/) indicate Genmom time segments. Ages to the right of the (/) indicate equivalent time segment from Licciardi et. al., 1998. The black line indicates the ice extent from the Licciardi et. al., 1998 reconstruction

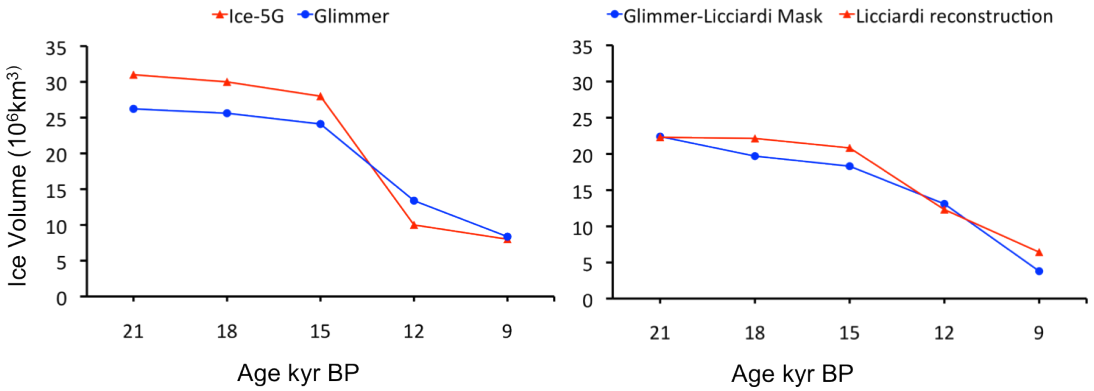

Figure 4.13. Ice volumes for the deglaciation simulations obtained by confining the LIS to the margins from Ice-5G (Peltier, 2004) and Licciardi et. al., 1998.

4.7.1. Sensitivity to CO_2 and Insolation

Large changes during the last deglaciation occurred both in greenhouse gases (GHG) and insolation. To test the individual effects of these forcings we re-run the GENMOM climate simulations for the deglaciation time segments using fixed GHG and insolation cases. For the fixed GHG case, we fix CO_2 concentrations at the 21ka concentration, and only allow insolation to vary across the deglaciation. For the fixed insolation case, we fix insolation at 21ka limits, and allow CO_2 to vary across the deglaciation.

4.8.1 CO_2 and Insolation effects

In Figure 14 are the ice thicknesses for the CO_2only case and the insolation only case. A cursory glance of the two indicates very little difference, with both following a similar trend in deglaciation to the standard approach using all forcings. The insolation forcing is stronger, leading to less overall ice thickness through each time segment. These differences are however, marginal, and are more clear when looking at the total ice volume. The ice volumes for the two sensitivity cases and the all forcing case, using the Licciardi et. al., 1998 mask, is shown in Figure 16. In the CO_2 only case, deglaciation does not begin until 15ka, as the LIS maintains its volume, and grows marginally to 18ka. Up to 15ka, the all forcings and insolation only case follow in lock step as the LIS melts. Between 15ka and 12ka, the majority of melt occurs in all cases. During this interval boreal summer insolation peaks by 12ka, constituting ~45 w/m^2 at 60°N (see Alder et. al., 2014). At 12ka, CO_2 nears a point of doubling compared to LGM values (see Alder et. al., 2014), constituting a 3.7w/m^2 forcing (Forster et. al., 2007), much smaller than the insolation forcing. The effect of increasing CO_2 however is symmetric globally, whereas the insolation forcing varies with latitude. In each case, however, the LIS fully terminates. Insolation increases greatly through the deglaciation, but then decreases after 12ka, with studies noting that the drop in insolation by itself would possibly allow ice to persist into the Holocene if insolation was only allowed to vary (Heinemann et. al., 2014). Conversely, CO_2 continues to increase towards present day. Therefore, no assessment can be made here as to the role of each individual forcing. In fact, this analysis represents a scenario where the topography forcing (used in the climate modeling component) predominantly controls the climate, and thus the rate of accumulation and ablation over the LIS.

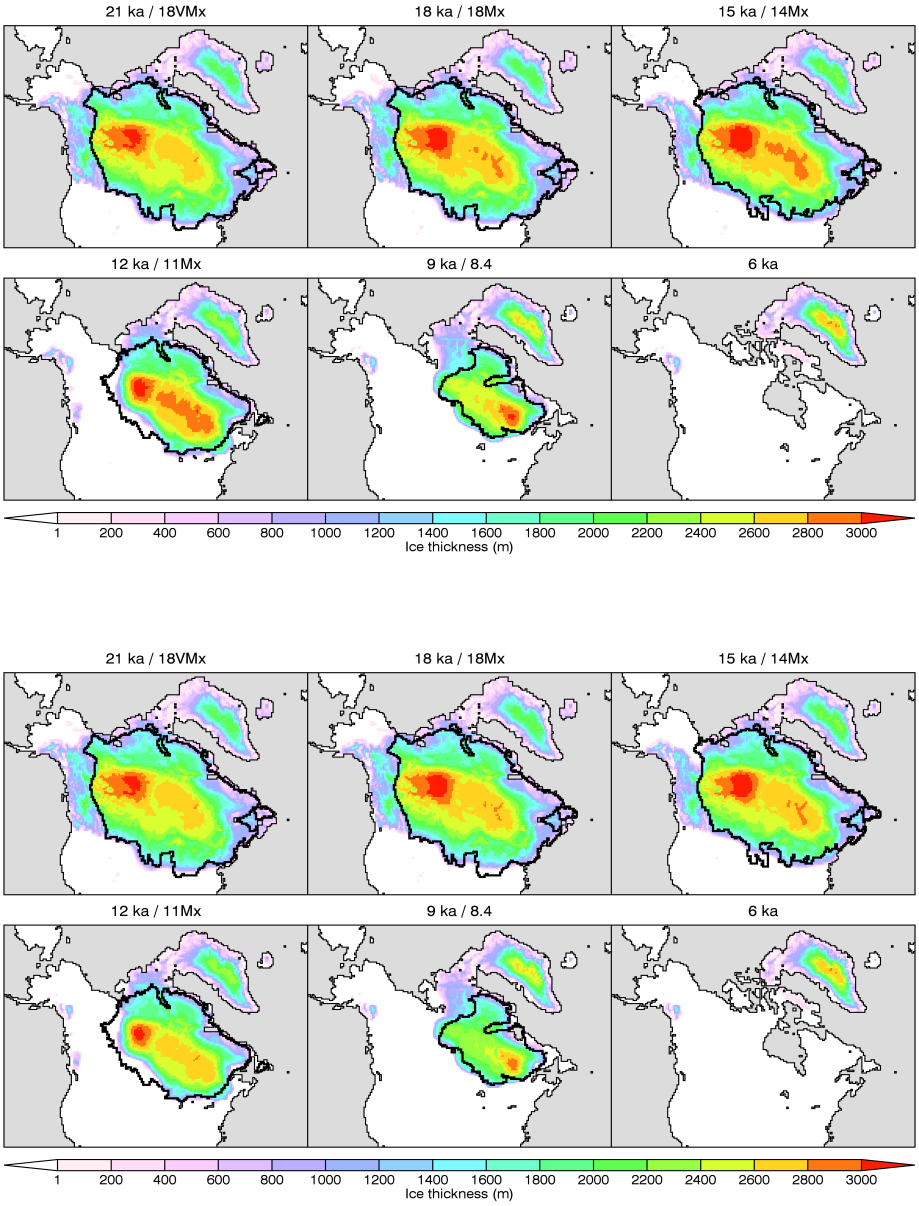

Figure 4.14. Resulting ice sheet thickness for the GHG only simulation of the last deglaciation (top) and the insolation only simulation (bottom). Black line indicates margins from Licciardi et. al., 1998.

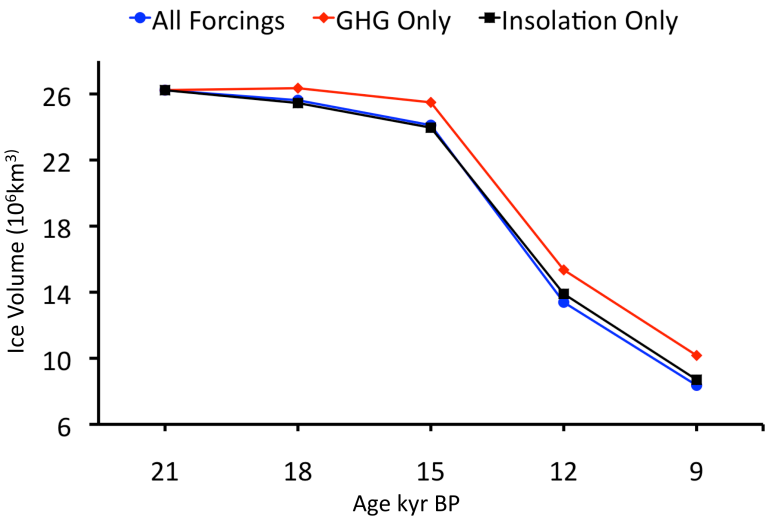

Figure 4.15. Resulting ice volume for the LIS (Licciardi et. al., 1998 margins) for the GHG only, insolation only, and all forcing cases.

4.9. Discussion and Conclusions

Following a similar experimental setup to Gregoire et. al. (2012), we were successful in obtaining an LGM LIS that corresponds well with the area reconstructions from Dyke (2004) and volume estimates from (Licciardi et. al., 1998). Accordingly, the simulation over the last deglaciation followed the expected pattern over the LIS. These simulations were not intended to serve as a complete simulation of the last deglaciation of the North American Ice Sheet. Because of the one way coupling between the climate and ice sheet, important feedbacks and interactions could not allow the ice sheet to develop outside of the initial boundary conditions. Instead, these simulations illustrate that the climate forcing produced by GENMOM is suitable for simulating reasonable ice sheet area and thickness. Since the climate of GENMOM was constrained by the Licciardi et. al. (1998) and Ice-4G (Peltier, 2004) topography, the climate produced in GENMOM

would be expected to follow from these large forcings. It should not be expected, however, that using the temperature and precipitation climatology from GENMOM for specific time segments, would produce an ice sheet of reasonable comparison to the topography boundary conditions used to simulate the climate in GENMOM, as well as ice-sheet thickness and volume.

Given the limitations in our experimental setup, the sensitivity simulations were unable to assess the relative contribution of insolation and GHG on the deglaciation of the LIS. Recently, Heinemann et. al. (2014) simulate the last deglaciation using an asynchronous ice-sheet-climate modeling approach. Each climate simulation is passed to the ice-sheet model, and the resulting ice-sheet topography feeds back into the next set of climate simulations. This is achieved using transient climate simulation of the last deglaciation from the EMIC, LOVECLIM (Timm et. al., 2007). This method allows the ice sheet and climate to communicate, thus allowing the ice sheet to evolve strictly to the climate in LOVECLIM, and not respond to a climate dictated by prescribed boundary conditions as in our experiment. Performing insolation and CO_2 experiments, Heinemann et. al. (2014) determine the termination of the LIS was forced chiefly by orbitally induced insolation changes at the beginning of the deglaciation. The full deglaciation of the LIS, however, could not be fully achieved without the influence of CO_2, especially into the Holocene. In fact, Heinemann et. al. (2014) find that ice stabilizes into the early Holocene under the insolation only experiment, following decreased insolation into the Holocene.

Our results offer a more subtle approach on the limitations of one-way coupling between an AOGCM and an ice-sheet model. The approach was successful in capturing

an LIS that follows reconstruction from the LGM through the deglaciation. This result confirms the robustness of the climatology produced in GENMOM. Conversely, this method falls short in simulating ice-sheet sensitivity to various forcings. Here the topography boundary conditions, which are used to create the climatology, have an overwhelming influence compared to changing the insolation or GHG boundary conditions. Therefore, as shown in Heinemann et al. (2014), an asynchronous approach is needed to more accurately capture ice-sheet climate interactions. With the advent of coupled ice-sheet climate models (Lipscomb et al., 2013), it will be possible to simulate these interactions in tandem, allowing for the study of various interactions and feedbacks.

10. Acknowledgements

We thank Stephen Price and Matthew Hoffman at Los Alamos National Laboratory for providing us with access to the Glimmer ice-sheet model and for answering questions regarding model setup. We also thank Jeremy Fyke at Los Alamos National Laboratory for providing feedback on the deglaciation simulations. Lastly we thank Lauren Gregoire at the University of Leeds for providing sediment masks, figures, and mapping projections used in the simulation.

11. References

Abe-Ouchi, A., Segawa, T., and Saito, F. 2007. Climatic conditions for modelling the northern hemisphere ice sheets throughout the ice age cycle. Climate of the Past, 3(3), 423–438.

Abe-Ouchi, A., Saito, F., Kawamura, K., Raymo, M.E., Okuno, J, Takahashi, K., Blatter, H. 2013 Insolation-driven 100,000-year glacial cycles and hysteresis of ice-sheet volume**.** *Nature*; 500 (7461): 190 DOI: 10.1038/nature12374

Alder, J. R. and Hostetler, S. W. 2014. Global climate simulations at 3000 year intervals for the last 21 000 years with the GENMOM coupled atmosphere–ocean model, CPD, 10(4), 2925–2978.

Amante, C. and Eakins, B. 2009. ETOPO1 1 Arc-Minute global relief model: Procedures, data sources and analysis. Technical Report 24, NOAA Technical Memorandum NESDIS NGDC.

Berger, A. and Loutre, M. 1992. Astronomical solutions for paleoclimate studies over the last 3 million years. Earth and Planetary Science Letters, 111(2-4), 369–382.

Bonelli, S., Charbit, S., Kageyama, M., Woillez, M., Ramstein, G., Dumas, C., and Quiquet, A. 2009. Investigating the evolution of major northern hemisphere ice sheets during the last glacial-interglacial cycle. Climate of the Past, 5(3), 329–345.

Brook, E. J., S. Harder, J. Severinghaus, E.J. Steig, and C.M. Sucher. 2000, On the origin and timing of rapid changes in atmospheric methane during the last glacial period, Global Biogeochem. Cycles, 14(2), 559–572.

Charbit, S., Ritz, C., Philippon, G., Peyaud, V., and Kageyama, M. 2007. Numerical reconstructions of the northern hemisphere ice sheets through the last glacial-interglacial cycle. Climate of the Past, 3, 15–37.

Dyke, A.S., Dredge, L.A., Vincet, J. 1982. Configuration and Dynamics of the Laurentide Ice Sheet During the Late Wisconsin Maximum. Géographie physique et Quaternaire, Volume 36, issue 1-2, 1982, p.5-14
Dyke, A. S. and Prest, V. K. 1987. Late wisconsinan and holocene history of the laurentide
ice sheet. G ´eographie physique et Quaternaire, 41(2), 237–263.

Dyke, A. S., Moore, A., and Robertson, L. 2003. Deglaciation of north america. Geological Survey of Canada Open File, 1574. Thirty-two digital maps at 1:7 000 000 scale with accompanying digital chronological database and one poster (two sheets) with full map series.

Forster, P., V. Ramaswamy, P. Artaxo, T. Berntsen, R. Betts, D.W. Fahey, J. Haywood, J. Lean, D.C. Lowe, G. Myhre, J. Nganga, R. Prinn, G. Raga, M. Schulz and R. Van Dorland, 2007: Changes in Atmospheric Constituents and in Radiative Forcing.In: Climate Change 2007: The Physical Science Basis. Contribution of Working Group I to the Fourth Assessment Report of the Intergovernmental Panel on Climate Change [Solomon, S., D. Qin, M. Manning, Z. Chen, M. Marquis, K.B. Averyt, M.Tignor and H.L. Miller (eds.)]. Cambridge University Press, Cambridge, United Kingdom and New York, NY, USA.

Ganopolski, A., Calov, R., and Claussen, M. 2010. Simulation of the last glacial cycle with a coupled climate ice-sheet model of intermediate complexity. Climate of the Past, 6(2), 229–244.

Gregoire, L J, A. J. Payne, and P. J. Valdes 2012, Deglacial rapid sea level rises caused by ice-sheet saddle collapses, Nature, 487(7406), 219–222, doi:10.1038/nature11257.

Hebeler, F., Purves, R. S., and Jamieson, S. S. 2008. The impact of parametric uncertainty and topographic error in ice-sheet modelling. Journal of Glaciology, 54, 899–919.

Heinemann, H., Timmermann, A., Timm, O.E., Saito, F., Abe-Ouchi, A. 2014. Deglacial ice–sheet meltdown: orbital pacemaking and CO_2 effects. Clim. Past Discuss., 10, 509-532, doi:10.5194/cpd-10-509-2014

Huybrechts, P. and T'siobbel, S. 1997. A three-dimensional climate-ice-sheet model applied to the last glacial maximum. Annals of Glaciology, 25, 333–339.

Kalnay, E., Kanamitsu, M., Kistler, R., Collins, W., Deaven, D., Gandin, L., Iredell, M., Saha, S., White, G., Woollen, J., Zhu, Y., Chelliah, M., Ebisuzaki, W., Higgins, W., Janowiak, J., Mo, K. C., Ropelewski, C., Wang, J., Leetmaa, A., Reynolds, R., Jenne, R., and Joseph, D. 1996. The NCEP/NCAR 40-year reanalysis project. Bulletin of the American Meteorological Society, 77(3), 437–471.

Laske, G. and Masters, G. 1997. A global digital map of sediment thickness. Eos, Transactions, American Geophysical Union, 78(F483).

Licciardi, J., P.U. Clark, J.W. Jenson, and D.R. Macayeal 1998, Deglaciation of a soft-bedded Laurentide ice sheet, *Quaternary Science Reviews,* 17, 427-448.

Lipscomb, W.H., Fyke, J.G., Vizcaíno, M., Sacks, W.J., Wolfe, J., Vertenstein, M., Craig, A., Kluzek, E., Lawrence, D.M., 2013. Implementation and Initial Evaluation of the Glimmer Community Ice Sheet Model in the Community Earth System Model. J. Climate, 26, 7352–7371. doi: http://dx.doi.org/10.1175/JCLI-D-12-00557.1

Lunt, D., Valdes, P., Haywood, A., and Rutt, I. 2008. Closure of the panama seaway during the pliocene: implications for climate and northern hemisphere glaciation. Climate Dynamics, 30(1), 1–18.

Marshall, S. J., Tarasov, L., Clarke, G. K. C., and Peltier, W. R. 2000. Glaciological reconstruction of the laurentide ice sheet: physical processes and modelling challenges. Canadian Journal of Earth Sciences, 37(5), 769–793.

Marshall, S. J., James, T. S., and Clarke, G. K. C. 2002. North american ice sheet reconstructions at the last glacial maximum. Quaternary Science Reviews, 21(1-3), 175–192.

Monnin, E., A. Indermühle, A. Dallenbach, J. Fluckiger, B. Stauffer, T. F. Stocker, D. Raynaud, and J. M. Barnola 2001, Atmospheric CO2 concentrations over the last glacial termination, *Science*, *291*(5501), 112–114, doi:10.1126/science.291.5501.112.

Pacanowski, R. C.1996. MOM 2 Version 2.0 (Beta) Documentation: User's Guide and Reference Manual, NOAA GFDL Ocean Technical Report 3.2.
Peltier, W. R. 1994, Ice age Paleotopography, *Science*, 265, 195-201.
Rutt, I. C., Hagdorn, M., Hulton, N. R. J., and Payne, A. J. 2009. The glimmer community ice sheet model. Journal of Geophysical Research, 114(F2).

Snyder, J. P. (1987). Map Projections: A Working Manual. Number 1395 in U.S. Geological Survey professional paper. United States Government Printing Office, Washington, D.C.

Sowers, T., Alley, R.B., and Jubenville, J. 2003, Ice Core Records of Atmospheric N2O Covering the Last 106,000 Years, *Science*, 301, 945-948.

Stokes, C. R. and Tarasov, L. 2010. Ice streaming in the laurentide ice sheet: A first comparison between data-calibrated numerical model output and geological evidence. Geophysical Research Letters, 37.

Stone, E. J., Lunt, D. J., Rutt, I. C., and Hanna, E. 2010. Investigating the sensitivity of numerical model simulations of the modern state of the greenland ice-sheet and its future response to climate change. The Cryosphere, 4(3), 397–417.

Tarasov, L. and Peltier, W. R. 2004. A geophysically constrained large ensemble analysis of the deglacial history of the north american ice-sheet complex. Quaternary Science Reviews, 23(3-4), 359–388.

Thompson, S. L. and Pollard, D. 1995. A global climate model (Genesis) with a Land-Surface Transfer Scheme (LSX) .1. Present climate simulation, J. Climate, 8, 732–761.
Timm, O. and Timmermann, A. 2007. Simulation of the last 21 000 years using accelerated transient boundary conditions, J. Climate, 20, 4377–4401. 511, 513

Uppala, S. M., Kallberg, P. W., Simmons, A. J., Andrae, U., Bechtold, V. D., Fiorino, M., Gibson, J. K., Haseler, J., Hernandez, A., Kelly, G. A., Li, X., Onogi, K., Saarinen, S., Sokka, N., Allan, R. P., Andersson, E., Arpe, K., Balmaseda, M. A., Beljaars, A. C.

M., Berg, L. V. D., Bidlot, J., Bormann, N., Caires, S., Chevallier, F., Dethof, A., Dragosavac, M., Fisher, M., Fuentes, M., Hagemann, S., Holm, E., Hoskins, B. J., Isaksen, L., Janssen, P. A. E. M., Jenne, R., McNally, A. P., Mahfouf, J. F., Morcrette, J. J., Rayner, N. A., Saunders, R. W., Simon, P., Sterl, A., Trenberth, K. E., Untch, A., Vasiljevic, D., Viterbo, P., and Woollen, J. 2005. The ERA-40 re-analysis. Quarterly Journal of the Royal Meteorological Society, 131(612), 2961–3012.

Zweck, C. and Huybrechts, P. 2005. Modeling of the northern hemisphere ice sheets during the last glacial cycle and glaciological sensitivity. Journal of Geophysical Research- Atmospheres, 110(D7), –.

Chapter 5

Conclusions

This dissertation is a compilation of three distinct studies, which address major scientific questions in glacial geology, paleoclimatology, and atmospheric science.

5.1 Chapter Summaries

In Chapter 2, we present a new, high-resolution reconstruction of the Holocene deglaciation of the Scandinavian Ice Sheet (SIS). This reconstruction illustrates the asymmetric deglaciation of the SIS, with different areas experiencing rapid retreat in response to various forcings. Early deglaciation in Southern Sweden seems to coincide with the break up of the Norweigan Ice Stream, occurring before the Bolling warm period. In contrast, the eastern Baltic experiences rapid retreat in response to the warming during the Bolling. During the Holocene, southeast Finland rapidly deglaciates, due to a combination of warming and ice dynamics. The location of this portion of the SIS, sharing a margin with the Baltic Ice Lake, allows for enhanced calving, making it more sensitive to post Younger Dryas warming. Accordingly, the Swedish sector experiences rapid retreat, but this is more aligned with warming out of the Younger Dryas. Lastly, we combine new estimates of the SIS contribution to sea-level rise with

data for the Laurentide and Greenland Ice Sheet. This total is subtracted from the modeled eustatic sea-level estimate to yield a residual Holocene sea-level contribution. Based upon our estimates, ~23m of sea-level rise exists at the start of the Holocene, which we relate to an Antarctic source, suggesting more instability of the Antarctic Ice Sheet during the Holocene than previously thought.

The results of chapter 3 offer new insights into the role of the atmospheric circulation on the deglaciation of the Laurentide Ice Sheet. We find that the stationary wave largely affects the Cordilleran ice sheet (CIS) through enhanced moisture advection, while the eastern LIS is primarily affected by the storm track. Over the CIS, an enhanced stationary wave exists, as a result of the large topography forcing of the LIS within the mean flow. This results in increased accumulation over the CIS, and a positive feedback whereby increased ice thickness promotes a stronger stationary wave. Over the eastern LIS, the storm track dominates. At the start of the deglaciation, storm activity is weakened relative to present day. Through the deglaciation, however, the storm track strengthens as the ice area decreases, constituting a negative feedback. As the storm track strengthens and broadens though, wintertime accumulation is enhanced greatly. This additional mass during winter, provided by the storm track, may have played a potentially important role in modulating the high ablation during summer. We propose that this mechanism may have possibly allowed the eastern LIS to maintain itself longer throughout the deglaciation, and may explain why the LIS terminated over eastern North America.

In chapter 4, a simulation of the last deglaciation is carried out by one-way coupling the climate model, GENMOM to the ice-sheet model Glimmer. To ensure a

realistic LIS ice sheet was developed for the deglaciation experiments, parameter testing was performed to maximize the best fit LGM LIS between the best available reconstructions of LIS area and volume. Of the parameters testing, the basal sliding and positive degree day factors were shown to affect the ice sheet area and volume the most. Using a varying basal sliding mask, the formation of domes was possible within the LIS. Using this as our starting point at the LGM, climate was forced onto the ice sheet through the deglaciation at 3ka intervals. The resulting deglaciation followed reconstructions well, and proved the usefulness of the GENMOM climatology in capturing the deglaciation. We lastly evaluated the role of CO_2 and insolation through fixed boundary condition experiments. The resulting deglaciation for the CO_2 and insolation only climate forcings were very similar. Instead the topography boundary condition used to simulate climate in GENMOM seems to impact the overall climate forcings greatly, and is the main driver of the changes in climatology used to simulate the ice-sheet evolution. From this, we show that to properly evaluate the role of CO_2 and insolation, an asynchronous ice-sheet-climate modeling approach should be taken at the very least. At best, coupled ice-sheet-climate simulations need to be performed.

5.2. General Conclusions

The study of paleoclimatology seeks to provide a context for present and future changes to our climate system by studying how the climate system responded to forcings during the past. The findings presented in this thesis offer new insights into ice-sheet atmosphere interactions during the last deglaciation over the Laurentide Ice Sheet, and document the response of the Scandinavian ice sheet to climate change during the

Holocene, allowing for new insights into the response of the Antarctic ice-sheet during this interval.

Building upon past research highlighting the intimate coupling of the LIS and the atmospheric circulation, our findings add to previous analysis of interaction between the LIS topography and the glacial atmospheric circulation, particularly the storm track and stationary waves. Unlike previous studies, however, this analysis benefitted from the use of climate simulations throughout the last deglaciation, thus providing an understanding of feedbacks between the two as the ice sheet extent and volume decreased during the last deglaciation. These results highlight that although the demise of the large northern hemisphere ice sheets were forced primarily through changes in insolation and CO_2, the atmospheric reorganization with respect to the wintertime storm track and stationary wave can have a large influence on the pattern of deglaciation across the LIS. This not only has implications for the study of the deglaciation of the LIS, but also confirms the intimate coupling between the ice-sheet topography and the atmospheric circulation. These results, although they do not offer direct context towards future ice-sheet-atmosphere dynamics, do highlight the important role the atmosphere can play in shaping the trajectory of ice sheets, especially given the expected changes in the atmospheric circulation as a response to a warming climate, and the important role that atmosphere plays in heat and moisture transport globally.

This thesis also presents results reconstructing the first high-resolution ^{10}Be chronology for the Scandinavian Ice Sheet retreat during the Holocene. The chronology presented in this thesis has been combined with the existing chronology extending back to the Last Glacial Maximum to provide a novel perspective on the deglaciation of the

SIS. Once thought of as having a symmetric deglaciation pattern through time, the new SIS reconstruction shows instead an asymmetric deglaciation punctuated by episodes of rapid deglaciation along different sectors of the ice sheet at different time intervals. The results highlight the role of climate and ice dynamics in influencing the pattern of deglaciation.

Furthermore, reconstructing the deglaciation of the SIS allows for a closure to the budget of Northern hemispheric ice-sheet contribution to Holocene sea-level rise. Knowing the contributions from reconstructions for the Laurentide and Greenland ice sheet, along with the new data from the SIS, an assessment has been made as to the remaining source of Holocene sea-level rise. The remaining 23m of sea-level rise at 13 ka could only have come from Antarctica. Prior work has indicated that Antarctica remained relatively stable during the Holocene, however, this data was very limited in spatial and temporal resolution. Therefore, since little direct evidence exists constraining the sensitivity of Antarctica during the Holocene, this estimate provided in this thesis concludes a large Antarctic source is needed to close the sea-level budget. This would suggest Antarctica has remained less stable than previously thought during the Holocene, and may have implications for its sensitivity into the future.

Appendices

Appendix A - A high-resolution ^{10}Be chronology for the final deglaciation of the Scandinavian Ice Sheet and implications for Holocene sea-level rise

A.1 Field Sampling Methods

Our sampling was performed on large glacial erratic boulders, primarily of granitic or gneissic lithology. To limit the impact of post-depositional movement, we sampled erractic boulders greater than 1 m in diameter, which rested on stable geomorphic surfaces with minimal till cover, and in many cases rested on bedrock. Erratics sampled in Southern Sweden and Finland resided under forested canopy, while sites to the North in Finland and Sweden were sampled amongst sparse vegetation. Many sites in southern Sweden and Finland, and sites to the North near the Baltic Sea experienced submergence as the Baltic Ice Lake evolved towards the present day Baltic Sea following isostatic depression and rebound (Andren et. al., 2011). Accordingly, we sampled above the highest shoreline to avoid the impact of shielding that would have otherwise taken place during post-glacial submersion.

Sample collection was performed using a hammer and chisel, with samples taken from the top of the boulders, making sure to not sample along any sides, which would have been shielded. Care was also taken to avoid sampling heavily eroded surfaces exhibiting pitting and spallation. Geographic location and elevation were recorded using a handheld GPS (Table A1-A4). Because of the low relief topography of our sampling sites, topographic shielding was not an issue in our age calculation.

A.2. Sampling Processing

Sample preparation and Beryllium isolation was performed at the Cosmogenic Isotope Laboratory at Oregon State University. Rock samples were crushed and sieved to isolate the 250-710 μm fraction. Mafic grains were removed using a Frantz magnetic separator. Samples were then leached in HCL and dilute solutions of HNO_3 and HF repeatedly until sufficient quartz purity was reached, as determined by measurements on the ICP-OES at the University of Colorado-Boulder.

Anion exchange, cation exchange, and pH adjustment steps were performed to isolate the beryllium. A reference 0.8 mg ^{9}Be spike was added to each sample. This spike was developed at Oregon State University and has an average blank ratio of $1.0x10^{-15}$ (n=17). During each sample batch a procedural blank was processed to measure background levels of contamination in the cosmogenic lab. $^{10}Be/^{9}Be$ ratios were measured by accelerator mass spectrometry at PRIME Laboratory at Purdue University.

A.3. Exposure age calculation

^{10}Be ages were calculated using the CRONIS-Earth online calculator (v2.2) (Balco et al., 2008). Inputs needed to calculate ages are given in tables A1-A4. We use the Western Norway regional production rate of Goehring et al. (2012). We choose this production rate primarily for its proximity to our sites, making it most applicable versus other calibration datasets that reside geographically further away. For comparison, the Arctic production rate from Young et al. (2013) is 3.96±0.15 atoms g^{-1} yr^{-1} versus

4.26±0.13 atoms g^{-1} yr^{-1} for the Western Norway production. Young et al. (2013) argue for the Arctic production rate being used in its non-uplift corrected state following from closer agreement between the true ages and predicted ages used in their dataset, and for the agreement with one site which only experienced marginal uplift. Young et al. (2013) state that an uplift corrected Arctic production rate will become 4-4.5% higher. Therefore, accounting for this additional correction makes the Arctic and W. Norway production rates almost identical.

Ages and uncertainties are presented in table A5-A8 for each of the 5 scaling schemes (St: Lal (1991) and Stone (2000); De: Desilets et al. (2006); Du: Dunai (2001); Li: Lifton et al. (2005); and Lm: Lal (1991) and Stone (2000), time dependent scheme). We choose the Lm scaling method for the presentation of our ages, although using other scaling schemes does not significantly alter the results or interpretations of our ages. Where applicable, prior published chronologies are recalculated using the W. Norway production rate, and are shown in table S3a-e.

A.4. Sample averaging and removal of outliers

At site Swe-5, a complex exposure history yields ages that are too old. Swe-35/36/38 and Swe-41 are labeled outliers as the ages are too old and do not fit within the stratigraphic chronology that is known for the deglaciation of the SIS. Before applying statistical methods to eliminate outliers, we first test that our samples fall within a normally distributed population, using a Shapiro-Wilk test for normality. Samples with ages or uncertainties 3 or more standard deviations outside of the site mean are labeled outliers. After performing this test, we disregard 5 samples (see Table A1-A4). Next, we

identify 8 statistical outliers (see Table A1-A4) using Chauvenet's criterion, conditioned by samples that have <50% probability of falling within the normal distribution of the sample population following Rinterknecht et al. (2006).

Our criterion for presenting ages and uncertainties involves addressing the geologic uncertainty and analytic uncertainty of our sample populations. The geologic uncertainty is defined as the standard deviation of the boulder ages for each given site. This is compared to the analytic uncertainty, defined by the internal uncertainty of each sample age, which accounts for measurement uncertainty. In the case that the geologic uncertainty is larger than the analytic uncertainty, the site age is defined by the straight mean of the sample population and the standard error of the ages. Conversely, when the analytic uncertainty is larger than the geologic uncertainty, we define the site age as the error weighted mean of the sample population and the error weighted uncertainty (of the internal uncertainty).

A.5. Time-distance transects

To assess SIS retreat rates, we sampled perpendicular to mapped ice retreat contours (Lundqvist, 1986; Lunkka et al., 2004). Although the ice margin retreat may not have followed this trajectory perfectly, it serves as a decent metric for evaluating ice margin retreat rates. We draw 3 distinct transects for our analysis shown in Figure A1: Sweden transect (Black), Finland transect (Red), Northern Finland transect (Blue). The Sweden and Finland transect each begin at the dated LGM moraine in the Southern Baltic region (Rinterknecht et. al., 2008), and continue perpendicular to the ice retreat contours before terminating in Northwestern Sweden. The Northern Finland transect begins at the

Finland/Norway boarder and terminates in Northwestern Sweden. In the case that a sampled site does not lie on the transect, we project the age and uncertainty at that particular site along the ice retreat contour onto the transect.

To describe our ages in context with the Northern Hemisphere climate, we compare our time-distance diagram to the 30-90°N temperature stack derived from Marcott et. al., (2013) for the period during the Holocene, and Shakun et. al., (2012) for the period extending back to the LGM. This temperature stack is a compilation of numerous temperature proxies distributed amongst the Atlantic basin, and is drawn as the anolmaly from present day temperature. Because the age control points from these studies are primarily derived from ^{14}C dating of organic material, our errors reflect the external uncertainty, which account for the production rate uncertainty (see description of sample averaging in previous section).

A.6. Probablity distribution functions (Pdf's)

In the case of our site mean ages, we assume that all ages in those populations date the same retreat of the ice sheet from that given location. By representing the ages as a probability distribution (Figure A2), we can assess the distribution of those ages at given sites more closely. Accordingly the ages and uncertainties are represented by their respective Gaussian curves, given by the equation:

$$(1) \qquad y = \frac{1}{\sqrt{2\pi\sigma^2}} \exp\left[\frac{-(x-\mu)^2}{2\sigma^2}\right]$$

Where μ is the mean and σ is the standard deviation. These individual pdfs's are shown in red for each site. To obtain the total pdf (shown as the black curve), we simply add each individual pdf. The black curve allows for a representation of the maximum likelihood of the particular sites age, given the individual distributions of each sample.

In Figure A2, we notice that for the exception of sites Swe-3, Swe-7, and Fin-6, all sites share a single peak. Because many of the sites individual frequency distributions overlap, this gives us confidence that each sample is measuring the same event. For completeness, we show alongside of each pdf, the peak age of the total pdf, the mean age of the site (shown as blue line) and the standard error, the median of each site population, and the error weighted mean age with the error weighted uncertainty. The shaded bars represent the 1 and 2 standard deviations of the ages.

A.7 Estimate of ice volume and sea-level contribution

Beginning at 14.5ka, we estimate the SIS volume and sea level contribution throughout the remainder of the deglaciation using our newly established chronology. We split up the SIS retreat into 5 time intervals: 14.5ka, 13.5ka, 12ka, 11ka, 10.5ka (see Figure A3). Extending the volume estimates past 14.5ka would increase uncertainty as little chronology is established for the SIS retreat over the Nordic Sea and parts of Russia. Therefore, we use this newly established chronology and existing chronology to draw areas for the SIS over these time intervals. The areas drawn are bounded by the nearest age constraint at particular sites. Where there are no ages to constrain the area, we follow the mapped ice retreat contours to the site closest in age to the particular area interval

being drawn. In this regard, the ice-sheet areas are bounded by the nearest chronology and the mapped ice retreat.

To estimate the volume we use the area to volume scaling of Paterson (1994). This scaling was determined empirically through regression by using volume and area measurements on a logarithmic scale from Antarctica, Greenland, and other small ice caps, which all reside in distinct temperate, maritime, and polar climates. The relationship assumes a simplified circular ice cap, which is a reasonable with respect to the SIS during this time interval. This relationship also assumes that the ice sheet is resting on hard bedrock, making this a maximum estimate for volume. The equation used is:

$$\log(V) = 1.23(\log(A) - 1) \quad (2)$$

where V is the ice cap volume in km^3, and A is the areal extent in km^2. The uncertainty on this estimate is ±12%. Once volumes are calculated using the Paterson (1994) area-volume scaling, we convert to equivalent sea level by dividing the volumes by the global ocean volume 3.61×10^8 km^2.

To derive the LIS contribution to the estimated sea-level contribution, we use values from Carlson et al. (2008). These include reconstructions from Dyke (2004) for the Innuition and Keewatin domes, with revised chronology over the Labrador sector from Carlson et al. (2008). This chronology is extended and refined using ^{10}Be chronology from Ullman et al. (Submitted) over the Labrador sector, which constrains the final termination of the LIS with associated meltwater pulses, particularly at 8.2ka.

Once the SIS and LIS contributions to Holocene sea-level are constrained, we use the eustatic sea-level curve from Lambeck et al. (2014) to derive the remainder. Using ~1000 relative sea-level observations and near-field analyses for the northern hemisphere ice sheets over the past 35 ka, Lambeck et al. (2014) use an Earth Model to derive an ESL curve for the past 35ka. The data provided uses the high-viscosity lower-mantle solution.

From the ESL curve, the sea-level contributions are combined for the LIS and SIS, with errors added in quadrature, to calculate the remainder. Retreat rates are calculated as the sea-level difference between each successive time interval, divided by the time elapsed during that interval.

Table A.1. Cosmogenic sample inputs for the CRONUS calculator (Balco et. al., 2008) for Sweden transect

Sample	Latitude (DD)	Longitude (DD)	Modern Elevation (m asl)	Corrected Elevation (m)[b]	Thickness (cm)	Density	Quartz (g)	Mass ^{9}Be added (10^{-4}g)	^{10}Be/^{9}Be ratio (10^{-15})[c]	Uncertainty (10^{-15})[d]	^{10}Be (atoms g^{-1})[e]	Uncertainty (atoms g-1)	^{10}Be age (ka)	Site mean age (ka)[f,,i]
Southern Sweden														
Swe-1														
Swe-03	58.9408	14.8900	240.487	190.487	2	2.65	36.269	0.787	1.31E-13	6.50E-15	67516	3395	13.1 (0.7)	**13.3 (0.2)**
Swe-06	58.9408	14.8900	232.258	182.258	2	2.65	36.264	0.787	1.49E-13	4.10E-15	68733	1931	13.4 (0.4)	
Swe-07	58.71	14.6	232.25	182.25	2	2.65	29.8545	0.7848	1.00E-13	1.40E-14	62886	8804	12.3 (1.7)	
Swe-08	58.71	14.6	232.25	182.25	2	2.65	40.6485	0.8568	1.31E-13	5E-15	66056	2521	13.0 (0.5)	
Swe-2														
Swe-10	59.8	14.4	220	165	2	2.65	44.268	0.822	1.43E-13	6.00E-15	63367	2659	12.6 (0.5)	**12.6 (0.2)**
Swe-12	59.8	14.4	216	161	2	2.65	40.1092	0.8629	1.02E-13	4E-15	62438	2449	12.5 (0.5)	
Swe-13	59.75	14.4	203	148	2	2.65	41.574	0.859	1.02E-13	4.00E-15	62438	2449	12.7 (0.5)	
Swe-14	59.75	14.4	203	148	2	2.65	40.0512	0.8126	1.20E-13	6.00E-15	57902	2916	11.7 (0.6)	
Swe-17	59.75	14.4	188	133	2	2.65	41.898	0.82	1.4E-13	6E-15	65127	2828	13.4 (0.6)	
Swe-3														
Swe-18	60.6950	14.2000	270.053	210.053	2	2.65	49.478	0.8051	1.49E-13	3.80E-15	57645	1659	11.0 (0.3)	**11.1 (0.5)**
Swe-19	60.6950	14.2000	276	216	2	2.65	40.5867	0.8098	1.38E-13	6.00E-15	65436	3185	12.4 (0.6)	
Swe-25	60.6	14.1	267	207	2	2.65	40.7351	0.8629	1.11E-13	4.00E-15	55931	2246	10.7 (0.4)	
Swe-4														
Swe-26	61.62	14.85	423	323	2	2.65	40.8057	0.8629	1.34E-13	5.60E-15	67357	2818	11.4 (0.5)	**11.0 (0.2)**
Swe-27	61.61	14.83	422	322	2	2.65	40.394	0.7942	1.44E-13	7.00E-15	67392	3644	11.4 (0.6)	
Swe-30	61.61	14.83	428.5	328.5	2	2.65	40.65977	0.8136	1.37E-13	6E-15	65580	2872	11.0 (0.5)	
Swe-31	61.61	14.83	430	330	2	2.65	41.0617	0.8584	1.31E-13	4E-15	65197	2217	11.0 (0.4)	
Swe-33	61.61	14.83	429.8	329.8	2	2.65	40.8032	0.8112	1.34E-13	5.00E-15	63395	2382	10.7 (0.4)	
Swe-5														
Swe-42 (2)[g]	65.2210	19.6580	345.033	255.033	2	2.65	41.552	0.818	1.34E-13	4.6E-15	62683	2191	11.2 (0.4)	**11.3 (0.2)**
Swe-42	65.2210	19.6580	345.033	255.033	2	2.65	40.3924	0.851	1.4E-13	4E-14	70561	20160	12.6 (3.6)	
Swe-43	65.2210	19.6580	243	153	2	2.65	34	0.8192	9.40E-14	1.00E-14	54181	5764	11.3 (0.5)	
Swe-44	65.01	19.4	247	157	2	2.65	65.01	19.4	7.7E-14	4E-15	57736	2999	11.5 (1.0)	
Swe-45	65.01	19.4	239	149	2	2.65	44.39	0.8245	1.28E-13	6E-15	56875	2666	10.7 (1.1)	
Swe-46	65.01	19.4	249	159	2	2.65	6.6	0.8762	2.40E-14	1.31E-15	58480	5050	11.4 (0.6)	
Swe-48[h]	65.2210	19.6580	245.364	155.364	2	2.65	40.7131	0.8091	2.1E-13	4.10E-15	99405	1978	19.7 (0.4)	

[a] Age calculations use standard atmosphere, density of 2.65 g cm^{-3}, and zero erosion. Due to low topographic variation of sampling sites, no shieldiing correcdtion is necessary.

[b] Isostatic uplift correction is estimated by subtracting half of the total uplift from the modern elevation (Ristaniemi et al., 1987; Hendenstrom and Risberg, 1999; Eronen et al., 2000; Saarnisto, 2001; Berglund et al., 2005, Linden et al., 2006; Rosentau et al., 2012)

[c] All measurements are standardized to 07KNSTD.

[d] 1-sigma AMS uncertainty

[e] ^{10}Be atom conecntrations are blank-corrected (see text).

[f] Ages were calculated using the Cronus Earth online calculator (v 2.2) with the Western Norway production rate and the Lal/Stone time-dependent scaling scheme.

[g] Ages exluded based on ages/uncertainty 4 std's outside of the mean.

[h] Ages excluded using Chauvenet's criterion.

[i] Site mean age and uncertainty is calculated as either the straight mean and standar error or the error weighted age and error weighted uncertainty based on the geologic and analytic uncertainty (see text).

[J] Ages exlcuded based an too old age to be consistent with stratigraphical retreat of SIS.

[RR] Site excluded from analysis based on inherited ages.

Table A.2. Cosmogenic sample inputs for the CRONUS calculator (Balco et. al., 2008) for Sweden transect continued

Sample	Latitude (DD)	Longitude (DD)	Modern Elevation (m asl)	Corrected Elevation (m)[b]	Thickness (cm)	Density	Quartz (g)	Mass ^{9}Be added (10^{-4}g)	^{10}Be/^{9}Be ratio (10^{-15})[c]	Uncertainty (10^{-15})[d]	^{10}Be (atoms g^{-1})[e]	Uncertainty (atoms g-1)	^{10}Be age (ka)	Site mean age (ka)[f,,i]
Northern Sweden														
Swe-6														
Swe-51	65.76	18.5	461	381	2	2.65	40.0208	0.8655	1.27E-13	5E-15	65704	2587	10.4 (0.4)	**10.4 (0.2)**
Swe-53[h]	65.79	18.51	475	395	2	2.65	44.585	0.816	1.7E-13	6E-15	74431	2627	11.6 (0.4)	
Swe-55	65.76	18.5	496.5	416.5	2	2.65	42.972	0.8077	1.48E-13	9E-15	66548	4047	10.1 (0.6)	
Swe-56	65.76	18.5	490	410	2	2.65	34.7007	0.8946	1.12E-13	8.00E-15	69074	4934	10.6 (0.8)	
Swe-57	65.79	18.51	475	395	2	2.65	43.671	0.837	1.41E-13	1.00E-14	69074	4585	10.7 (0.7)	
Swe-7														
Swe-59	66.7	16.1	640	560	2	2.65	31	0.8556	1.25E-13	4.00E-15	82532	2641	10.9 (0.4)	**10.2 (0.2)**
Swe-61	66.7	16.3	640	560	2	2.65	25.7593	0.868	8.5E-14	4.00E-15	68519	3224	9.1 (0.4)	
Swe-62	66.7	16.05	640	560	2	2.65	20.25	0.8124	8.1E-14	7E-15	77739	6718	10.3 (0.9)	
Swe-63	66.7	16.3	640	560	2	2.65	20.2031	0.8697	6.3E-14	6E-15	64878	6179	8.6 (0.8)	
Swe-8														
Swe-66[h]	66.7	19.8	438	368	2	2.65	40.5494	0.8665	1.30E-13	7.80E-15	52654	3987	8.4 (0.6)	**10.0 (0.2)**
Swe-67	66.6	19.8	298.4	228.4	2	2.65	40.703	0.864	1.04E-13	5.00E-15	52492	2812	9.6 (0.5)	
Swe-72[g]	66.58	19.86	300	230	2	2.65	32.8072	0.8215	8.30E-14	2.40E-14	49618	15902	9.1 (2.9)	
Swe-73	66.69	19.865	290.8	220.8	2	2.65	40.3262	0.8671	1.08E-13	5.00E-15	55471	2851	10.2 (0.5)	
Swe-75	66.5000	19.8000	283	213	2	2.65	41.8646	0.827	1.14E-13	8E-15	53452	3795	9.9 (0.7)	
Swe-76	66.69	19.865	290.8	220.8	2	2.65	40.3262	0.8671	1.08E-13	5E-15	55553	2572	10.2 (0.5)	
Swe-9[RR]														
Swe-35	62.4960	14.6460	400.202	320.202	2	2.65	41.2293	0.8159	2.25E-13	6.20E-15	106090	2954	18.0 (0.5)	---------
Swe-36	62.41	14.6	375	295	2	2.65	40.0578	0.8127	1.98E-13	6.00E-15	96098	2912	16.7 (0.5)	
Swe-38	62.4960	14.6460	363.016	283.016	2	2.65	38.1463	0.7848	3.09E-13	4.60E-15	155967	2106	27.5 (0.4)	
Swe-39	62.41	14.6	363.9	283.9	2	2.65	38.1463	0.7848	1.20E-13	7E-15	59060	3445	10.4 (0.6)	
Swe-41	62.41	14.6	357	277	2	2.65	26.834	0.8601	1.76E-13	7E-15	134953	5367	23.9 (1.0)	

[a] Age calculations use standard atmosphere, density of 2.65 g cm^{-3}, and zero erosion. Due to low topographic variation of sampling sites, no shieldiing correcdtion is necessary.

[b] Isostatic uplift correction is estimated by subtracting half of the total uplift from the modern elevation (Ristaniemi et al., 1987; Hendenstrom and Risberg, 1999; Eronen et al., 2000; Saarnisto, 2001; Berglund et al., 2005, Linden et al., 2006; Rosentau et al., 2012)

[c] All measurements are standardized to 07KNSTD.

[d] 1-sigma AMS uncertainty

[e] ^{10}Be atom conecntrations are blank-corrected (see text).

[f] Ages were calculated using the Cronus Earth online calculator (v 2.2) with the Western Norway production rate and the Lal/Stone time-dependent scaling scheme.

[g] Ages exluded based on ages/uncertainty 4 std's outside of the mean.

[h] Ages excluded using Chauvenet's criterion.

[i] Site mean age and uncertainty is calculated as either the straight mean and standar error or the error weighted age and error weighted uncertainty based on the geologic and analytic uncertainty (see text).

[j] Ages exlcuded based an too old age to be consistent with stratigraphical retreat of SIS.

Table A.3. Cosmogenic sample inputs for the CRONUS calculator (Balco et. al., 2008) for Finland transect

Sample	Latitude (DD)	Longitude (DD)	Modern Elevation (m asl)	Corrected Elevation (m)[b]	Thickness (cm)	Density	Quartz (g)	Mass ^{9}Be added (10^{-4}g)	^{10}Be/^{9}Be ratio (10^{-15})[c]	Uncertainty (10^{-15})[d]	^{10}Be (atoms g^{-1})[e]	Uncertainty (atoms g-1)	^{10}Be age (ka)	Site mean age (ka) [f,,i]
Southern Finland														
Fin-1														
Fin-01	61.0760	26.8060	126	71	2	2.65	41.8646	0.7836	1.2029E-13	6.542E-15	53244	3249	11.7 (0.7)	**11.9 (0.3)**
Fin-02	61.0760	26.8060	126	71	2	2.65	31.0601	0.7814	9.1744E-14	7.0003E-15	54384	4672	11.9 (1.0)	
Fin-05	61.0700	26.8000	124	69	2	2.65	41.4552	0.8598	1.08E-13	5.00E-15	53272	2747	11.7 (0.6)	
Fin-08	61.0600	26.8000	137.7	82.7	2	2.65	41.0152	0.7988	1.21E-13	5.00E-15	56041	2580	12.1 (0.6)	
Fin-2														
Fin-10	61.8120	27.2470	128	73	2	2.65	40.7527	0.781	1.1692E-13	4.6827E-15	52971	2388	11.6 (0.5)	**12.1 (0.3)**
Fin-11	61.8120	27.2470	128	73	2	2.65	38.8052	0.7844	1.1498E-13	6.2775E-15	54935	3367	12.0 (0.7)	
Fin-14	61.8000	27.2300	129	74	2	2.65	24.7929	0.8555	7.10E-14	2.80E-15	58084	2567	12.7 (0.8)	
Fin-15	61.8000	27.2300	129	74	2	2.65	31.467	0.8546	8.60E-14	6.00E-15	55462	4315	12.1 (1.0)	
Fin-3														
Fin-19[h]	62.5500	26.0000	174	114	2	2.65	41.1498	0.8701	8.60E-14	1.00E-14	43074	5604	8.7 (1.1)	**12.0 (0.3)**
Fin-17	62.5500	26.0000	174	114	2	2.65	25.7845	0.8755	7.57E-14	3.99E-15	59867	3624	12.5 (0.9)	
Fin-20	62.5500	26.0000	174	114	2	2.65	20.9552	0.8794	5.83E-14	2.35E-15	56582	2690	11.8 (0.7)	
Fin-22	62.5500	26.0000	174	114	2	2.65	35.68	0.8286	1.04E-13	3.76E-15	57778	2089	12.0 (0.6)	
Fin-23	62.5500	26.0000	178.3	118.3	2	2.65	28.9444	0.857	8.10E-14	4.00E-15	56924	3140	11.8 (0.8)	
Fin-4														
Fin-25[g]	63.2300	24.6340	210	140	2	2.65	39.7263	0.7843	2.7496E-13	6.3095E-14	129213	36820	26.2 (7.5)	**12.1 (0.3)**
Fin-25 (2)[h]	63.2300	24.6340	210	140	2	2.65	33.9406	0.868	1.12E-13	7.00E-15	68003	4754	13.8 (1.0)	
Fin-28	63.2300	24.6350	194	124	2	2.65	41.7535	0.7831	1.31E-13	4.535E-15	58160	2264	12.0 (0.5)	
Fin-29	63.2300	24.6350	194	124	2	2.65	25.8	1.032	7.90E-14	8.00E-15	56331	6407	11.6 (1.3)	
Fin-30	63.2300	24.6350	194	124	2	2.65	38.976	0.842	1.20E-13	7.47E-15	62016	3860	12.8 (0.8)	
Fin-31	63.2300	24.6350	194	124	2	2.65	34.7473	0.8568	1.09E-13	7.47E-15	58949	4409	12.1 (0.9)	

[a] Age calculations use standard atmosphere, density of 2.65 g cm^{-3}, and zero erosion. Due to low topographic variation of sampling sites, no shieldiing correcdtion is necessary.

[b] Isostatic uplift correction is estimated by subtracting half of the total uplift from the modern elevation (Ristaniemi et al., 1987; Hendenstrom and Risberg, 1999; Eronen et al., 2000; Saarnisto, 2001; Berglund et al., 2005, Linden et al., 2006; Rosentau et al., 2012)

[c] All measurements are standardized to 07KNSTD.

[d] 1-sigma AMS uncertainty

[e] ^{10}Be atom conecntrations are blank-corrected (see text).

[f] Ages were calculated using the Cronus Earth online calculator (v 2.2) with the Western Norway production rate and the Lal/Stone time-dependent scaling scheme.

[g] Ages exluded based on ages/uncertainty 4 std's outside of the mean.

[h] Ages excluded using Chauvenet's criterion.

[i] Site mean age and uncertainty is calculated as either the straight mean and standar error or the error weighted age and error weighted uncertainty based on the geologic and analytic uncertainty (see text).

[j] Ages exlcuded based an too old age to be consistent with stratigraphical retreat of SIS.

Table A.4. Cosmogenic sample inputs for the CRONUS calculator (Balco et. al., 2008) for Finland transect continued

Sample	Latitude (DD)	Longitude (DD)	Modern Elevation (m asl)	Corrected Elevation (m)[b]	Thickness (cm)	Density	Quartz (g)	Mass ^{9}Be added (10^{-4}g)	^{10}Be/^{9}Be ratio (10^{-15})[c]	Uncertainty (10^{-15})[d]	^{10}Be (atoms g^{-1})[e]	Uncertainty (atoms g-1)	^{10}Be age (ka)	Site mean age (ka) [f,,i]
Northern Finland														
Fin-5														
Fin-44	70.0700	27.7100	65	30	2	2.65	28.956	0.822	7.80E-14	7.00E-15	53244	3249	11.8 (0.7)	**12.1 (0.3)**
Fin-45	70.0700	27.7100	50	15	2	2.65	50.332	0.832	1.10E-13	1.90E-14	54384	4672	12.3 (1.1)	
Fin-46	70.1600	27.7000	52.42	17.42	2	2.65	28.72	0.8774	7.26E-14	4.30E-15	51642	3508	11.6 (0.9)	
Fin-47	70.1600	27.7000	52.42	17.42	2	2.65	28.18	0.8723	8.02E-14	4.95E-15	57887	4083	13.0 (1.1)	
Fin-48	70.1700	27.8000	55.5	20.5	2	2.65	43.4074	0.8473	1.07E-13	5.00E-15	53272	2747	12.0 (0.8)	
Fin-6														
Fin-49	68.1950	26.9870	154	74	2	2.65	45.2531	0.7862	1.2415E-13	4.8706E-15	51028	2250	10.9 (0.5)	**11.9 (0.8)**
Fin-50	68.1950	26.9870	154	74	2	2.65	30.698	1.032	7.80E-14	7.00E-15	50241	3375	10.8 (0.7)	
Fin-51	68.1950	26.9870	154	74	2	2.65	42.4352	0.7817	1.1466E-13	6.9074E-15	49919	1850	10.7 (0.4)	
Fin-54	68.9000	26.9800	154.29	74.29	2	2.65	44.0745	0.8568	1.26E-13	8.48E-15	58466	3945	12.5 (0.8)	
Fin-56	68.9000	26.9800	154.29	74.29	2	2.65	44.8604	0.8119	1.57E-13	8.00E-15	67670	3833	14.4 (0.8)	
Fin-7														
Fin-15-11	66.38	24.33	188	98	2	2.65	34.968	0.812	9.50E-14	3.10E-15	52774	1722	11.1 (0.4)	**11.1 (0.3)**
Fin-16-11	66.38	24.33	188	98	2	2.65	40.5443	0.8757	1.03E-13	7.50E-15	53258	3874	11.1 (0.8)	
Fin-17-11	66.38	24.33	188	98	2	2.65	40.1	0.8601	1.14E-13	4.00E-15	58171	2275	12.2 (0.5)	
Fin-18-11	66.38	24.33	189.9	99.9	2	2.65	40.0914	0.8529	1.04E-13	8.00E-15	52845	4507	11.1 (0.9)	
Fin-19-11[h]	66.38	24.33	189.9	99.9	2	2.65	40.2385	0.8507	1.30E-13	7.93E-15	65708	4010	13.8 (0.8)	
Fin-20-11	66.38	24.33	192	102	2	2.65	34.954	0.8102	9.80E-14	4.00E-15	53950	2459	11.3 (0.5)	
Fin-21-11	66.38	24.33	192	102	2	2.65	40.799	0.8448	9.70E-14	5.00E-15	47967	2746	10.0 (0.6)	
Fin-8														
Fin-08-11[h]	66.42	27.12	209	109	2	2.65	20.2572	0.8719	1.40E-13	4.00E-14	143284	45557	29.8 (9.6)	**11.1 (0.2)**
Fin-09-11	66.42	27.12	209	109	2	2.65	32.987	0.784	9.50E-14	7.00E-15	54014	3980	11.2 (0.8)	
Fin-10-11[g]	66.42	27.12	210.3	110.3	2	2.65	47.904	0.784	1.57E-13	2.22E-14	61183	9614	12.7 (2.1)	
Fin-12-11	66.42	27.12	210.3	110.3	2	2.65	38.1879	0.8695	1.02E-13	7.71E-15	55558	4200	11.5 (0.9)	
Fin-13-11[h]	66.42	27.12	209	109	2	2.65	40.0853	0.8768	1.51E-13	4.00E-15	78574	2340	16.3 (0.5)	
Fin-14-11	66.42	27.12	209	109	2	2.65	38.872	0.782	1.10E-13	3.20E-15	52938	1540	11.0 (0.3)	

[a] Age calculations use standard atmosphere, density of 2.65 g cm^{-3}, and zero erosion. Due to low topographic variation of sampling sites, no shieldiing correcdtion is necessary.

[b] Isostatic uplift correction is estimated by subtracting half of the total uplift from the modern elevation (Ristaniemi et al., 1987; Hendenstrom and Risberg, 1999; Eronen et al., 2000; Saarnisto, 2001; Berglund et al., 2005, Linden et al., 2006; Rosentau et al., 2012)

[c] All measurements are standardized to 07KNSTD.

[d] 1-sigma AMS uncertainty

[e] ^{10}Be atom conecntrations are blank-corrected (see text).

[f] Ages were calculated using the Cronus Earth online calculator (v 2.2) with the Western Norway production rate and the Lal/Stone time-dependent scaling scheme.

[g] Ages exluded based on ages/uncertainty 4 std's outside of the mean.

[h] Ages excluded using Chauvenet's criterion.

[i] Site mean age and uncertainty is calculated as either the straight mean and standar error or the error weighted age and error weighted uncertainty based on the geologic and analytic uncertainty (see text).

[j] Ages exlcuded based an too old age to be consistent with stratigraphical retreat of SIS.

Table A.5. Cosmogenic age results for Sweden in kilo annum (ka) for the different latitude/altitude scaling schemes from the CRONUS Calculator (Balco et. al., 2008)

Sample	Internal Uncertainty	Lal/Stone Constant	External Uncertainty	Desilets	External Uncertainty	Dunai	External Uncertainty	Lifton	External Uncertainty	Lal/Stone Time Varying	External Uncertainty
Sweden											
Swe-1											
Swe-03	0.7	13.1	0.8	13.2	0.8	13.2	0.8	13.2	0.8	13.1	0.8
Swe-06	0.4	13.5	0.7	13.6	0.7	13.6	0.7	13.6	0.7	13.5	0.7
Swe-07	1.7	12.3	1.8	12.4	1.8	12.4	1.8	12.4	1.8	12.3	1.8
Swe-08	0.5	13.0	0.7	13.0	0.7	13.1	0.7	13.0	0.7	13.0	0.7
Swe-2											
Swe-10	0.5	12.6	0.7	12.7	0.7	12.7	0.7	12.7	0.7	12.6	0.7
Swe-12	0.5	12.5	0.7	12.5	0.7	12.5	0.7	12.6	0.7	12.5	0.7
Swe-13	0.5	12.7	0.7	12.7	0.7	12.7	0.7	12.7	0.7	12.7	0.7
Swe-14	0.6	11.7	0.8	11.8	0.8	11.8	0.8	11.8	0.8	11.7	0.8
Swe-17	0.6	13.4	0.8	13.4	0.8	13.4	0.8	13.4	0.8	13.4	0.8
Swe-3											
Swe-18	0.3	11.0	0.5	11.1	0.5	11.1	0.5	11.1	0.5	11.0	0.5
Swe-19	0.6	12.4	0.8	12.5	0.8	12.5	0.8	12.5	0.8	12.4	0.8
Swe-25	0.4	10.7	0.6	10.7	0.6	10.7	0.6	10.8	0.6	10.7	0.6
Swe-4											
Swe-26	0.5	11.4	0.7	11.6	0.7	11.6	0.7	11.6	0.7	11.4	0.7
Swe-27	0.6	11.4	0.8	11.6	0.8	11.6	0.8	11.6	0.8	11.4	0.8
Swe-30	0.5	11.0	0.7	11.2	0.7	11.2	0.7	11.2	0.7	11.0	0.7
Swe-31	0.4	11.0	0.6	11.1	0.6	11.1	0.6	11.1	0.6	11.0	0.6
Swe-33	0.4	10.7	0.6	10.8	0.6	10.8	0.6	10.8	0.6	10.7	0.6
Swe-5											
Swe-35	0.5	18.0	0.9	18.3	0.9	18.2	0.9	18.2	0.9	18.0	0.9
Swe-36	0.5	16.7	0.8	17.0	0.8	16.9	0.8	16.9	0.8	16.7	0.8
Swe-38	0.4	27.5	1.2	27.9	1.2	27.8	1.2	27.6	1.2	27.5	1.2
Swe-39	0.6	10.4	0.7	10.5	0.7	10.5	0.7	10.5	0.7	10.4	0.7
Swe-41	1.0	23.9	1.3	24.2	1.4	24.2	1.4	24.1	1.4	23.9	1.3
Swe-6											
Swe-42 (2)	0.4	11.2	0.6	11.3	0.6	11.3	0.6	11.4	0.6	11.2	0.6
Swe-42	3.6	12.6	3.6	12.8	3.7	12.7	3.7	12.8	3.7	12.6	3.6
Swe-43	1.1	10.7	1.2	10.8	1.2	10.7	1.2	10.8	1.2	10.7	1.2
Swe-44	0.6	11.4	0.7	11.5	0.7	11.4	0.7	11.5	0.8	11.4	0.7
Swe-45	0.5	11.3	0.7	11.4	0.7	11.3	0.7	11.4	0.7	11.3	0.7
Swe-46	1.0	11.5	1.1	11.6	1.1	11.5	1.1	11.6	1.1	11.5	1.1
Swe-48	0.4	19.7	0.9	19.8	0.9	19.7	0.9	19.7	0.9	19.7	0.9
Swe-7											
Swe-51	0.4	10.4	0.6	10.6	0.6	10.5	0.6	10.5	0.6	10.4	0.6
Swe-53	0.4	11.6	0.6	11.8	0.6	11.7	0.6	11.8	0.6	11.6	0.6
Swe-55	0.6	10.1	0.7	10.4	0.8	10.3	0.7	10.3	0.8	10.1	0.7
Swe-56	0.8	10.6	0.9	10.8	0.9	10.7	0.9	10.8	0.9	10.6	0.9
Swe-57	0.7	10.7	0.8	11.0	0.8	10.9	0.8	10.9	0.8	10.7	0.8
Swe-8											
Swe-59	0.4	10.9	0.6	11.2	0.6	11.1	0.6	11.2	0.6	10.9	0.6
Swe-61	0.4	9.1	0.6	9.3	0.6	9.2	0.6	9.2	0.6	9.1	0.6
Swe-62	0.9	10.3	1.0	10.6	1.0	10.5	1.0	10.5	1.0	10.3	1.0
Swe-63	0.8	8.6	0.9	8.8	0.9	8.7	0.9	8.7	0.9	8.6	0.9
Swe-9											
Swe-66	0.6	8.4	0.7	8.5	0.7	8.5	0.7	8.5	0.7	8.4	0.7
Swe-67	0.5	9.6	0.6	9.7	0.6	9.6	0.6	9.7	0.6	9.6	0.6
Swe-72	2.9	9.1	2.9	9.2	3.0	9.1	2.9	9.1	3.0	9.1	2.9
Swe-73	0.5	10.2	0.7	10.3	0.7	10.3	0.7	10.3	0.7	10.2	0.7
Swe-75	0.7	9.9	0.8	10.0	0.8	10.0	0.8	10.0	0.8	9.9	0.8
Swe-76	0.5	10.2	0.6	10.3	0.6	10.3	0.6	10.4	0.6	10.2	0.6

Table A.6. Cosmogenic age results for Finland in kilo annum (ka) for the different latitude/altitude scaling schemes from the CRONUS Calculator (Balco et. al., 2008)

Sample	Internal Uncertainty	Lal/Stone Constant	External Uncertainty	Desilets	External Uncertainty	Dunai	External Uncertainty	Lifton	External Uncertainty	Lal/Stone Time Varying	External Uncertainty
Finland											
Fin-1											
Fin-01	0.7	11.7	0.9	11.6	0.8	11.6	0.8	11.7	0.9	11.7	0.9
Fin-02	1.0	11.9	1.1	11.9	1.1	11.9	1.1	11.9	1.1	11.9	1.1
Fin-05	0.6	11.7	0.8	11.6	0.8	11.6	0.8	11.7	0.8	11.7	0.8
Fin-08	0.6	12.2	0.7	12.1	0.7	12.1	0.7	12.1	0.7	12.2	0.7
Fin-2											
Fin-10	0.5	11.6	0.7	11.5	0.7	11.5	0.7	11.6	0.7	11.6	0.7
Fin-11	0.7	12.0	0.9	11.9	0.9	11.9	0.9	12.0	0.9	12.0	0.9
Fin-14	0.6	12.7	0.8	12.6	0.8	12.6	0.7	12.6	0.8	12.7	0.8
Fin-15	0.9	12.1	1.1	12.0	1.1	12.0	1.1	12.1	1.1	12.1	1.1
Fin-3											
Fin-19	1.2	9.0	1.2	9.0	1.2	9.0	1.2	9.0	1.2	9.0	1.2
Fin-17	0.8	12.5	0.9	12.5	0.9	12.5	0.9	12.5	0.9	12.5	0.9
Fin-20	0.6	11.8	0.7	11.8	0.7	11.8	0.7	11.8	0.7	11.8	0.7
Fin-22	0.4	12.0	0.6	12.0	0.6	12.0	0.6	12.0	0.6	12.0	0.6
Fin-23	0.7	11.8	0.8	11.8	0.8	11.8	0.8	11.9	0.8	11.8	0.8
Fin-4											
Fin-25	7.5	26.2	7.6	26.3	7.6	26.2	7.6	26.1	7.6	26.2	7.6
Fin-25 (2)	1.0	13.8	1.1	13.8	1.1	13.7	1.1	13.8	1.1	13.8	1.1
Fin-28	0.5	12.0	0.7	12.0	0.7	11.9	0.7	12.0	0.7	12.0	0.7
Fin-29	1.3	11.6	1.4	11.6	1.4	11.6	1.4	11.6	1.4	11.6	1.4
Fin-30	0.8	12.8	0.9	12.8	0.9	12.7	0.9	12.8	0.9	12.8	0.9
Fin-31	0.9	12.1	1.0	12.1	1.0	12.1	1.0	12.2	1.0	12.1	1.0
Fin-5											
Fin-44	0.7	11.8	0.9	11.7	0.9	11.6	0.8	11.8	0.9	11.8	0.9
Fin-45	1.1	12.3	1.2	12.2	1.2	12.1	1.1	12.2	1.2	12.3	1.2
Fin-46	0.8	11.6	0.9	11.5	0.9	11.4	0.9	11.6	0.9	11.6	0.9
Fin-47	0.9	13.0	1.1	12.9	1.0	12.8	1.0	12.9	1.1	13.0	1.1
Fin-48	0.6	12.0	0.8	11.8	0.8	11.8	0.8	11.9	0.8	12.0	0.8
Fin-6											
Fin-49	0.5	10.9	0.6	10.9	0.6	10.8	0.6	10.9	0.6	10.9	0.6
Fin-50	0.7	10.8	0.8	10.7	0.8	10.6	0.8	10.8	0.8	10.8	0.8
Fin-51	0.4	10.7	0.6	10.7	0.6	10.6	0.6	10.7	0.6	10.7	0.6
Fin-54	0.8	12.5	1.0	12.4	1.0	12.3	1.0	12.5	1.0	12.5	1.0
Fin-56	0.8	14.4	1.0	14.4	1.0	14.3	1.0	14.4	1.0	14.4	1.0
Fin-7											
Fin-08-11	9.6	29.9	9.6	29.9	9.6	29.7	9.6	29.7	9.6	29.9	9.6
Fin-09-11	0.8	11.2	0.9	11.2	0.9	11.1	0.9	11.2	0.9	11.2	0.9
Fin-10-11	2.0	12.7	2.1	12.7	2.1	12.6	2.1	12.7	2.1	12.7	2.1
Fin-12-11	0.9	11.5	1.0	11.5	1.0	11.5	1.0	11.6	1.0	11.5	1.0
Fin-13-11	0.5	16.3	0.8	16.3	0.8	16.2	0.8	16.3	0.8	16.3	0.8
Fin-14-11	0.3	11.0	0.5	11.0	0.5	10.9	0.5	11.0	0.5	11.0	0.5
Fin-8											
Fin-15-11	0.4	11.1	0.6	11.1	0.6	11.0	0.6	11.1	0.6	11.1	0.6
Fin-16-11	0.8	11.2	0.9	11.2	0.9	11.1	0.9	11.2	0.9	11.2	0.9
Fin-17-11	0.5	12.2	0.7	12.2	0.7	12.1	0.7	12.2	0.7	12.2	0.7
Fin-18-11	0.9	11.1	1.0	11.1	1.0	11.0	1.0	11.1	1.0	11.1	1.0
Fin-19-11	0.8	13.8	1.0	13.7	1.0	13.7	1.0	13.8	1.0	13.8	1.0
Fin-20-11	0.5	11.3	0.7	11.3	0.7	11.2	0.7	11.3	0.7	11.3	0.7
Fin-21-11	0.6	10.0	0.7	10.0	0.7	10.0	0.7	10.0	0.7	10.0	0.7

Table A.7. Cosmogenic sample information for existing chronology

Sample	Latitude (DD)	Longitude (DD)	Modern Elevation (m asl)	Corrected Elevation (masl)[a]	Thickness (cm)	Density	^{10}Be (atoms g^{-1})[e]	Uncertainty (atoms g-1)[d]	^{10}Be age (ka)	1 sigma analaytical uncertainty (ka)	Mean Age (ka)[f,i]
LGM moraine (from Rinterknecht et al., 2006)[c]											
LIT-1	54.289	25.096	150	----	2.00	2.8	87981	7449	19.0	1.6	**21.7 (1.8)**
LIT-4"	54.25	25.609	200	----	2.00	2.8	23433	3622	4.8	0.7	
LIT-5	54.178	25.588	207	----	2.70	2.8	102851	6688	21.2	1.4	
LIT-6	54.288	25.322	162	----	1.50	2.8	151141	9347	32.3	2.0	
LIT-7	54.263	25.258	193	----	1.50	2.8	98713	6991	20.4	1.5	
BEL-2	54.889	26.773	177	----	2.00	2.8	67782	5989	14.2	1.3	
BEL-3	54.881	25.951	196	----	3.50	2.8	87198	5761	18.2	1.2	
BEL-6	54.888	26.507	201	----	2.20	2.8	113709	7332	23.4	1.5	
BEL-7	54.795	26.791	188	----	3.20	2.8	135090	9922	28.5	2.1	
BEL-8"	54.723	26.361	153	----	3.50	2.8	47282	3558	10.3	0.8	
BEL-9	55.056	27.621	179	----	2.50	2.8	72772	5324	15.3	1.1	
BEL-11^^	54.922	27.195	200	----	2.50	2.8	118451	22601	24.5	4.7	
BEL-17""	54.78	27.06	210	----	4.00	2.8	347494	23873	72.9	5.1	
BEL-18""	54.781	27.082	214	----	1.00	2.8	468697	28273	96.1	5.9	
BEL-19	54.906	26.906	207	----	4.00	2.8	85743	6109	17.8	1.3	
Middle Lithuanian (from Rinterknecht et al., 2008)[c]											
MLIT-1	55.59	24.309	57	----	2.0	2.8	71371	5125	16.9	1.2	**14.9 (0.3)**
MLIT-2	55.67	24.19	50	----	1.5	2.8	51246	4098	12.2	1.0	
MLIT-3	56.125	21.607	55	----	1.5	2.8	72013	5036	16.9	1.2	
MLIT-4	56.125	21.607	55	----	1.5	2.8	62594	5506	14.7	1.3	
MLIT-5	56.125	21.643	68	----	2.0	2.8	64867	4898	15.1	1.1	
MLIT-6	56.125	21.643	68	----	2.0	2.8	74477	5387	17.4	1.3	
MLIT-7	56.125	21.643	68	----	1.0	2.8	44744	4359	10.3	1.0	
MLIT-8	56.125	21.643	68	----	1.5	2.8	66315	5000	15.4	1.2	
MLIT-9""	56.125	21.643	68	----	1.0	2.8	119155	7340	27.6	1.7	
MLIT-11	57.361	25.842	183	----	1.0	2.8	70804	5140	14.5	1.1	
MLIT-13	57.498	26.941	162	----	1.5	2.8	80030	5137	16.9	1.1	
MLIT-14	57.412	26.964	194	----	1.5	2.8	58268	5078	11.9	1.0	
MLIT-15	57.483	27.195	179	----	1.5	2.8	69666	5456	14.4	1.1	
MLIT-16	57.058	27.364	124	----	2.0	2.8	59713	6800	13.1	1.5	
MLIT-17	57.034	27.166	106	----	3.0	2.8	66794	5094	15.1	1.2	
MLIT-19	57.023	27.016	96	----	2.0	2.8	62089	5435	14.1	1.2	
MLIT-20"	56.832	27.553	116	----	1.5	2.8	21815	3508	4.8	0.8	
MLIT-21	56.906	26.288	173	----	2.0	2.8	66400	5426	13.9	1.1	
MLIT-22	56.972	26.242	216	----	2.0	2.8	74208	6414	14.9	1.3	
MLIT-23	56.648	26.259	120	----	2.0	2.8	68800	6134	15.2	1.4	
BALTI-6	55.507	25.07	87	----	2.0	2.8	68530	4876	15.7	1.1	
BALTI-7	55.383	22.175	67	----	2.0	2.8	59295	4548	13.9	1.1	
BALTI-13	56.58	27.403	168	----	2.0	2.8	81335	6014	17.2	1.3	
BALTI-15	56.424	26.076	88	----	3.0	2.8	66958	4900	15.5	1.1	
BALTI-16	56.152	26.461	105	----	2.0	2.8	75052	5165	16.9	1.2	
BALTI-17	56.123	26.001	115	----	1.5	2.8	62715	4319	13.9	1.0	
BALTI-18	56.169	25.466	97	----	1.5	2.8	67531	5225	15.3	1.2	
LAT-2	57.313	24.758	58	----	2.0	2.8	78702	6058	18.5	1.4	
LAT-7	56.655	26.287	120	----	2.0	2.8	66544	5901	14.7	1.3	
LAT-12""	57.019	22.688	81	----	1.0	2.8	119389	10191	27.2	2.3	
LAT-13	56.578	21.952	57	----	1.5	2.8	65144	4675	15.3	1.1	
NLIT-4	56.564	27.978	120	----	2.0	2.8	68676	5118	15.2	1.1	
EST-18	57.761	27.016	156	----	1.5	2.8	60242	5082	12.7	1.1	
EST-19	57.754	27.023	195	----	2.0	2.8	87451	6033	17.9	1.2	
EST-21	57.697	27.033	290	----	0.8	2.8	65774	4601	12.1	0.8	
EST-23	57.703	27.278	243	----	3.5	2.8	61983	4808	12.2	1.0	

[a]Age calculations use standard atmosphere, density of 2.65 g cm^{-3}, and zero erosion. Due to low topographic variation of sampling sites, no shielding correcdtion is necessary.

[b]Where applicable, Isostatic uplift correction is estimated by subtracting half of the total uplift from the modern elevation (Ristaniemi et al., 1987; Hendenstrom and Risberg, 1999; Eronen et al., 2000; Saarnisto, 2001; Berglund et al., 2005, Linden et al., 2006; Rosentau et al., 2012)

[c]All measurements are standardized to NIST_Certified.

[d]1-sigma AMS uncertainty

[e]^{10}Be atom conecntrations are blank-corrected (see text).

[f]Ages were calculated using the Cronus Earth online calculator (v 2.2) with the Western Norway production rate and the Lal/Stone time-dependent scaling scheme.

[h]Ages excluded using Chauvenet's criterion.

[i]Site mean age and uncertainty is calculated as either the straight mean and standar error or the error weighted age and error weighted uncertainty based on the geologic and analytic uncertainty (see text).

"Ages exluded: Ages too young to fit within chronology

""Ages excludes: Ages too old to fit within chronology

^^Age excluded: Current too low

** Age removed based upon Geomorphic considerations.

Table A.8. Cosmogenic sample information for existing chronology.

Sample	Latitude (DD)	Longitude (DD)	Modern Elevation (m asl)	Corrected Elevation (masl)[b]	Thickness (cm)	Density	^{10}Be (atoms g^{-1})[e]	Uncertainty (atoms g-1)[d]	^{10}Be age (ka)	1 sigma analaytical uncertainty (ka)	Mean Age (ka)[f,i]
North Lithuanian (from Rinterknecht et al., 2008)[c]											
EST-13	58.508	26.778	81	----	3.0	2.8	63880	4927	14.8	1.1	**14.5 (0.7)**
EST-16	58.059	26.379	158	----	1.5	2.8	67936	4808	14.3	1.0	
LAT-1	57.352	22.725	50	----	0.5	2.8	66829	6076	15.6	1.4	
LAT-3	57.621	25.224	58	----	2.0	2.8	67382	5442	15.9	1.3	
LAT-4	57.748	25.163	56	----	2.0	2.8	62064	5449	14.6	1.3	
LAT-8	56.801	24.84	56	----	1.5	2.8	56495	4041	13.3	1.0	
LAT-9[h]	57.848	24.868	57	----	1.6	2.8	43948	3583	10.3	0.8	
NLIT-1	56.198	23.84	50	----	2.0	2.8	62980	5468	15.0	1.3	
NLIT-2	56.097	21.276	38	----	1.5	2.8	54530	4398	13.1	1.1	
NLIT-3	56.076	21.217	25	----	2.0	2.8	64680	4681	15.8	1.1	
Pomeranian (from Rinterknecht et al., 2005)[c]											
Western - Odra Lobe											
POM-12"	52.886	14.791	70	----	1.0	2.8	30870	3002	7170	697	**16.6 (0.5)**
POM-13	52.886	14.791	80	----	1.0	2.8	87292	6227	20135	1441	
POM-14	53.366	14.651	99	----	3.0	2.8	76216	5772	17484	1328	
POM-15"	53.352	14.644	88	----	2.0	2.8	35852	4170	8230	958	
POM-16	53.167	14.736	96	----	1.5	2.8	65994	4705	14996	1072	
POM-17	53.018	14.954	60	----	1.5	2.8	51029	4026	12034	951	
POM-18	53.613	15.437	102	----	1.0	2.8	74206	7835	16676	1766	
POM-19	53.759	14.853	22	----	2.0	2.8	61383	4950	15108	1221	
POM-21	53.712	16.255	133	----	2.0	2.8	68634	5107	15063	1124	
POM-22	53.891	15.838	110	----	1.5	2.8	71878	6531	16072	1465	
PO-05-02	52.980	13.870	73	----	3	2.8	83000	3901	19000	1010	
PO-05-03	52.980	13.860	75	----	5	2.8	92000	4876	16542	614	
MVP-1	53.327	13.450	113	----	1.3	2.8	73315	5062	15660	1084	
MVP-2""	53.324	13.257	94	----	2.3	2.8	110498	25241	24332	5582	
MVP-3	53.304	13.252	76	----	0.8	2.8	82326	5388	18205	1195	
MVP-5	53.748	13.583	39	----	3.5	2.8	80370	4060	18879	956	
MVP-9	53.704	13.571	30	----	2.3	2.8	78227	5666	18368	1334	
MVP-12	53.668	10.951	51	----	3.5	2.8	75543	6687	17506	1554	
MVP-13	53.668	10.951	50	----	3.5	2.8	63218	5676	14652	1318	
MVP-15	53.866	11.828	115	----	1.8	2.8	49904	8729	10642	1865	
MVP-16	53.927	11.711	82	----	1.1	2.8	81709	3614	17954	796	
MVP-17	53.572	13.144	59	----	1.5	2.8	56086	6908	12665	1563	
MVP-18	53.449	12.965	90	----	3.7	2.8	80011	8228	17854	1842	
MVP-19	53.450	12.965	99	----	1.0	2.8	69792	4212	15071	912	
MVP-20	53.450	12.965	100	----	2.3	2.8	88418	4108	19308	900	
MVP-23	53.665	11.978	45	----	2.2	2.8	65048	8381	14994	1936	
[a]Age calculations use standard atmosphere, density of 2.65 g cm^{-3}, and zero erosion. Due to low topographic variation of sampling sites, no shieldiing correcdtion is necessary.											
[b]Where applicable, Isostatic uplift correction is estimated by subtracting half of the total uplift from the modern elevation (Ristaniemi et al., 1987; Hendenstrom and Risberg, 1999; Eronen et al., 2000; Saarnisto, 2001; Berglund et al., 2005, Linden et al., 2006; Rosentau et al., 2012)											
[c]All measurements are standardized to NIST_Certified.											
[d]1-sigma AMS uncertainty											
[e]^{10}Be atom conecntrations are blank-corrected (see text).											
[f]Ages were calculated using the Cronus Earth online calculator (v 2.2) with the Western Norway production rate and the Lal/Stone time-dependent scaling scheme.											
[h]Ages excluded using Chauvenet's criterion.											
[i]Site mean age and uncertainty is calculated as either the straight mean and standar error or the error weighted age and error weighted uncertainty based on the geologic and analytic uncertainty (see text).											
"Ages exluded: Ages too young to fit within chronology											
""Ages excludes: Ages too old to fit within chronology											
^^Age excluded: Current too low											
** Age removed based upon Geomorphic considerations.											

Table A.10. Cosmogenic sample information for existing chronology

Sample	Latitude (DD)	Longitude (DD)	Modern Elevation (m asl)	Corrected Elevation (masl)[b]	Thickness (cm)	Density	^{10}Be (atoms g^{-1})[e]	Uncertainty (atoms g-1)[d]	^{10}Be age (ka)	1 sigma analaytical uncertainty (ka)	Mean Age (ka)[f,i]
Pomeranian (from Rinterknecht et al., 2005)[c]											
Eastern Lobe											
POM-1	53.724	19.751	99	----	1.0	2.8	92097	6276	20809	1423	**16.3 (0.5)**
POM-2	53.844	19.824	107	----	2.0	2.8	68138	4762	15366	1077	
POM-3	54.086	20.91	117	----	2.0	2.8	79234	5772	17688	1293	
POM-4	53.957	20.86	167	----	1.5	2.8	59453	4226	12551	895	
POM-5	53.901	21.203	175	----	2.0	2.8	73356	6069	15443	1282	
POM-8	54.068	21.61	138	----	3.0	2.8	74349	6533	16381	1444	
POM-10	54.15	21.996	173	----	1.0	2.8	68842	5535	14387	1160	
POM-11	53.901	22.017	177	----	1.0	2.8	77292	5339	16110	1117	
POL-1	53.774	21.629	117	----	2.0	2.8	77039	5936	17218	1331	
POL-2	54.215	21.859	128	----	2.0	2.8	77096	6373	17014	1411	
POL-3""	54.195	21.946	130	----	2.0	2.8	119747	10373	26446	2303	
POL-4	54.236	22.79	240	----	2.0	2.8	90221	6790	17810	1347	
POL-5	54.204	22.753	243	----	2.0	2.8	93906	7175	18488	1419	
POL-6""	54.165	22.968	211	----	2.0	2.8	410588	30728	84847	6485	
POL-7	54.164	22.97	195	----	2.0	2.8	101223	7233	20916	1502	
BALTI-2	55.698	25.799	113	----	3.5	2.8	67204	5015	15223	1139	
BALTI-3	55.31	25.431	142	----	2.0	2.8	74111	5494	16111	1198	
BALTI-4	55.434	25.509	167	----	2.0	2.8	78424	6380	16615	1357	
BALTI-5	55.494	25.657	154	----	2.0	2.8	61937	4694	13283	1010	
BALTI-8**	55.666	23.156	132	----	2.0	2.8	57037	4762	12471	1044	
BALTI-9**	55.718	23.212	123	----	3.0	2.8	51941	3877	11555	864	
BALTI-10**	55.635	23.174	120	----	1.0	2.8	73685	5025	16193	1108	
BALTI-11**	55.635	23.174	120	----	2.0	2.8	49898	4360	11043	967	
BALTI-12""	57.095	25.901	227	----	1.0	2.8	167932	10143	33146	2019	
LIT-2	55.544	25.846	187	----	2.0	2.8	83087	7334	17250	1529	
LIT-3	55.544	25.846	187	----	2.0	2.8	87424	6903	18154	1440	
LIT-8	54.273	24.021	190	----	3.8	2.8	70209	5637	14785	1191	
LIT-9	54.52	24.315	176	----	2.6	2.8	70891	5385	14982	1142	
GRUDA-1	55.073	26.017	201	----	2.0	2.8	82295	5940	16877	1223	
LES-1""	53.346	20.45	196	----	2.0	2.8	112386	8501	23264	1769	
LES-2"	53.388	20.493	179	----	2.0	2.8	32223	3462	6754	727	
LES-3"	53.481	20.222	212	----	3.0	2.8	34515	3455	7059	708	
LES-4	53.494	20.239	172	----	2.0	2.8	73962	5383	15639	1142	
LES-5""	53.579	20.094	180	----	2.0	2.8	192392	11556	40613	2462	
LES-6	53.601	20.061	151	----	2.0	2.8	80752	5844	17440	1267	
LES-7"	53.625	20.042	132	----	2.0	2.8	26384	3283	5790	721	
LES-8	53.511	19.9	255	----	2.0	2.8	101364	11043	19770	2165	
LES-10	53.576	19.942	270	----	2.0	2.8	67819	5686	13012	1095	
LES-11	53.522	19.838	218	----	2.0	2.8	79384	7748	16037	1571	
LES-12	53.563	19.953	275	----	2.0	2.8	84598	7005	16166	1345	
LES-13""	53.553	19.925	302	----	2.0	2.8	191466	13310	35809	2515	
LAT-5	57.151	25.585	200	----	2.0	2.8	98950	8426	20164	1726	
BEL-13	55.658	27.683	151	----	2.8	2.8	71772	7044	15564	1533	
BEL-14	55.639	27.375	150	----	1.7	2.8	61926	4691	13310	1011	
BEL-15	55.699	26.994	144	----	0.5	2.8	69890	6224	14962	1337	
BEL-15A	55.699	26.994	144	----	0.5	2.8	73939	6205	15833	1333	
BEL-16	55.544	27.076	152	----	2.0	2.8	66330	4604	14269	993	

[a] Age calculations use standard atmosphere, density of 2.65 g cm^{-3}, and zero erosion. Due to low topographic variation of sampling sites, no shieldiing correcdtion is necessary.

[b] Where applicable, Isostatic uplift correction is estimated by subtracting half of the total uplift from the modern elevation (Ristaniemi et al., 1987; Hendenstrom and Risberg, 1999; Eronen et al., 2000; Saarnisto, 2001; Berglund et al., 2005, Linden et al., 2006; Rosentau et al., 2012)

[c] All measurements are standardized to NIST_Certified.

[d] 1-sigma AMS uncertainty

[e] ^{10}Be atom conecntrations are blank-corrected (see text).

[f] Ages were calculated using the Cronus Earth online calculator (v 2.2) with the Western Norway production rate and the Lal/Stone time-dependent scaling scheme.

[h] Ages excluded using Chauvenet's criterion.

[i] Site mean age and uncertainty is calculated as either the straight mean and standar error or the error weighted age and error weighted uncertainty based on the geologic and analytic uncertainty (see text).

"Ages exluded: Ages too young to fit within chronology

""Ages excludes: Ages too old to fit within chronology

^^Age excluded: Current too low

** Age removed based upon Geomorphic considerations.

Table A.9. Cosmogenic sample information for existing chronology

Sample	Latitude (DD)	Longitude (DD)	Modern Elevation (m asl)	Corrected Elevation (masl)[a]	Thickness (cm)	Density	^{10}Be (atoms g^{-1})[e]	Uncertainty (atoms g-1)[d]	^{10}Be age (ka)	1 sigma analaytical uncertainty (ka)	Mean Age (ka)[f,i]
Vimmerby Moraine (from Johnsen et al., 2009)											
S1	57.3947	14.9039	208	163	2	2.65	76100	4300	14.0	0.8	**15.3 (0.4)**
S3	57.3866	14.8983	211	166	2	2.65	89800	4700	16.8	0.9	
S4	57.3808	14.8787	217	172	2	2.65	80000	4100	14.9	0.8	
S7	57.6695	15.8057	145	100	2	2.65	76200	4000	14.9	0.8	
S8	57.67	15.8064	136	91	2	2.65	79900	4200	16.2	0.9	
S9	57.6688	15.8031	140	95	2	2.65	75100	5800	14.8	1.1	
Stroeven et al., 2011											
130	69.3203	23.4976	540	490	2	2.7	80200	4300	11.3	0.6	**11.8 (0.3)**
131	69.3203	23.4976	540	490	2	2.7	84600	4600	11.9	0.6	
132	69.3894	23.5266	365	315	2	2.7	72900	2800	12.1	0.5	
133	69.39	23.5263	355	305	2	2.7	68900	4500	11.5	0.8	
19	67.155	18.8475	890	865	0.5	2.7	93000	16400	9.3	1.6	**10 (0.8)**
62	67.1528	18.8739	945	850	1	2.7	84300	12900	8.6	1.3	
63	67.1578	18.8833	930	717	5	2.7	105100	18600	12.4	2.2	
114	67.1274	18.7507	797	717	2	2.7	84600	4400	9.7	0.5	
Linge et al., 2007											
Helgelandsbukken, Svartisen											
OL02-01**	66.47	15.15	1640	----	2	2.65	359000	24000	20.7	1.391	**10.7 (0.3)**
OL02-09	66.47	15.15	1442	----	2	2.65	164000	13000	10.677	0.849	
OL02-10	66.47	15.15	1440	----	2	2.65	171000	12000	11.223	0.79	
OL02-04**	66.47	15.15	1350	----	2	2.65	239000	1600	16.84	0.113	
OL02-11	66.47	15.15	1310	----	2	2.65	158000	10000	11.463	0.728	
OL02-08	66.47	15.15	1229	----	2	2.65	129000	8000	10.141	0.631	
OL02-07	66.47	15.15	1215	----	2	2.65	124000	9000	9.719	0.707	
OL02-05 **	66.47	15.15	1111	----	2	2.65	127000	9000	11.016	0.783	
OL02-06	66.47	15.15	1111	----	2	2.65	124000	9000	10.755	0.783	
Mangerud et al., 2013											
Nordlifjell											
NFJ08-1	60.0493	6.08075	963	----	1.52	2.7	1.41E+05	3.60E+03	13.53	0.34	**14.2 (0.64)**
NFJ08-2	60.04917	6.08059	966	----	1.21	2.7	1.53E+05	3.90E+03	14.67	0.37	
NFJ08-3	60.04943	6.08258	960	----	1.78	2.7	1.43E+05	3.20E+03	14.03	0.32	
NFJ08-4	60.04932	6.08136	960	----	1.6	2.7	1.56E+05	3.30E+04	15.06	0.32	
NFJ08-5	60.05013	6.0812	960	----	2.33	2.7	1.42E+05	3.80E+04	13.75	0.37	
Eidfjord-Osa Moraine at Osa											
OSA08-1	60.55712	7.12253	1160	----	3.18	2.65	1.36E+05	2.60E+03	11.12	0.22	**11.3 (0.22)**
OSA08-2	60.55683	7.12243	1160	----	1.89	2.65	1.38E+05	2.90E+03	11.17	0.24	
OSA08-3	60.55682	7.12232	1160	----	1.52	2.65	1.37E+05	2.90E+03	11.17	0.24	
OSA08-4	60.55687	7.12261	1160	----	3.28	2.65	1.41E+05	3.00E+03	11.61	0.25	
OSA08-5	60.5567	7.12136	1160	----	0.98	2.65	1.42E+05	3.00E+03	11.51	0.25	
Briner et al., 2014											
Beyond Lysefjorden											
42-11NOR-31	58.933889	6.038333	104	----	2	2.65	68225.2	1403.3	14.6	0.3	**14.5 (0.2)**
42-11NOR-30	58.933889	6.038333	108	----	2	2.65	66146.5	1459.6	14.4	0.3	
42-11NOR-29	58.933889	6.038333	113	----	1	2.65	66024.2	1487.2	13.9	0.3	
Inner Lysefjorden moraine											
45-11NOR-13	59.11	6.4	593	----	1	2.65	88580.6	2184.7	11.7	0.3	**11.5 (0.4)**
45-11NOR-15	59.11	6.4	591	----	3	2.65	86399.8	1715.2	11.6	0.2	
44-11NOR-14	59.11	6.4	593	----	2.5	2.65	83182.1	1649.4	11.1	0.2	
44-11NOR-12	59.11	6.4	715	----	1.5	2.65	91682.1	1821	10.9	0.2	
44-11NOR-20	59.11	6.4	603	----	1.5	2.65	91913.4	3074.5	12.1	0.4	
44-11NOR-17	59.11	6.4	684	----	2	2.65	91806.3	1730.7	11.3	0.2	
Beyond Trolgaren moraine											
46-11NOR-73	59.28	6.6	863	----	1	2.65	114591.8	2464.4	12	0.3	**11.4 (0.4)**
46-11NOR-74	59.28	6.6	863	----	1	2.65	105561.3	2281.9	11.1	0.2	
46-11NOR-75	59.28	6.6	849	----	3	2.65	103594.3	2857.2	11.2	0.3	

[a] Age calculations use standard atmosphere, density of 2.65 g cm^{-3}, and zero erosion. Due to low topographic variation of sampling sites, no shieldiing correcdtion is necessary.

[b] Where applicable, Isostatic uplift correction is estimated by subtracting half of the total uplift from the modern elevation (Ristaniemi et al., 1987; Hendenstrom and Risberg, 1999; Eronen et al., 2000; Saarnisto, 2001; Berglund et al., 2005, Linden et al., 2006; Rosentau et al., 2012)

[c] All measurements are standardized to NIST_Certified.

[d] 1-sigma AMS uncertainty

[e] ^{10}Be atom conecntrations are blank-corrected (see text).

[f] Ages were calculated using the Cronus Earth online calculator (v 2.2) with the Western Norway production rate and the Lal/Stone time-dependent scaling scheme.

[h] Ages excluded using Chauvenet's criterion.

[i] Site mean age and uncertainty is calculated as either the straight mean and standar error or the error weighted age and error weighted uncertainty based on the geologic and analytic uncertainty (see text).

"Ages exluded: Ages too young to fit within chronology

"" Ages excludes: Ages too old to fit within chronology

^^Age excluded: Current too low

** Age removed based upon Geomorphic considerations.

Table A.11. Cosmogenic sample information for existing chronology.

Sample	Latitude (DD)	Longitude (DD)	Modern Elevation (m asl)	Corrected Elevation (masl)[b]	Thickness (cm)	Density	^{10}Be (atoms g^{-1})[e]	Uncertainty (atoms g-1)[d]	^{10}Be age (ka)	1 sigma analaytical uncertainty (ka)	Mean Age (ka)[f,i]
FIN-1	60.7310	24.9600	140	95	3.0	2.8	62202	4475	13368	965	**13.6 ± 0.7**
FIN-2	60.7310	24.9600	140	95	1.7	2.8	57330	4561	12184	972	
FIN-3	60.7310	24.9600	140	95	2.0	2.8	52593	3934	11202	840	
FIN-4	60.7310	24.9620	140	95	2.0	2.8	58046	4310	12367	921	
FIN-5	60.7310	24.9620	140	95	3.4	2.8	63074	4442	13602	961	
FIN-6	60.7310	24.9620	140	95	2.6	2.8	56761	4059	12154	872	
FIN-7	60.7310	24.9620	140	95	2.5	2.8	64904	4600	13892	988	
FIN-8	60.7310	24.9620	140	95	2.0	2.8	65435	4515	13947	966	
FIN-9	60.7310	24.9620	140	95	2.0	2.8	63284	4468	13487	955	
SS1 (from Tschudi et. al., 2000)											
Sal-1	61.0000	25.3900	160	115	4.0	2.8	75000	5000	13927	932	
Sal-3	61.0000	25.3900	160	115	3.0	2.8	70700	4800	13016	887	
Sal-4b	61.0200	25.4000	160	115	2.0	2.8	69500	4900	12686	897	
Sal-5	61.0200	25.4000	160	115	2.0	2.8	72600	5400	13254	989	
[a]Age calculations use standard atmosphere, density of 2.65 g cm^{-3}, and zero erosion. Due to low topographic variation of sampling sites, no shieldiing correcdtion is necessary.											
[b]Where applicable, Isostatic uplift correction is estimated by subtracting half of the total uplift from the modern elevation (Ristaniemi et al., 1987; Hendenstrom and Risberg, 1999; Eronen et al., 2000; Saarnisto, 2001; Berglund et al., 2005, Linden et al., 2006; Rosentau et al., 2012)											
[c]All measurements are standardized to NIST_Certified.											
[d]1-sigma AMS uncertainty											
[e]^{10}Be atom conecntrations are blank-corrected (see text).											
[f]Ages were calculated using the Cronus Earth online calculator (v 2.2) with the Western Norway production rate and the Lal/Stone time-dependent scaling scheme.											
[h]Ages excluded using Chauvenet's criterion.											
[i]Site mean age and uncertainty is calculated as either the straight mean and standar error or the error weighted age and error weighted uncertainty based on the geologic and analytic uncertainty (see text).											
"Ages exluded: Ages too young to fit within chronology											
""Ages excludes: Ages too old to fit within chronology											
^^Age excluded: Current too low											
** Age removed based upon Geomorphic considerations.											

Table A.12. Cosmogenic sample information for existing chronology.

Sample	Latitude (DD)	Longitude (DD)	Modern Elevation (m asl)	Corrected Elevation (masl)[a]	Thickness (cm)	Density	^{10}Be (atoms g^{-1})[e]	Uncertainty (atoms g-1)[d]	^{10}Be age (ka)	1 sigma analaytical uncertainty (ka)	Mean Age (ka)[f,i]
Skåne (Anjar et. al., 2014)											
SVE0836	56.28	12.52	188	148	3	2.8	62202	4475	13368	965	16.1 (0.6)
SVE0837	56.28	12.52	180	140	1.7	2.8	57330	4561	12184	972	
SVE0839	56.28	12.52	118	78	2	2.8	52593	3934	11202	840	
SVE0840	56.28	12.52	120	80	2	2.8	58046	4310	12367	921	
SVE0841	56.28	12.52	86	46	3.4	2.8	63074	4422	13602	961	
Småland (Anjar et. al., 2014)											
AL06	56.14	14.67	140	100	3	2.65	82600	3300	16387	657	15.8 (0.6)
AL08	56.51	14.67	132	92	4	2.65	86400	3500	17404	708	
SJ004	56.84	14.76	191	151	2.5	2.65	95900	3500	17937	658	
SJ005	56.83	14.79	185	145	4	2.65	83900	3300	15970	631	
SJ006	56.83	14.79	183	143	5	2.65	83700	3400	16091	656	
SVE0825	56.96	15.75	157	117	2	2.65	55700	2100	10723	405	
SVE0826	56.75	15.75	155	115	3	2.65	97100	7300	19276	1456	
SVE0828	56.96	15.75	160	120	6	2.65	97100	7300	19276	1456	
RA05	57.23	14.21	183	143	3.5	2.65	79800	3000	15130	571	
RA06	57.23	14.21	185	145	4	2.65	80200	3500	15235	667	
RA07	57.23	14.2	177	137	4.5	2.65	79500	3300	15286	637	
SVE0819	58.1	14.94	205	165	2	2.65	80900	2900	14791	532	
SVE0821	58.1	14.94	203	163	2	2.65	78300	3600	14392	664	
SVE0822""	58.1	14.94	200	160	2.5	2.65	188600	5800	34971	1085	
Leven Moraine (Anjar et. al., 2014)											
SVE0814	58.76	12.03	125	85	3	2.65	74200	3600	14824	722	14.3 (0.7)
SVE0815¨	58.76	12.03	130	90	5	2.65	536900	15200	111024	3232	
SVE0816	58.199	13.32	145	105	3	2.65	66100	2900	12939	570	
SVE0817	58.189	13.31	130	90	6	2.65	74400	4900	15156	1002	
SVE0818¨	58.196	13.32	140	100	7	2.65	35000	3700	7097	752	
Halland Coastal Moraine (Larsen et. al., 2012)											
SVE0801	57.02	12.46	65	---	3	2.65	78200	4700	16004	966	16.9 (0.6)
SVE0802	57.05	12.42	85	---	3.5	2.65	80800	3400	16257	687	
SVE0803	57.05	12.42	40	---	1.5	2.65	68900	3000	14296	625	
SVE0804ll	57.05	12.42	85	---	2	2.65	93600	4300	18620	859	
SVE0805	57.13	12.38	76	---	2	2.65	87400	3100	17541	625	

[a]Age calculations use standard atmosphere, density of 2.65 g cm^{-3}, and zero erosion. Due to low topographic variation of sampling sites, no shieldiing correcdtion is necessary.

[b]Where applicable, Isostatic uplift correction is estimated by subtracting half of the total uplift from the modern elevation (Ristaniemi et al., 1987; Hendenstrom and Risberg, 1999; Eronen et al., 2000; Saarnisto, 2001; Berglund et al., 2005, Linden et al., 2006; Rosentau et al., 2012)

[c]All measurements are standardized to NIST_Certified.

[d]1-sigma AMS uncertainty

[e]^{10}Be atom conecntrations are blank-corrected (see text).

[f]Ages were calculated using the Cronus Earth online calculator (v 2.2) with the Western Norway production rate and the Lal/Stone time-dependent scaling scheme.

[h]Ages excluded using Chauvenet's criterion.

[i]Site mean age and uncertainty is calculated as either the straight mean and standar error or the error weighted age and error weighted uncertainty based on the geologic and analytic uncertainty (see text).

"Ages exluded: Ages too young to fit within chronology

""Ages excludes: Ages too old to fit within chronology

^^Age excluded: Current too low

** Age removed based upon Geomorphic considerations.

llSVE0804 calculated using Larsen et. al., (2012) correction for submergence.

Table A.13. Cosmogenic exposure ages, elevation, and error used in Figure 3 of Chapter 2, to infer Antarctic Ice Sheet thinning during the Holocene.

Stone et. al. 2003

Sample	normalized elevation (m)	^{10}Be age (ka)	^{10}Be error (ka)
99-MBL-038-PAS	346	3.515	0.371
99-MBL-043-PAS	189	1.798	0.173
99-MBL-044-PAS	63	1.72	0.344
99-MBL-069-BLD	357	6.738	0.62
99-MBL-073-BLD	231	3.623	0.349
99-MBL-076-BLD	207	2.97	0.42
01-MBL-002-VVB	167	6.328	0.568
01-MBL-005-VVB	165	6.117	0.55
01-MBL-007-VVB	111	3.84	0.362
01-MBL-008-VVB	92	3.289	0.304
01-MBL-055-DAR	376	9.265	0.843
01-MBL-058-DAR	375	9.175	0.839
01-MBL-064-DAR	288	6.877	0.619
01-MBL-070-DAR	184	4.542	0.412
01-MBL-073-DAR	149	3.805	0.346
99-MBL-061-REA	389	3.084	0.331
99-MBL-062-REA	389	3.348	0.31
01-MBL-151-REA	333	3.321	0.316
01-MBL-153-REA	304	2.718	0.261
99-MBL-066-REA	187	2.698	0.25
01-MBL-161A-REA	72	2.566	0.278
01-MBL-163-REA	62	2.347	0.257
99-MBL-080-GAP	252	2.336	0.274
99-MBL-081-GAP	250	2.447	0.254
99-MBL-083/3-GAP	145	1.911	0.195
99-MBL-084-GAP	137	0.581	0.083
01-MBL-157/3-GAP	126	0.297	0.098

Mackintosh et. al., 2007

Sample	normalized elevation (m)	^{10}Be age (ka)	^{10}Be error (ka)
Mt. Henderson			
FM-Hend-27-2	242	9.01	0.7
FM-Hend-14-3	10	6.442	0.9
N. Masson Range			
FM-NMas-4B-1	329	11.899	0.9
FM-NMas-1-2 s	281	7.029	0.5
FM-NMas-18-3	266	10.672	0.7
FM-NMas-24-5	114	10.068	0.6
FM-NMas-23-6	102	7.192	0.5
FM-NMas-20-7	55	10.094	0.7
FM-NMas-21-8	0	7.6	0.5
Brown Range			
FM-Brown-29-3	2	13.1	0.9
FM-Brown-43-4	23	1.004	0.19
FM-Brown-20-5	143	5.1	2.9

Bentley et. al., 2010

Sample	normalized elevation (m)	^{10}Be age (ka)	^{10}Be error (ka)
PAT-01-MJB	192	8.2	0.8
PAT-03-MJB	109	5.7	1.8
PAT-04-MJB	98	9	1
PAT-05-MJB	54	6.6	1
CF-228-08	166	5.4	0.5
CF-229-08	166	4.6	0.4
CF-230-08	130	8.8	0.8
CF-231-08	130	0.3	0
MAR-05-MJB	372	6.8	0.6
MAR-06-MJB	346	7.4	0.7
MAR-08-MJB	182	6.2	0.5
MAR-09-CJF	485	15.1	1.3
MAR-10-MJB	154	11.4	1
MAR-11-CJF	460	15.4	1.4
MAR-11-MJB	0	2.1	0.2
MAR-12-MJB	0	2.8	0.3
MAR-26-CJF	59	6	0.6

Johnson et. al., 2014

Sample	normalized elevation (m)	^{10}Be age (ka)	^{10}Be error (ka)
MTM-01	7.9	142	0.3
MTM-02	7.9	127	0.3
MTM-03	7.9	86	0.3
MTM-04	6.3	20	0.2
MTM-05	7	22	0.3
MTM-06	6	0	0.2
JF-01	8.1	106	0.3
JF-02	7.9	89	0.3
JF-04	7.9	75	0.3
JF-06	7.7	20	0.3
JF-07	8.1	7	0.3

Figure A.1. Map of study site locations, with the corresponding number of samples processed and used. Note site Swe-9 was not used due to inheritance.

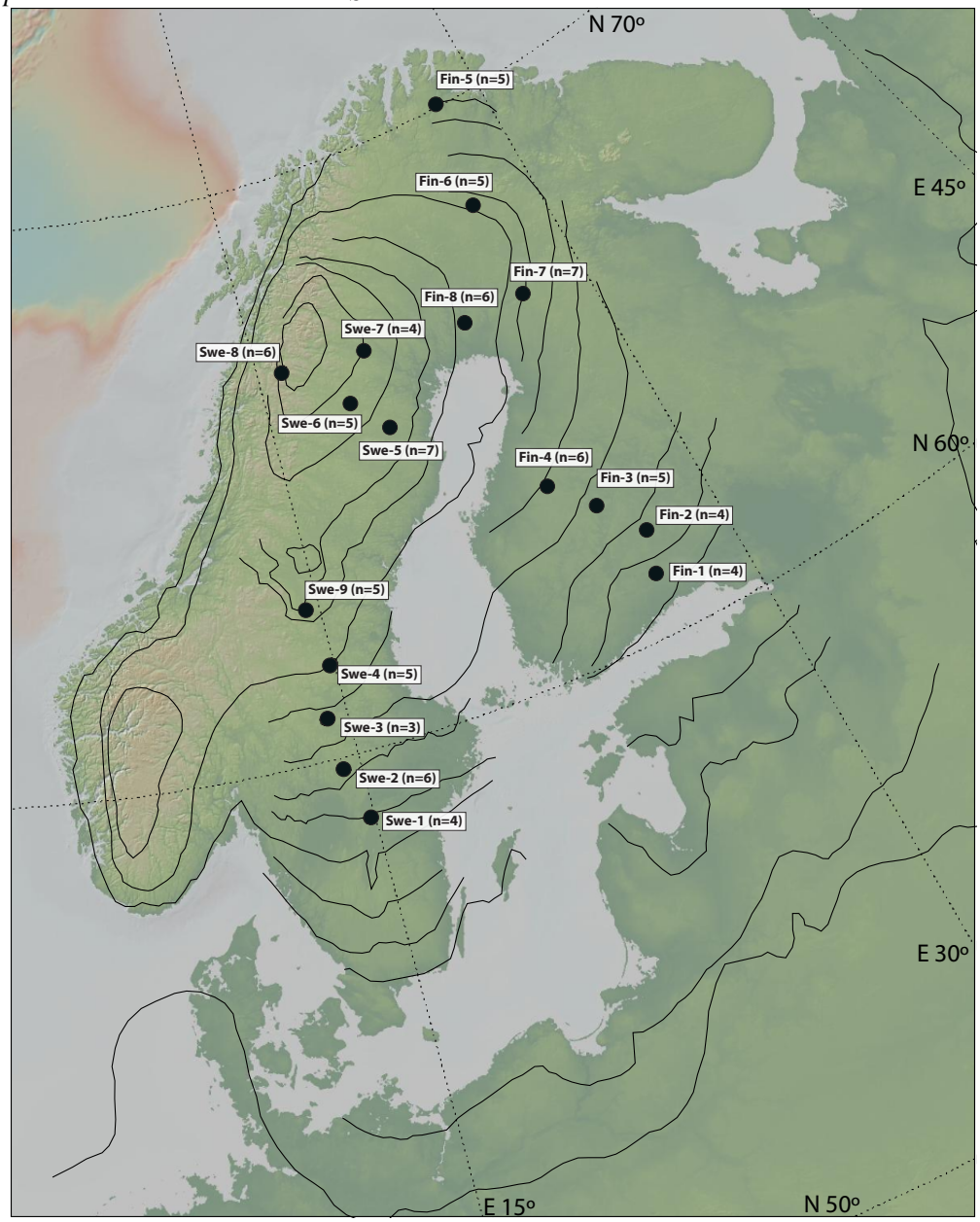

Figure A.2. Map showing current study sites (circles) as well as previous chronologies used in this study (squares). Colors indicate the particular study where ages were obtained. Colored lines and numbers denote the three transects used to create time-distance diagrams in Figure 2 in chapter 2.

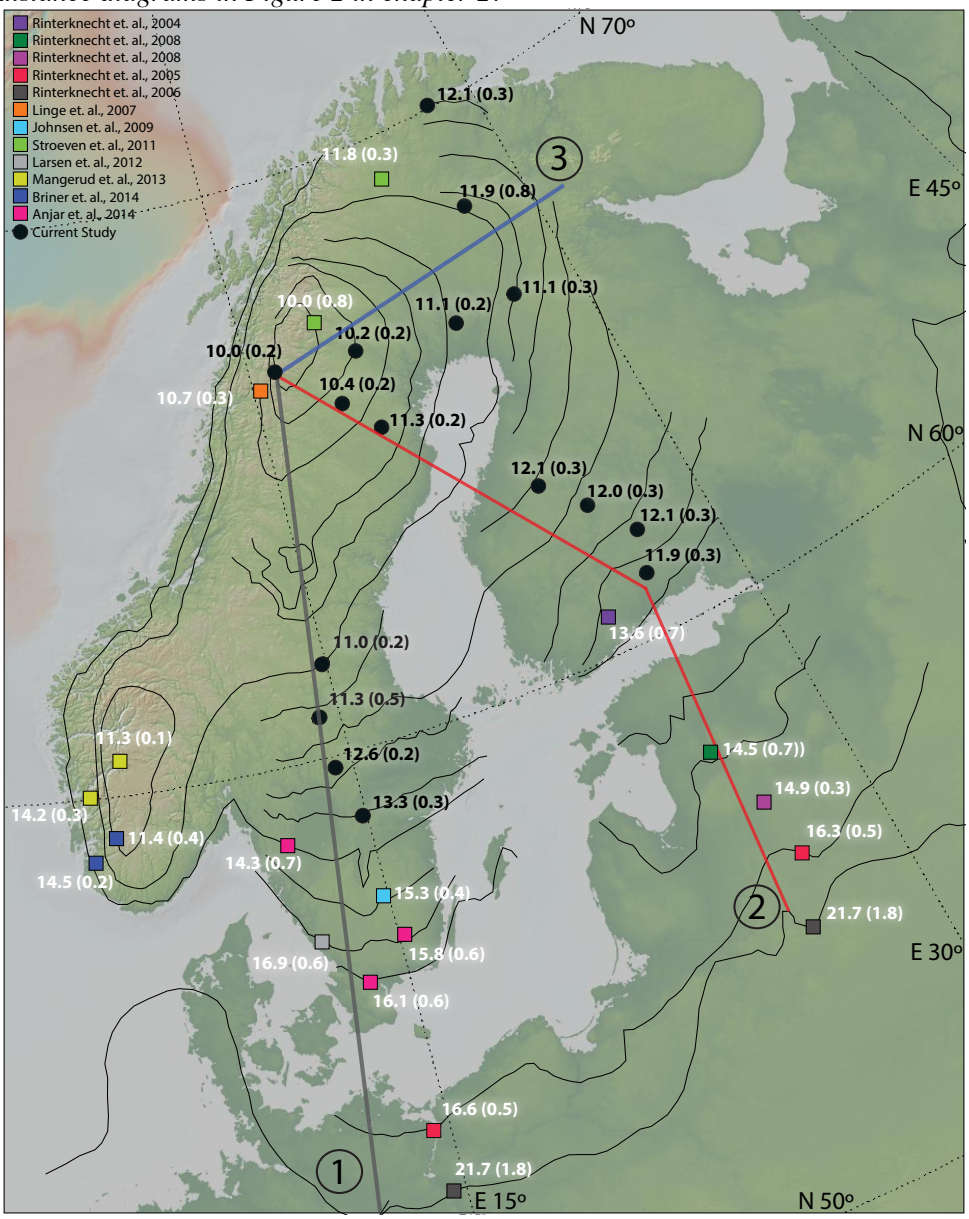

Figure A.3. Map showing areas and corresponding time intervals used to create the volume estimates for the SIS (see Figure 2 and 3 in chapter 2). Map also showsthe current study ages as well as previous chronology used to determine ice areas through time.

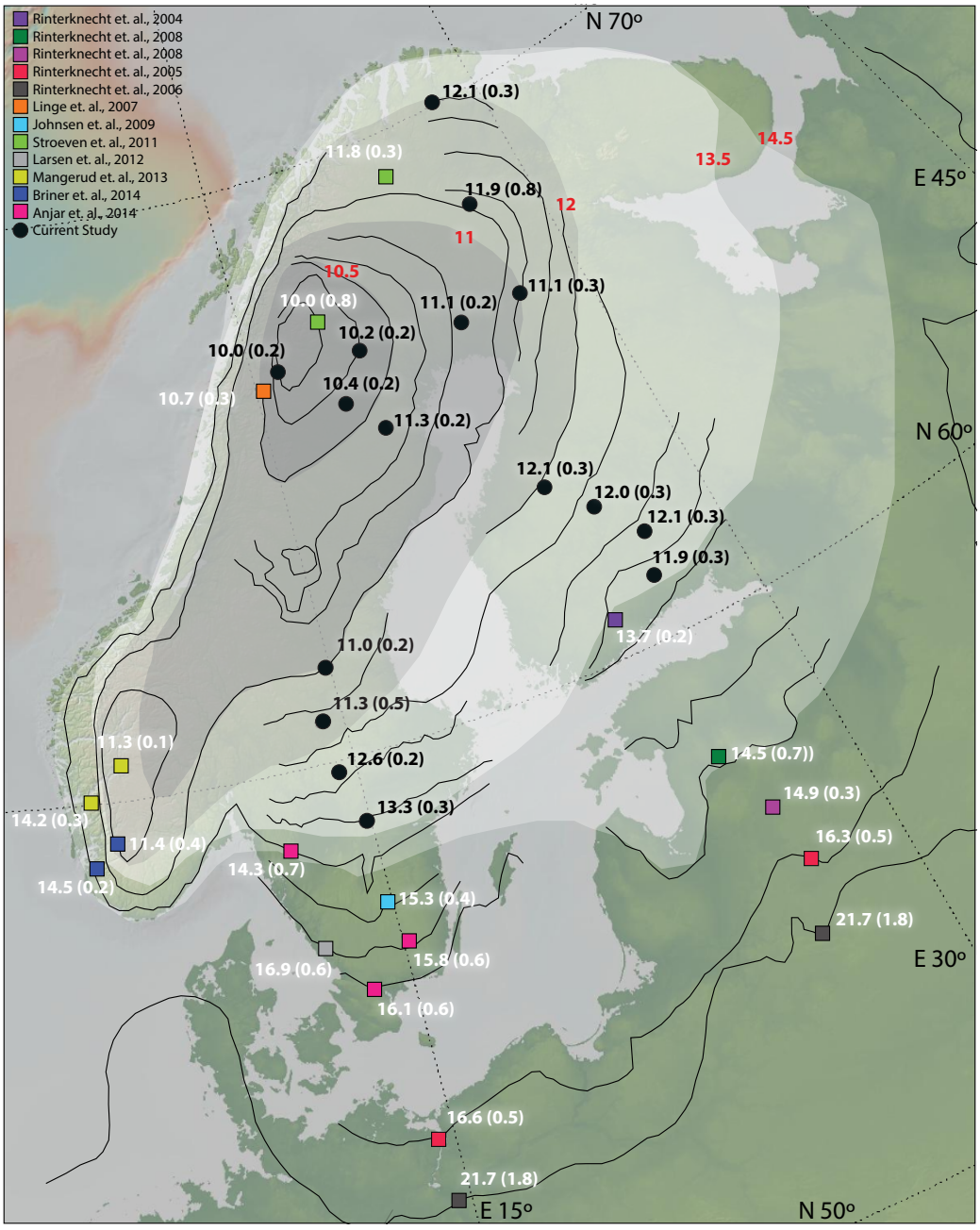

Figure A.4. Probability distribution diagrams for the current studies ages. PDFs are for site locations shown in Figure 1. Mean age uncertainty is the standard deviation of the ages. Error weighted mean uncertainty is the standard error of the ages. Light gray shading denotes the 2 sigma uncertainty of the external uncertainty. Dark gray shading denotes the 1 sigma uncertainty of the external uncertainty.

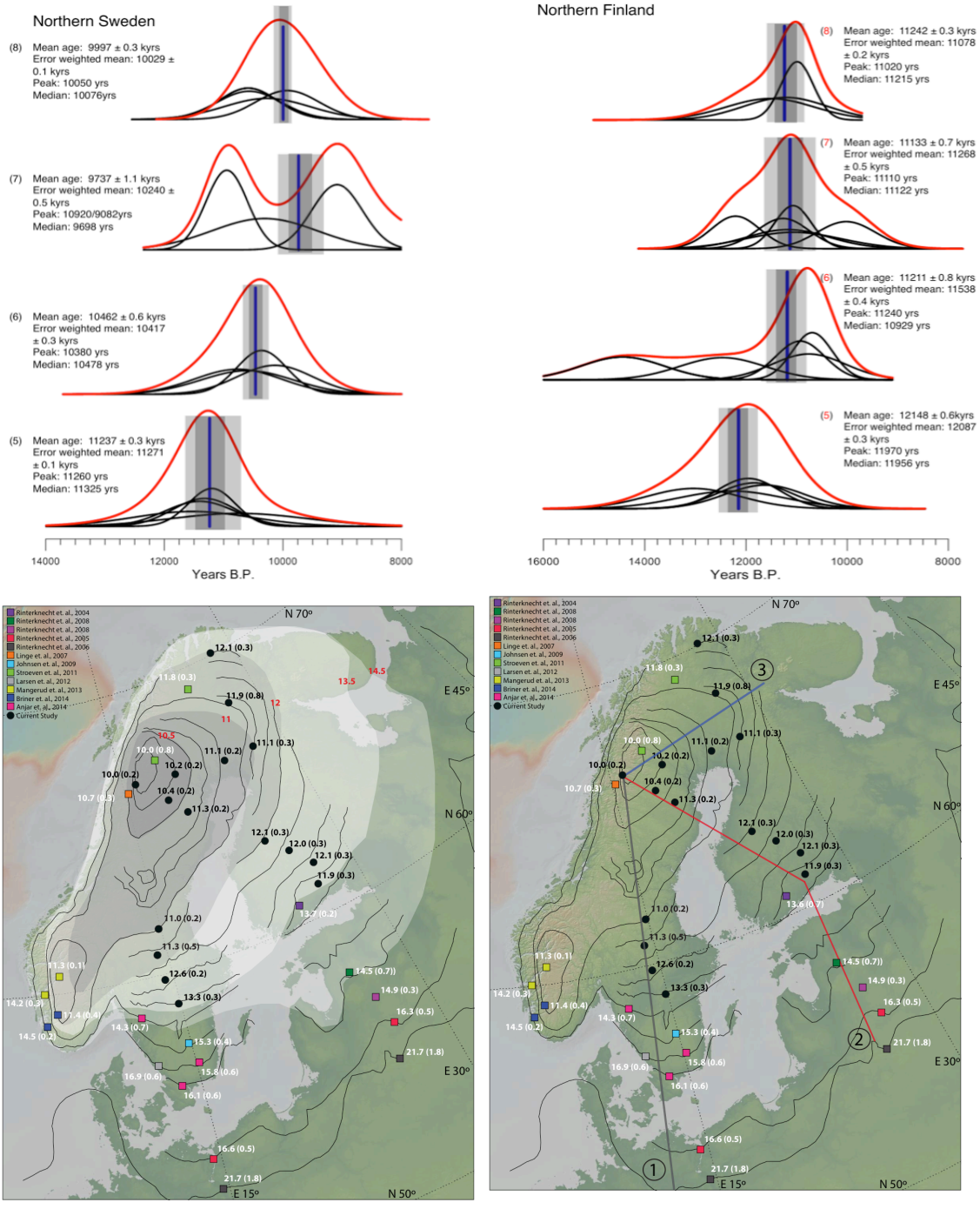

Figure A.5. Comparison of time series of ESL (m) from 13ka to 8ka for the current study SIS, and Ice-5G (Peltier, 2004).

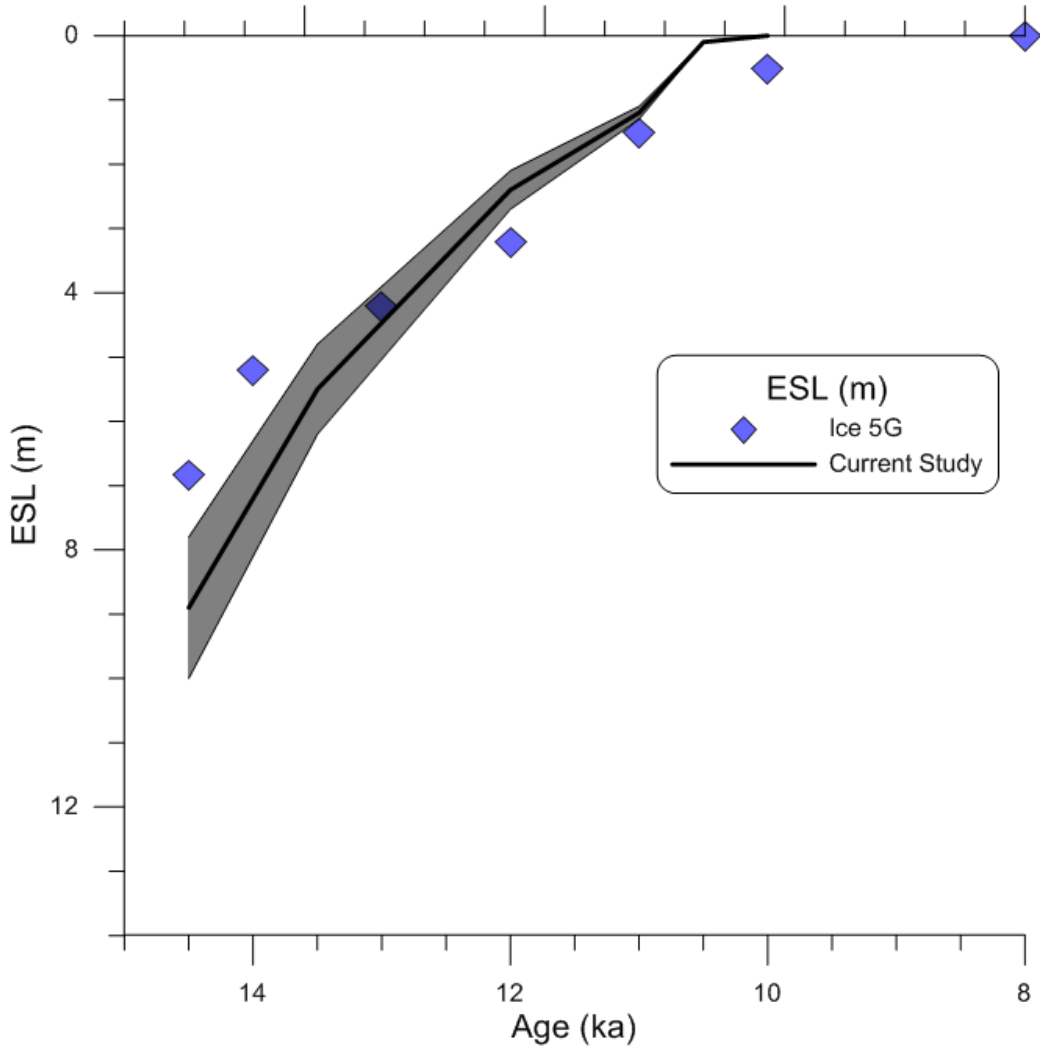

A.8. References

Andrén, T., Björck, S., Andrén, E., Conley, D., Lambeck, K., Zillén, L., Anjar, J., 2011. The development of the Baltic Sea basin during the last 130 ka. In: Harff, J.,Björck, S., Hoth, P. (Eds.), The Baltic Sea Basin as a Natural Laboratory. Springer-Verlag, Berlin, Heidelberg, pp. 75-97

Balco, G. A., Stone, J. O., Lifton, N. A., and Dunai, T. J. 2008. A complete and easily accessible means of calculating surface exposure ages or erosion rates from ^{10}Be and ^{26}Al measurements. *Quaternary Geochronology,* **3,** 174-195

Carlson, A., Legrande, A. N., Oppo, D., Came, R.E., Schmidt, G. A., Anslow, F.S., Licciardi, J.M., Obbink, E.A. 2008. Rapid early Holocene deglaciation of the Laurentide ice sheet. Nature Geoscience. 1, 620-624.

Desilets, D., Zreda, M. G., and Prabu, T. 2006. The energy dependence of cosmogenic nuclide scaling models: New measurments at low latitudes. *Earth and Planetary Science Letters* **246,** 265-276.

Dunai, T. J. 2001. Influence of secular variation of the geomagnetic field on the production rates of in situ produced cosmogenic nuclides. *Earth and Planetary Science Letters* **193,** 197-212.

Dyke, A.S., 2004. An outline of North American Deglaciation with emphasis on central and northern Canada. In: Ehlers, J., Gibbard, P.L. (Eds.), Quaternary Glaciations: Extent and Chronology. Elsevier, Amsterdam, pp. 373–424.

Goehring, B., Strand, O.L., Mangerud, J., Inge Svendsen, J, Gyllencreutz, R., Schaefer, J., Finkel, R. 2012. Late Glacial and Holocene Be-10 production rates for western Norway. Journal of Quaternary Science, v. 27, pp. 89-96.

Lal, D. 1991. Cosmic ray labeling of erosion surfaces: In-situ nuclide production rates and erosion models. *Earth and Planetary Science Letters* **104,** 424-439.

Lambeck, K., Rouby, H., Purcell, A., Sun, Y., Sambridge, M. In press. Sea Level and Global Ice Volumes From the Last Glaicial Maximum to the Holocene. *PNAS*.

Lifton, N. A., Bieber, J. W., Clem, J. M., Duldig, M. L., Evenson, P., Humble, J. E., and Pyle, R. 2005. Addressing solar modulation and long-term uncertanties in scaling secondary cosmic rays for in situ comogenic nuclide applications. *Earth and Planetary Science Letters* **239,** 140-161.

Lundqvist, Jan, 1986a, Late Weichselian glaciation and deglaciation in Scandinavia. in V. Sibrava, D. Q. Bowen, and G. M. Richmond, ed., pp. 269-292, Quaternary Glaciations in the Northern Hemisphere. Pergammon Press, New York. 514 pp.

Lunkka, J. P., Johansson, P., Saarnisto, M. And Sallasmaa, O. 2004. Glaciation of Finland. In Ehlers, J., Gibbard, P. (Eds), Extent and Chronology of Glaciations. INQUA Commission on Glaciation. Elsevier, p. 93 – 100.

Marcott, S.A., Shakun, J.D., Clark, P.U., Mix, A.C. 2013. A Reconstruction of Regional and Global Temperature for the Past 11,300 Years. **339** (6124), 1198-1201. DOI:10.1126/science.1228026.

Paterson, W.S.B. 1994. The Physics of Glaciers. 3rd edition, Pergamom, Tarrytown, N.Y.

Rinterknecht, V. R., Bitinas, A., Clark, P. U., Raisbeck, G. M., Yiou, F.,Brook, E. J. 2008. Timing of the last deglaciation in Lithuania. BOREAS. 37, 3, p. 426-433.

Rinterknecht, V., Clark, P. U., Raisbeck, G. M., Yiou, F., Bitinas, A., Brook, E. J., Marks, L., Zelcs, V., Lunkka, J. P., Pavlovskaya, I. E., Piotrowski, J. A., Raukas, A. 2006. The Last Deglaciation of the Southeastern Sector of the Scandinavian Ice Sheet. Science. 311, 5766, p. 1449-1452.

Shakun, J. D., Clark, P. U., He, F., Marcott, S. A., Mix, A. C., Liu, Z., Otto-Bliesner, B. L, Schmittner, A., and Bard, E. 2012. Global warming preceded by increasing carbon dioxide concentrations during the last deglaciation. Nature,484, 49-54.

Stone, J. O. 2000. Air pressure and cosmogenic isotope production. *Journal of Geophysical Research* **105,** 23,753 - 23,759.

Young, N.E., Schaefer, J.M., Briner, J.P., and Goehring, B.M. 2013. A precise 10Be production-rate calibration for the Arctic. *Journal of Quaternary Science*, v. **28**, p. 515-526.

Bibliography

Abe-Ouchi, A., Segawa, T., and Saito, F. 2007. Climatic conditions for modelling the northern hemisphere ice sheets throughout the ice age cycle. Climate of the Past, 3(3), 423–438.

Abe-Ouchi, A., Saito, F., Kawamura, K., Raymo, M.E., Okuno, J, Takahashi, K., Blatter, H. 2013 Insolation-driven 100,000-year glacial cycles and hysteresis of ice-sheet volume**.** *Nature*; 500 (7461): 190 DOI: 10.1038/nature12374

Alder, J.R., and S.W. Hostetler. (2014). Global climate simulations at 3000 year intervals for the last 21,000 years with the GENMOM coupled atmosphere-ocean model. C*limates of the past discussion,* **10**(4), 2925-2978.

Alder, J. R., S. W. Hostetler, D. Pollard, and A. Schmittner (2011), Evaluation of a present-day climate simulation with a new coupled atmosphere-ocean model GENMOM, *Geosci. Model Dev.*, ***4***(1), 69–83, doi:10.5194/gmd-4-69-2011.
Alley, R. B., Brook, E. J, Anandakrishnan, S. (2002). A northern lead in the orbital band: north-south phasing of Ice-Age events. *Quat. Sci. Rev.* **21**, 431–441.

Amante, C. and Eakins, B. 2009. ETOPO1 1 Arc-Minute global relief model: Procedures, data sources and analysis. Technical Report 24, NOAA Technical Memorandum NESDIS NGDC.

Andrén, T., Björck, S., Andrén, E., Conley, D., Lambeck, K., Zillén, L., Anjar, J., 2011. The development of the Baltic Sea basin during the last 130 ka. In: Harff, J.,Björck, S., Hoth, P. (Eds.), The Baltic Sea Basin as a Natural Laboratory. Springer-Verlag, Berlin, Heidelberg, pp. 75-97

Anjar, J., Laresen, N. K., Hakansson, L., Moller, P., Linge, H., Fabel, D., Xu, S. 2014. A 10 Be-based reconstruction of the last deglaciation in southern Sweden. *Boreas*. **43,** 132–148.

Balco, G. A., Stone, J. O., Lifton, N. A., and Dunai, T. J. 2008. A complete and easily accessible means of calculating surface exposure ages or erosion rates from ^{10}Be and ^{26}Al measurements. *Quaternary Geochronology,* **3,** 174-195

Bard, E., Hameline, B., Arnold, M., Montaggiono, L., Cabioch, G., Faure, G., Rougerie, F. 1996. Deglacial sea-level record from Tahiti corals and the timining of global meltwater discharge. Nature. **382**, 241-244.

Bentley, M.J., Fogwill, J., Le Brocq, A.M., Hubbard, A.L., Sugden, D.E., Dunai, T.J., Freeman, S.P.H.T. 2010. Deglacial history of the West Antarctic Ice Sheet in the Weddell

Sea embayment: Constraints on past ice volume change. *Geology*. **38**, pp 411-414. Doi:10.1130/G30754.1

Berger, A. L. (1978), Long-term variations of daily insolation and Quaternary climatic changes, *Journal of the Atmospheric Sciences*, ***35***(12), 2362–2367.

Bonelli, S., Charbit, S., Kageyama, M., Woillez, M., Ramstein, G., Dumas, C., and Quiquet, A. 2009. Investigating the evolution of major northern hemisphere ice sheets during the last glacial-interglacial cycle. Climate of the Past, 5(3), 329–345.

Boulton, G.S., Dongelmans, P., Punkari, M., Broadgate, M., 2001. Paleoglaciology of an ice sheet through a glacial cycle: the European ice sheet through the Weichselian. Quaternary Science Reviews **20**, 591–625.

Boos, W. R. (2012), Thermodynamic Scaling of the Hydrological Cycle of the Last Glacial Maximum, *J. Climate*, ***25***(3), 992–1006, doi:10.1175/JCLI-D-11-00010.1.

Briner, J.P., Svendsen, J.I., Mangerud, J., Lohne, Ø.S., Young, N.E. (2014). A ^{10}Be chronology of the southwestern Scandinavian Ice Sheet history during the Late Glacial period. Journal of Quaternary Science, v. **29,** p. 370-380.

Bromley, G.R.M., Putnam, A.E., Rademaker, K.M., Lowell, T.V., Schaefer, J.M., Hall, B., Winckler, G., Birkel, S.D., Borns, H.W. 2014. Younger Dryas deglaciation of Scotland driven by warming summers. *PNAS*. **117**(11):6215-9 DOI: 10.1073/pnas.1321122111.

Brook, E. J., S. Harder, J. Severinghaus, E.J. Steig, and C.M. Sucher (2000), On the origin and timing of rapid changes in atmospheric methane during the last glacial period, Global Biogeochem. Cycles, **14(**2), 559–572.

Carlson, A., Legrande, A. N., Oppo, D., Came, R.E., Schmidt, G. A., Anslow, F.S., Licciardi, J.M., Obbink, E.A. 2008. Rapid early Holocene deglaciation of the Laurentide ice sheet. Nature Geoscience. **1**, 620-624.

Carlson, A.E., and Clark, P.U. 2012, Ice-sheet sources of sea-level rise and freshwater discharge during the last deglaciation: Reviews of Geophysics, v. **50**, doi: 10.1029/ 2011RG000371.

Cato, I. 1987: On the definitive connection of the Swedish Time Scale with the present. Sverige Geologiska Undersokning Ca. **68**, 1-55.

Chang, E. K. M., Y. Guo, X. Xia, and M. Zheng (2012), Storm Track Activity in IPCC AR4/CMIP3 Model Simulations, *J. Climate*, 120630072710003, doi:10.1175/JCLI-D-11-00707.1.

Charbit, S., Ritz, C., Philippon, G., Peyaud, V., and Kageyama, M. 2007. Numerical reconstructions of the northern hemisphere ice sheets through the last glacial-interglacial cycle. Climate of the Past, 3, 15–37.

Clark, P.U., Mix, A.C. 2002. Ice sheets and sea level of the Last Glacial Maximum. Quaternary Science Reviews. **21**, 1-7.

Cook, K.H. and I.M. Held. 1988. Stationary waves of the ice age climate. J. Climate, **1**(8), 807–819.

Desilets, D., Zreda, M. G., and Prabu, T. 2006. The energy dependence of cosmogenic nuclide scaling models: New measurments at low latitudes. *Earth and Planetary Science Letters* **246,** 265-276.

Dong, B., and P. J. Valdes (1998), Simulations of the Last Glacial Maximum climates using a general circulation model: prescribed versus computed sea surface temperatures, *Climate Dynamics*, **14**, 571-591.

Donohoe, A and D.S. Battisti (2009), Causes of reduced Atlantic storm activity in a CAM3 simulation of the last glacial maximum, *Journal of Climate,* **22**, 4793–4808.

Donner, J. 1995. The Qauternary History of Finland. (World and regional Geology 7). Cambridge, Cambridge University Press, 200pp.

Dunai, T. J. 2001. Influence of secular variation of the geomagnetic field on the production rates of in situ produced cosmogenic nuclides. *Earth and Planetary Science Letters* **193,** 197-212.

Dyke, A.S., 2004. An outline of North American Deglaciation with emphasis on central and northern Canada. In: Ehlers, J., Gibbard, P.L. (Eds.), Quaternary Glaciations: Extent and Chronology. Elsevier, Amsterdam, pp. 373–424.

Dyke, A.S., Dredge, L.A., Vincet, J. 1982. Configuration and Dynamics of the Laurentide Ice Sheet During the Late Wisconsin Maximum. Géographie physique et Quaternaire, Volume 36, issue 1-2, 1982, p.5-14

Dyke, A. S. and Prest, V. K. 1987. Late wisconsinan and holocene history of the laurentide ice sheet. G ´eographie physique et Quaternaire, 41(2), 237–263.

Fairbanks, R. 1989. A 17,000-year glacio-eustatic sea level record: influence of glacial melting rates on the Younger Dryas event and deep-ocean circulation. Nature. **342**, 637-642.

Fettweis, X., M. Tedesco, M. R. Van de Broeke, and J. Ettema (2011), Melting trends over the Greenland ice sheet 52 (1958–2009) from spaceborne microwave data and regional climate models, *The Cryosphere*, **5**, 359-375.

Forster, P., V. Ramaswamy, P. Artaxo, T. Berntsen, R. Betts, D.W. Fahey, J. Haywood, J. Lean, D.C. Lowe, G. Myhre, J. Nganga, R. Prinn, G. Raga, M. Schulz and R. Van Dorland, 2007: Changes in Atmospheric Constituents and in Radiative Forcing.In: Climate Change 2007: The Physical Science Basis. Contribution of Working Group I to the Fourth Assessment Report of the Intergovernmental Panel on Climate Change [Solomon, S., D. Qin, M. Manning, Z. Chen, M. Marquis, K.B. Averyt, M.Tignor and H.L. Miller (eds.)]. Cambridge University Press, Cambridge, United Kingdom and New York, NY, USA.

Ganopolski, A., Calov, R., and Claussen, M. 2010. Simulation of the last glacial cycle with a coupled climate ice-sheet model of intermediate complexity. Climate of the Past, 6(2), 229–244.

Goehring, B., Strand, O.L., Mangerud, J., Inge Svendsen, J, Gyllencreutz, R., Schaefer, J., Finkel, R. 2012. Late Glacial and Holocene Be-10 production rates for western Norway. Journal of Quaternary Science, v. **27**, pp. 89-96.

Gregoire, L J, A. J. Payne, and P. J. Valdes 2012, Deglacial rapid sea level rises caused by ice-sheet saddle collapses, Nature, 487(7406), 219–222, doi:10.1038/nature11257.

Gyllencreutz, R., Mangerud, J., Svendsen, JI., Lohne, O. 2007. DATED-A GIS based reconstruction and dating database of the Eurasian deglaciation. Geologic Survey of Finland, Special Paper **46**, 113-120.

He, F., J. D. Shakun, P. U. Clark, A. E. Carlson, Z. Liu, B. L. Otto-Bliesner, and J. E. Kutzbach (2013), Northern Hemisphere forcing of Southern Hemisphere climate during the last deglaciation, Nature, **494**(7435), 81-85.

Hebeler, F., Purves, R. S., and Jamieson, S. S. 2008. The impact of parametric uncertainty and topographic error in ice-sheet modelling. Journal of Glaciology, 54, 899–919.

Heine, K., Reuther, A. U., Thieke, H. U., Schulz, R., Schlaak, N. & Kubik, P. W. 2009: Timing of Weichselian ice marginal positions in Brandenburg (northeastern Germany) using cosmogenic in situ 10Be. Zeitschrift für Geomorphologie **53**, 433–454.

Heinemann, H., Timmermann, A., Timm, O.E., Saito, F., Abe-Ouchi, A. 2014. Deglacial ice–sheet meltdown: orbital pacemaking and CO_2 effects. Clim. Past Discuss., 10, 509-532, doi:10.5194/cpd-10-509-2014

Hofer, D., C. C. Raible, A. Dehnert, and J. Kuhlemann (2012), The impact of different glacial boundary conditions on atmospheric dynamics and precipitation in the North Atlantic region, *Clim. Past*, ***8***(3), 935–949, doi:10.5194/cp-8-935-2012.

Hoskins, B. J. and D. J. Karoly, 1981: The steady linear response of a spherical

atmosphere to thermal and orographic forcing. J. Atmos. Sci., **38**, 1179–1196.

Hostetler, S.W., P.U. Clark, P.J. Bartlein, A.C. Mix, and N.G. Pisias (1999), Atmospheric transmission of North Atlantic Heinrich Events, *J. Geophysical Research,* **104**(D4), 3947-3952.

Huybrechts, P. and T'siobbel, S. 1997. A three-dimensional climate-ice-sheet model applied to the last glacial maximum. Annals of Glaciology, 25, 333–339.

Johansson, P. 1995. The deglaciation in the eastern part of the Weichselian ice divide in Finnish Lapland. Geological Survey of Finland Bulletin, **383**, 72pp.

Johnsen, T.F., Alexanderson, H., Fabel, D. and Freeman, S.P.H.T. 2009.
New 10Be cosmogenic ages from the Vimmerby moraine confirm the timing of Scandinavian Ice Sheet deglacia- tion in southern Sweden. Geogr. Ann. **91** A (2): 113-120.

Johnson, J.S., Bentley, M.J., Smith, J.A., Finkel, R.C., Rood, D.H., Gohl, K., Balco, G., Larter, R.D., Schaefer, J.M. 2014. Rapid thinning of Pine Island Glacier in the Early Holocene. *Science*. **343**, 999. Doi:10.1126/science/1247385.

Kageyama, M., P. Valdes, G. Ramstein, C. Hewitt, and U. Wyputta (1999), Northern Hemisphere storm tracks in present day and Last Glacial Maximum climate simulations: A comparison of European PMIP models, *J. Climate*, **12,** 742.

Kalnay, E., Kanamitsu, M., Kistler, R., Collins, W., Deaven, D., Gandin, L., Iredell, M., Saha, S., White, G., Woollen, J., Zhu, Y., Chelliah, M., Ebisuzaki, W., Higgins, W., Janowiak, J., Mo, K. C., Ropelewski, C., Wang, J., Leetmaa, A., Reynolds, R., Jenne, R., and Joseph, D. 1996. The NCEP/NCAR 40-year reanalysis project. Bulletin of the American Meteorological Society, 77(3), 437–471.

Kapsner, W. R., R. B. Alley, C. A. Shuman, S. Anandarkrishnan, and P. M. Grootes (1995), Dominant influence of atmospheric circulation on snow accumulation in Greenland over the past 18,000 years, *Nature*, ***373***(6509), 52–54.

Laîné, A., M. Kageyama., D. Salas-Mélia., A. Voldoire., G Riviere., G. Ramstein., S. Planton., S. Tyteca., and J.Y. Peterschmitt (2009), Northern Hemisphere storm tracks during the Last Glacial Maximum in the PMIP2 ocean-atmosphere coupled models: Energetic study, seasonal cycle, precipitation, *Climate Dyn.*, **32,** 593–614.

Lal, D. 1991. Cosmic ray labeling of erosion surfaces: In-situ nuclide production rates and erosion models. *Earth and Planetary Science Letters* **104,** 424-439.

Lambeck, K., Rouby, H., Purcell, A., Sun, Y., Sambridge, M. In press. Sea Level and Global Ice Volumes From the Last Glaicial Maximum to the Holocene. *PNAS*.

Larsen, N. K., Linge, H., Håkansson, L. & Fabel, D. 2012: Investigating the last deglaciation of the Scandinavian Ice Sheet in south- west Sweden with 10Be exposure dating. Journal of Quaternary Science **27**, 211–220.

Laske, G. and Masters, G. 1997. A global digital map of sediment thickness. Eos, Transactions, American Geophysical Union, 78(F483).

Lecavalier, B.S., Milne, G.A., Simpson, M. J.R., Wake, L., Huybrechts, P., Tarasov, L., Kjeldsen, K. K., Funder, S., Long, A. J., Woodroffe, S., Dyke, A.S., Larsen, N. K. 2014. A model of Greenland ice sheet deglaciation constrained by observations of relative sea level and ice extent. *Quaternary Science Reviews,* **102**, 54-84
doi: 10.1016/j.quascirev.2014.07.018

Li, C. and J.J. Wettstein, 2012: Thermally driven and Eddy-driven Jet Variability in Reanalysis. *J. Climate,* **25**, 1587-1596, doi:10.1175/JCLI-D-11-00145.1.

Li, C., and D. S. Battisti (2008), Reduced Atlantic Storminess during Last Glacial Maximum: Evidence from a Coupled Climate Model, *J. Climate*, ***21***(14), 3561–3579, doi:10.1175/2007JCLI2166.1.

Liakka, J., Nilsson, J. 2010. The impact of topographically forced stationary waves on local ice-sheet climate. *J. Glaciology.* **56**, 534-544.

Licciardi, J.M., Clark, P.U., Jenson, J.W., and MacAyeal, D.R., 1998, Deglaciation of a soft-bedded Laurentide Ice Sheet: Quaternary Science Reviews, v. **17**, p. 427-448.

Lifton, N. A., Bieber, J. W., Clem, J. M., Duldig, M. L., Evenson, P., Humble, J. E., and Pyle, R. 2005. Addressing solar modulation and long-term uncertanties in scaling secondary cosmic rays for in situ comogenic nuclide applications. *Earth and Planetary Science Letters* **239,** 140-161.

Lindeman, M. and J. Oerlemans, 1987. Northern Hemisphere ice sheets and planetary waves: a strong feedback mechanism. *Journal of Climatology*, **7**, 109-117.

Linge, H., Olsen, L., Brook, E.J., Darter, J.R., Mickelson, D.M., Raisbeck, G.M. & Yiou, F. 2007. Cosmogenic nuclide surface exposure ages from Nordland, northern Norway: implications for deglaciation in a coast to inland transect. Norwegian Journal of Geology, vol. **87**, pp. 269-280. ISSN 029-196X.

Lipscomb, W.H., Fyke, J.G., Vizcaíno, M., Sacks, W.J., Wolfe, J., Vertenstein, M., Craig, A., Kluzek, E., Lawrence, D.M., 2013. Implementation and Initial Evaluation of the Glimmer Community Ice Sheet Model in the Community Earth System Model. J. Climate, 26, 7352–7371. doi: http://dx.doi.org/10.1175/JCLI-D-12-00557.1

Liu, Z., B. L. Otto-Bliesner, F. He, E. C. Brady, R. Tomas, P. U. Clark, A. E. Carlson, J.

Lynch-Stieglitz, W. Curry, E. Brook, D. Erickson, R. Jacob, J. Kutzbach, and J. Cheng (2009): Transient Simulation of Last Deglaciation with a New Mechanism for Bølling-Allerød Warming. Science, **325**, 310-314, doi:10.1126/science.1171041.

Lundqvist, Jan, 1986a, Late Weichselian glaciation and deglaciation in Scandinavia. in V. Sibrava, D. Q. Bowen, and G. M. Richmond, ed., pp. 269-292, Quaternary Glaciations in the Northern Hemisphere. Pergammon Press, New York. 514 pp.

Lundqvist, J. & Wohlfarth, B. A. 2001. Timing and east-west correlation of South Swedish ice marginal lines during the late Weichselian. Quaternary Science Reviews **20** (10), 1127–1148.

Lundqvist, J. 2004. Glacial history of Sweden. In: Ehlers, J., Gibbard, P.I. (eds), Quaternary glaciations: extent and chronology, Part 1: Europe. Developments in Quaternary Science 2. Amsterdam: Elsevier, 271–294.

Lunt, D., Valdes, P., Haywood, A., and Rutt, I. 2008. Closure of the panama seaway during the pliocene: implications for climate and northern hemisphere glaciation. Climate Dynamics, 30(1), 1–18.

Lunkka, J. P., Johansson, P., Saarnisto, M. And Sallasmaa, O. 2004. Glaciation of Finland. In Ehlers, J., Gibbard, P. (Eds), Extent and Chronology of Glaciations. INQUA Commission on Glaciation. Elsevier, p. 93 – 100.

Mackintosh, A., White, D., Fink, D., Gore, D.B., Pickard, J., Fanning, P.C. 2007. Exposure ages from mountain dipsticks in Mac. Robertson Land, East Antarctica, indicate little change in ice-sheet thickness since the Last Glacial Maximum. *Geology*. **35**, pp. 551-554. Doi:10.1130/G23503A.1

Manabe, S., and A. J. Broccoli (1985), The influence of continental ice sheets on the climate of an ice age, *J. Geophys. Res.*, 90, 2167-2190, doi:10.1029/JD090iD01p02167.
Marshall, S.J., and G.K.C. Clarke (1999), Modeling North American freshwater runoff through the last glacial cycle, *Quaternary Research,* **52**, 300–315.

Mangerud J, Goehring BM, Lohne ØS, et al. 2013. Collapse of marine-based outlet glaciers from the Scandinavian Ice Sheet. Quaternary Science Reviews **67**: 8–16.

Marcott, S.A., Shakun, J.D., Clark, P.U., Mix, A.C. 2013. A Reconstruction of Regional and Global Temperature for the Past 11,300 Years. **339** (6124), 1198-1201. DOI:10.1126/science.1228026.

Marshall, S. J., Tarasov, L., Clarke, G. K. C., and Peltier, W. R. 2000. Glaciological reconstruction of the laurentide ice sheet: physical processes and modelling challenges. Canadian Journal of Earth Sciences, 37(5), 769–793.

Marshall, S. J., James, T. S., and Clarke, G. K. C. 2002. North american ice sheet reconstructions at the last glacial maximum. Quaternary Science Reviews, 21(1-3), 175–192.

Monnin, E., A. Indermühle, A. Dallenbach, J. Fluckiger, B. Stauffer, T. F. Stocker, D. Raynaud, and J. M. Barnola (2001), Atmospheric CO2 concentrations over the last glacial termination, *Science*, ***291***(5501), 112–114, doi:10.1126/science.291.5501.112.

Pacanowski, R. C. 1996. MOM 2 Version 2.0 (Beta) Documentation: User's Guide and Reference Manual, NOAA GFDL Ocean Technical Report 3.2, 329 pp.

Paterson, W.S.B. 1994. The Physics of Glaciers. 3rd edition, Pergamom, Tarrytown, N.Y.

Peixoto, J. P., and A. H. Oort (1992), Physics of Climate, American Institute of Physics, 520 pp.

Peltier, W.R., 2004. Global Glacial Isostasy and the Surface of the Ice-Age Earth: The ICE-5G (VM2) Model and GRACE, Ann. Rev. Earth and Planet. Sci., **32**, 111-149.

Pollard, D., and S. L. Thompson (1997), Climate and ice-sheet mass balance at the last glacial maximum from the GENESIS version 2 global climate model, *Quaternary Science Reviews*, ***16***(8), 841–863.

Rasmussen, S.O., Andersen, K.K., Svenson, A.M., Steffensen, J.P., Vinther, B.M., Clausen, H.B., Siggard-Andersen, M.L., Johnsen, S.J., Larsen, L.B., Dahl-Jensen, D., Bigler, M., Rothlisberger, R., Fischer, H., Goto-Azuma, K., Hansson, M.E., Ruth, U. 2006. A new Greenland ice core chronology for the last glacial termination. *J. Geophys. Res.*, **111**, D06102, doi:10.1029/2005JD006079.

Rinterknecht, V. R., Bitinas, A., Clark, P. U., Raisbeck, G. M., Yiou, F.,Brook, E. J. 2008. Timing of the last deglaciation in Lithuania. BOREAS. **37**, 3, p. 426-433.

Rinterknecht, V., Pavlovskaya, I. E., Clark, P. U., Raisbeck, G. M., Yiou, F., Brook, E. J. 2007. Timing of the last deglaciation in Belarus. Boreas. **36**, 3, p. 307-313.

Rinterknecht, V., Clark, P. U., Raisbeck, G. M., Yiou, F., Brook, E. J., Tschudi, S., Lunkka, J. P. 2004. Cosmogenic ^{10}Be dating of the Salpausselkä I Moraine in southwestern Finland. Quaternary Science Reviews. **23**, 23-24, p. 2283-2289.

Rinterknecht, V., Marks, L., Piotrowski, J. A., Raisbeck, G. M., Yiou, F., Brook, E. J. & Clark, P. U. 2005. Cosmogenic 10Be ages on the Pomeranian Moraine, Poland. Boreas. **34**, 2, p. 186-191.

Rinterknecht, V., Clark, P. U., Raisbeck, G. M., Yiou, F., Bitinas, A., Brook, E. J., Marks, L., Zelcs, V., Lunkka, J. P., Pavlovskaya, I. E., Piotrowski, J. A., Raukas, A.

2006. The Last Deglaciation of the Southeastern Sector of the Scandinavian Ice Sheet. Science. **311**, 5766, p. 1449-1452.

Roe, G.H. and R.S. Lindzen. 2001a. The mutual interaction between continental-scale ice sheets and atmospheric stationary waves. *J. Climate*, **14**(7), 1450–1465.

Rutt, I. C., Hagdorn, M., Hulton, N. R. J., and Payne, A. J. 2009. The glimmer community ice sheet model. Journal of Geophysical Research, 114(F2).

Saarnisto, J., and T. Saarinen. 2001. Deglaciation chronology of the Scandanavian Ice Sheet from the Lake Onega Basin to the Salpausselka End Moraines. Global and Planetary Change. **31**: 387-405.

Shakun, J. D., Clark, P. U., He, F., Marcott, S. A., Mix, A. C., Liu, Z., Otto-Bliesner, B. L, Schmittner, A., and Bard, E. 2012. Global warming preceded by increasing carbon dioxide concentrations during the last deglaciation. Nature,**484**, 49-54.

Shepherd, A., Irvins, E.R., Geruo, A., Barletta, V.R., Bentley, M.J., Bettadpur, S., Briggs, K.H., Bromwich, D.H., Forsberg, R., Galin, N., Horwath, M., Jacobs, S., Joughin, I., King, M.A., Lenaerts, J.T.M., Li, J., Lightenberg, S.R.M., Luckman, A., Luthcke, S.B., McMillan, M., Meister, R., Milne, G., Mouginot, J., Muir, A., Nicolas, J.P., Paden, J., Payne, A.J., Pritchard, H., Rignot, E., Rott, H., Sorensen, L.S., Scambos, T.A., Scheuchl, B., O. Schrama, E.J., Smith, B., Sundal, A.V., van Angelen, J.H., van de Berg, W.J., van den Broeke, M.R., Vaughan, D.G., Velicogna, I., Wahr, J., Whitehouse, P., Wingham, D.J., Yi, D., Young, D., Zwally, H.J. 2012. A Reconciled Estimate of Ice-Sheet Mass Balance. *Science*. **338**, pp. 1183-1189. DOI: *10.1126/science.1228102*

Shinn, R.A., Barron, E.J. 1989. Climate Sensitivity to Continental Ice Sheet Size and Configuration.*J. Climate*.**2**,1517-1537.

Simmons, A., S. Uppala, D. Dee, and S. Kobayashi (2007), Era-Interim: New ECMWF reanalysis products from 1989 onwards, *ECMWF Newsletter,* **110**, 25-35, ECMWF, Reading, United Kingdom.

Snyder, J. P. (1987). Map Projections: A Working Manual. Number 1395 in U.S. Geological Survey professional paper. United States Government Printing Office, Washington, D.C.

Sollid, J.L., Andersen, S., Hamre, M., Kjeldsen, O., Salvigsen, O., Sturos, S., Tveita, T., Wilhelmsen, A. 1973. Deglaciation of Finmark, North Norway. Norsk Geografisk Tidskrift, **27**, 233-325.

Sowers, T., Alley, R.B., and Jubenville, J. (2003), Ice Core Records of Atmospheric N2O Covering the Last 106,000 Years, *Science*, **301**, 945-948.

Stone, J.O., Balco, G.A., Sugden, D.E., Caffee, M.W., Sass,L.C., Cowdery, S.G., Siddoway, C. 2003. Holocene deglaciation of Marie Byrd Land, West Antarctica. Science.**299**, 99-102.

Stroeven, A.P., Fabel, D., Harbor, J.M., Fink, D., Caffee, M.W., Dahlgren, T., 2011. Importance of sampling across an assemblage of glacial landforms for interpreting cosmogenic ages of deglaciation. Quaternary Research **76**, 148-156.

Stokes, C. R. and Tarasov, L. 2010. Ice streaming in the laurentide ice sheet: A first comparison between data-calibrated numerical model output and geological evidence. Geophysical Research Letters, 37.

Stromberg, B. 1989: Late Weichselian deglaciation and clay varve chronologyin east central Sweden. Sverige Geologiska Undersokning Ca **73**, 1-70.

Stone, E. J., Lunt, D. J., Rutt, I. C., and Hanna, E. 2010. Investigating the sensitivity of numerical model simulations of the modern state of the greenland ice-sheet and its future response to climate change. The Cryosphere, 4(3), 397–417.

Stone, J. O. 2000. Air pressure and cosmogenic isotope production. *Journal of Geophysical Research* **105,** 23,753 - 23,759.

Tarasov, L., and Peltier, W. R. 2004. A geophysically constrained large ensemble analysis of the deglacial history of the North American ice sheet complex, Quat. Sci. Rev. vol **23**, 359-388.

Thompson, S. L. and Pollard, D. 1997. Greenland and Antarctic mass balances for present and doubled CO2 from the GENESIS version 2 global climate model, J. Climate, **10**, 871–900.

Thompson, S. L. and Pollard, D. 1995. A global climate model (Genesis) with a Land-Surface Transfer Scheme (LSX) .1. Present climate simulation, J. Climate, 8, 732–761.

Timm, O. and Timmermann, A. 2007. Simulation of the last 21 000 years using accelerated transient boundary conditions, J. Climate, 20, 4377–4401. 511, 513

Tschudi, S., Ivy-Ochs, S., Schlu ¨ chter, C., Kubik, P.W., Rainio, H. 2000.^{10}Be dating of Younger Dryas Salpausselka ¨I formation in Finland. Boreas **29**, 287–293.

Ullman, D.J., Carlson, A.E., Clark, P.U., Cuzzone, J., Winsor, K., Caffee, M. In Prep. Abrupt collapse of the Labrador Dome of the Laurentide Ice Sheet linked to 8.2 ka event.

Uppala, S. M., Kallberg, P. W., Simmons, A. J., Andrae, U., Bechtold, V. D., Fiorino, M., Gibson, J. K., Haseler, J., Hernandez, A., Kelly, G. A., Li, X., Onogi, K., Saarinen, S., Sokka, N., Allan, R. P., Andersson, E., Arpe, K., Balmaseda, M. A., Beljaars, A. C.

M., Berg, L. V. D., Bidlot, J., Bormann, N., Caires, S., Chevallier, F., Dethof, A., Dragosavac, M., Fisher, M., Fuentes, M., Hagemann, S., Holm, E., Hoskins, B. J., Isaksen, L., Janssen, P. A. E. M., Jenne, R., McNally, A. P., Mahfouf, J. F., Morcrette, J. J., Rayner, N. A., Saunders, R. W., Simon, P., Sterl, A., Trenberth, K. E., Untch, A., Vasiljevic, D., Viterbo, P., and Woollen, J. 2005. The ERA-40 re-analysis. Quarterly Journal of the Royal Meteorological Society, 131(612), 2961–3012.

Weaver, A.J., Saenko, O.A., Clark, P.U., Mitrovica, J.X. 2003. Meltwater Pulse 1A from Antarctica as a Trigger of the Bølling-Allerød Warm Interval. *Science*. **299**, pp. 1709-1713.

Weber, M.E., Clark, P.U., Kuhn, G., Timmerman, A., Sprenk, D., Gladstone, R., Zhang, X., Lohman, G., Menviel, L., Chikamoto, M.O., Friedrich, T., Ohlwein, C. 2014. Millennial-scale variability in Antarctic ice-sheet discharge during the last deglaciation. Nature. **510**, 134-138. Doi:10.1038/nature13397

Wettstein, J.J., and J.M. Wallace, 2010: Observed Patterns of Month-to-Month Storm Track Variability and Their Relationship to the Background Flow. *J. Atmos. Sci.*, **67**, 1420-1437, doi: 10.1175/2009JAS3194.1.

Whitehouse, P. L., Bentley, M.J., Milne, G., King, M.A., Thomas, I.D. 2012. A new glacial isostatic adjustment model for Antarctica: calibrated and tested using observations of relative sea-level change and present-day uplift rates. *Geophysical Journal International*. **190**, pp. 1464-1482. doi: 10.1111/j.1365-246X.2012.05557.x

Wohlfarth, B., Björck, S., Possnert, G. & Brunnberg, L. 1995. A comparison between radiocarbon dated Late Weichselian calendar-year chronologies. *Journal of Coastal Research* Special Issue No. 17: Holocene Cycles: Climate, Sea Levels and Sedimentation, pp. 45–48.

Yin, J. H. (2005), A consistent poleward shift of the storm tracks in simulations of 21st century climate, *Geophysical Research Letters*, ***32***(18), L18701, doi:10.1029/2005GL023684**.**

Young, N.E., Schaefer, J.M., Briner, J.P., and Goehring, B.M. 2013. A precise 10Be production-rate calibration for the Arctic. *Journal of Quaternary Science*, v. **28**, p. 515-526.

Zweck, C. and Huybrechts, P. 2005. Modeling of the northern hemisphere ice sheets during the last glacial cycle and glaciological sensitivity. Journal of Geophysical Research- Atmospheres, 110(D7), –.